University of Louisville

ThinkIR: The University of Louisville's Institutional Repository

Electronic Theses and Dissertations

12-2023

The impact of environmental pollutants on alcohol-associated liver disease pathogenesis.

Tyler Charles Gripshover
University of Louisville

Follow this and additional works at: https://ir.library.louisville.edu/etd

Part of the Toxicology Commons

Recommended Citation

THE IMPACT OF ENVIRONMENTAL POLLUTANTS ON ALCOHOL-

ASSOCIATED LIVER DISEASE PATHOGENESIS

By

Tyler Charles Gripshover
B.S., Eastern Kentucky University, 2018
M.S., University of Louisville, 2021

A Dissertation
Submitted to the Faculty of the
School of Medicine of the University of Louisville
in Partial Fulfillment of the Requirements
for the Degree of

Doctor of Philosophy
in Pharmacology and Toxicology

Department of Pharmacology and Toxicology
University of Louisville
Louisville, KY

December 2023

THE IMPACT OF ENVIRONMENTAL POLLUTANTS ON ALCOHOL-

ASSOCIATED LIVER DISEASE PATHOGENESIS

By

Tyler Charles Gripshover
B.S., Eastern Kentucky University, 2018
M.S., University of Louisville, 2021

A Dissertation Approved on

11/08/2023

By the following Dissertation Committee:

_____

Matthew C. Cave, M.D.

_____

Barbara J. Clark, Ph.D.

_____

Joshua L. Hood, M.D., Ph.D.

_____

Irina A. Kirpich, Ph.D., MPH

_____

Shesh N. Rai, Ph.D.

_____

Banrida Wahlang, Ph.D.

DEDICATION

This dissertation is dedicated to my family for their encouragement and support over my life for my academic pursuits. Although I have been away from home the past nine years, you are all always in my thoughts and deepest gratitude for what you have done for me as a person. Additionally, my best friends since middle school, Klay, Michael, and Zach, have made a substantial impact on my life. Although we have started our own lives and have grown apart some, you will always be with me for the remainder of my life.

Finally, I am dedicating this dissertation to my remarkable wife, Amanda. You have been the greatest inspiration and motivation to me to be the best I absolutely can be. As my wife and soon to be mother to our child, I am eager to spend the rest of my life with you and endure any and all positive and negative things that may happen to us.

Isaiah 40:31

ACKNOWLEDGEMENTS

ABSTRACT

THE IMPACT OF ENVIRONMENTAL POLLUTANTS ON ALCOHOL-
ASSOCIATED LIVER DISEASE PATHOGENESIS

Tyler Charles Gripshover

November 8, 2023

Steatotic liver disease is brought upon by differing etiologies and its global prevalence is expected to keep increasing over the next several decades. Particularly, alcohol-associated liver disease (ALD) manifests from excessive alcohol consumption where the liver retains lipids and progresses with metabolic dysfunction. Previous studies have demonstrated that environmental pollutants, polychlorinated biphenyls (PCBs) promote metabolic dysfunction associated steatotic liver disease (MASLD), in diet-induced obesity models. However, it is unknown if environmental pollutants may also promote ALD pathogenesis. Thus, this dissertation focuses on characterizing the effects of PCB126 in a rodent ALD model followed by multiple 'Omics approaches to identify mechanisms for modified disease pathogenesis. C57BL/6J mice were orally gavaged 0.2mg/kg PCB126 or vehicle prior to the chronic-binge alcohol feeding model. Mice were then provided a 5% EtOH or control diet for ten days. The following day, mice were provided 5 g/kg EtOH bolus, prior to euthanasia and tissue collection.

PCB126 exposure significantly enhanced hepatomegaly in EtOH-fed mice as observed by increased liver weight and steatosis. Carbohydrate metabolism was disrupted wherein blood glucose and hepatic glycogen were significantly reduced. Gene expression analyses supported both endpoints by suggesting a net retention of hepatic lipids and general loss of glycolysis and gluconeogenesis functionality. Albumin levels were reduced ~50% at the transcriptional and protein level by PCB126 in EtOH-fed mice. Finally, differential aryl hydrocarbon receptor activation was observed by PCB126 exposure and EtOH feeding. RNA sequencing reveals that PCB126 uniquely alters the transcriptome in EtOH-fed mice. Significant gene ontology (GO) biological processes suggested "peptidyl tyrosine modifications" are prevalent. Western blotting revealed PCB126 further decreasing phosphorylated JAK2. Significant GO Molecular Function processes suggested metal ion binding is deficient, and metallomic analyses show decreased hepatic metals, supporting this observation. Phosphoproteomics demonstrated that phospho-peptide levels were reduced in EtOH+PCB126 mice. The phosphoproteome was globally impacted by EtOH feeding; however, PCB126 altered specific phospho-peptides. Particularly, PCB126 increased the phosphorylation of progesterone receptor membrane component 1 (PGRMC1) at serine-181 which may conformationally inhibit other phosphoacceptor residues.

Overall, the findings implicated that PCB126 promoted ALD pathogenesis and reprogramed intermediary metabolism at all macromolecule levels. Multiple 'Omics suggest that signaling is disrupted by altered protein phosphorylation and loss of essential metal levels. Future studies must consider the disease modifying effects toxicants have on ALD.

TABLE OF CONTENTS

CHAPTER I: INTRODUCTION

CHAPTER II: THE ENVIRONMENTAL POLLUTANT, POLYCHLORINATED BIPHENYL 126, ALTERS LIVER FUNCTION IN A RODENT MODEL OF ALCOHOL ASSOCIATED LIVER DISEASE

CHAPTER III: PCB126 MODIFIES THE MURINE HEPATIC TRANSCRIPTOME AND METALLOME TO PROMOTE ALCOHOL-ASSOCIATED LIVER DISEASE PATHOGENESIS

CHAPTER IV: POLYCHLORINATED BIPHENYL 126 MODIFIES THE HEPATIC PHOSPHOPROTEOME IN A RODENT ALCOHOL MODEL

CHAPTER V: MAJOR FINDINGS AND COMPREHENSIVE CONCLUSIONS

APPENDICIES

LIST OF FIGURES

CHAPTER I

INTRODUCTION

Steatotic Liver Disease

Steatotic liver disease (SLD) is a clinical state of the liver in which excess lipids are stored, and this may be accompanied by inflammation and fibrosis. SLD is thought of as a multifactorial disease where genetics, environment, diet, and/or comorbid diseases can all influence susceptibility to the development and progression of this disease. SLD exists along a pathological spectrum that often begins with steatosis which may progress with inflammation (steatohepatitis) and if not treated, can further result in tissue scarring (fibrosis/cirrhosis) and fulminant liver failure (Schlageter et al., 2014). Historically, 'simple' steatosis is thought to be a benign condition where accumulated lipids will be either catabolized or transported to adipose tissue for storage. Steatosis is the first pathological consequence in the SLD spectrum, recent research suggests that it may alter signaling and prime the liver to developing fibrosis (Adams and Ratziu, 2015; El-Zayadi, 2008). Furthermore, hepatic fibrosis is primarily a compensatory repair mechanism to acute injury where activated myofibroblasts deposit collagen (Heyens et al., 2021). With extensive injury, the rate of collagen degradation is much slower than collage deposition, resulting in a harmful accumulation

(McKleroy et al., 2013). Bridging fibrotic scars typically occurs with inflammation and activated hepatic stellate cells where collagen deposition extends from the portal triad to several central veins and between central veins (Suk and Kim, 2015). The final stage of the SLD spectrum results from severe cirrhotic scarring that may form nodules surmounting to hepatocellular carcinoma and liver failure. SLD is also largely associated with other comorbidities such as obesity, type 2 diabetes mellitus, cardiovascular diseases, and metabolic syndrome (Glass et al., 2019). The initiating disease may rather be one of these comorbidities, where SLD develops alongside with, for example, obesity. Indeed, a relationship exists between these progressive diseases where some individuals progress more rapidly than others and have risk factors for other cardiometabolic diseases.

While this pathological spectrum has been extensively studied, etiological differences have been identified to help characterize the onset of SLD. For instance, cases of Metabolic Dysfunction Associated Steatotic Liver Disease (MASLD) have been attributed to excess diet or poor nutritional caloric intake that may be comorbid with other cardiometabolic diseases (Rosato et al., 2019). MASLD is the most common chronic liver disease in developed countries affecting roughly 25% of adults in the United States and has a global prevalence estimated at 24% (Glass et al., 2019; Younossi et al., 2018). In contrast, alcohol-associated liver disease (ALD), which also manifests through the SLD spectrum, is caused by excessive alcohol consumption (Crabb et al., 2020). Recently, a third subtype of SLD has been characterized which is known as toxicant-associated steatotic liver disease or steatohepatitis (TASLD/TASH) (Wahlang et al., 2013a; Cave et al.,

2010). This disease can be established after significant toxicant or pollutant exposure and has demonstrated to enhance dyslipidemia and inflammation in diet-induced obesity models (Cave et al., 2010; Cave et al., 2011; Wahlang et al., 2013b).

Often in clinical ALD cases, nutritional calorie intake may be in a deficit of protein and essential micronutrients that are vital to maintaining health (McClain et al., 2011). These deficits usually are associated with more poor liver disease prognosis and increased severity. The malnutrition aspect of ALD may be due to the replacement of nutritional macromolecules and micronutrients with those, albeit limited, found in alcoholic beverages. Excessive alcohol consumption results in satiety and therefore less consumption of nutritional food; importantly, it also disrupts intermediary metabolism and limits absorption of critical nutrition. Alcohol, chiefly ethanol (EtOH), is primarily metabolized in the liver where alcohol dehydrogenase (ADH) and cytochrome P450 2E1 (CYP2E1) convert it to toxic intermediate, acetaldehyde. Acetaldehyde is directly toxic, carcinogenic, and is largely responsible for the toxicological effects observed in humans and model systems. It should also be noted that CYP2E1 also generates a wealth of reactive oxygen species (ROS), which contributes to disease development. Acetaldehyde is then converted to acetate which can be used in homeostatic metabolism processes (Seitz et al., 2018). A myriad of mechanisms have been proposed relating to alcohol's negative effects including: downregulation of fatty acid β-oxidation, increased fatty acid synthesis, dysregulated hormone and adipokine

function, and proinflammatory cytokine induction (Seitz et al., 2018; Mandrekar and Szabo, 2009).

The economic burden of chronic liver diseases is immense and is expected to keep increasing with increasing obesity and metabolic syndrome rates. Inpatient liver disease hospitalizations in the United States between 2012 and 2016 increased from $14.9 billion to $18.8 billion. Overall, national inpatient hospitalization costs for those with chronic liver diseases are estimated over $80 billion (Hirode et al., 2020b). With the prevalence of MASLD and other chronic liver diseases expected to increase for the foreseeable future, hospitalizations and economic costs will likely follow (Le et al., 2022; Hirode et al., 2020a). While MASLD accounts for approximately 59% of chronic liver diseases and ALD accounts for approximately 2%, this is nonetheless an emerging epidemic (Cheemerla and Balakrishnan, 2021). To further this issue's complexity, SLD may manifest and progress at different rates from patient to patient. For example, only about 10-30% of people progress from simple, bland steatosis to metabolic dysfunction-associated steatohepatitis (MASH), and only about 25-40% of people with MASH will develop fibrotic scarring (Dyson et al., 2014). Besides individual genetic predisposition differences, there must be external, modifying factors that account for why some individuals progress more rapidly along this pathological spectrum.

Persistent Organic Pollutants

Persistent organic pollutants (POPs), also known as "forever chemicals" are global pollutants. This is primarily due to their long biological half-lives and resistance to

degradation, either by physical, chemical, and enzymatic means. The historic Stockholm Convention initially began with twelve hazardous compounds that fit this description. Today, over thirty compounds have been recognized and over 150 countries have ratified its legislation to ban or limit the use of various POPs. Some of the original notorious "dirty dozen" POPs recognized include chlordane, dichlorodiphenyltrichloroethane (DDT), and polychlorinated biphenyls (PCBs). Newly added POPs include some perfluorinated compounds (PFCs), lindane, and short-chain chlorinated paraffins (SCCPs). Unfortunately, due to improper waste disposal and POP's chemical nature, these pollutants are still being detected in the environment and in human tissues. While total levels are trending down, these chemicals tend to recirculate in the environment and bioaccumulate in the food chain (Wong et al., 2021; Montone et al., 2023).

One prominent class of POPs of interest to our group are PCBs. PCBs are environmental toxicants that were manufactured by Monsanto Corporation in the United States from the 1930's until their subsequent ban in the late 1970's (Markowitz and Rosner, 2018). Based on the chlorine atom substitution on the biphenyl ring, there are up to 209 PCB congeners; many of these congeners were produced and sold as mixtures under the trade name 'Aroclor' (Clair et al., 2018). These compounds are generally categorized by their molecular geometry as either coplanar or non-coplanar and based on the number of chlorine atoms around the biphenyl ring (Jin et al., 2020). Additionally, PCBs are further classified as dioxin-like or non-dioxin-like PCBs, based on their similarity to 2,3,7,8-tetrachlorodibenzo-p-dioxin (TCDD) toxic physiological consequences (Safe et al.,

1985). These chemicals were commercially used for electrical equipment, motor oil, insulators, plastics, and adhesives (EPA, 2022). The primary route of human exposure to PCBs are through ingestion of contaminated foods, particularly meat, and water followed by inhalation and dermal exposures (Carpenter, 2006). Epidemiology and experimental animal models have demonstrated that exposure to PCBs is associated with liver injury, steatohepatitis, and obesity (Cave et al., 2022; Clair et al., 2018; Deng et al., 2019). A recognized key molecular initiating event in PCB toxicity lies in the activation of the aryl hydrocarbon receptor (AhR), by dioxin-like PCBs, or the activation of the constitutive androstane receptor (CAR) and pregnane x receptor (PXR), by non-dioxin-like PCBs (Jin et al., 2020; Wahlang et al., 2021).

Significance of Study

Previously, our group has demonstrated that MASLD models paired with PCB exposures promotes, and often, exacerbates liver disease and metabolic disruption (Wahlang et al., 2013a; Wahlang et al., 2013b; Hardesty et al., 2019b; Al-Eryani et al., 2015). To date, there are few reports that study the complex interaction of environmental chemical exposure and alcohol consumption in ALD development. We postulate that a complex interaction occurs between environmental toxicants and ethanol to enhance toxicity that may be dependent on dose, duration, sequence of exposure, sex, and other factors. This theory resides in the fact that the liver is a primary target of xenobiotic toxicity where both alcohol and PCBs have demonstrated negative health outcomes. Currently, there is limited

knowledge on how environmental pollutant exposures may enhance hepatic disease induced by alcohol consumption. It is becoming increasingly apparent that lifestyle factors coupled with chemical exposure may impact not only hepatic health and function, but also contribute to worsening disease prognosis (Al-Dayyat et al., 2018; Bailey et al., 2009; Nivukoski et al., 2020; Wahlang et al., 2019a).

Objective and Hypothesis

The objective of the current study is to develop and characterize a novel alcohol-plus-toxicant model to understand how environmental pollutants (PCB126) may enhance the lifestyle related disease, ALD. Furthermore, we aim to take a high throughput 'Omics approach to explore how the hepatic transcriptome, metallome, and phosphoproteome are impacted to influence metabolism and promote liver disease. With respect to our 'Omics approaches, our goal is to employ these data to suggest possible mechanisms that play, in part, to enhanced metabolism dysfunction and liver disease.

We hypothesize that PCB126 will promote ALD pathogenesis by enhancing dyslipidemia and altering intermediary metabolism resulting in compromised liver function. Additionally, our 'Omics approaches will be utilized to suggest potential mechanisms as to how PCB126 alters the transcriptome, metallome, and phosphoproteome in alcohol fed mice exposed to PCB126 in relation to disrupted hepatic signaling.

CHAPTER II

THE ENVIRONMENTAL POLLUTANT, POLYCHLORINATED BIPHENYL 126,
ALTERS LIVER FUNCTION IN A RODENT MODEL OF ALCOHOL
ASSOCIATED LIVER DISEASE

Introduction

ALD is a subtype of SLD that etiologically stems from excessive alcohol

consumption. ALD is progressive in that it persists with excessive alcohol intake

until the disease reaches an irreversible pathological state, such as cirrhosis. This

disease is characterized by hepatic steatosis, disrupted energy metabolism,

oxidative stress, and leaky gut (Louvet and Mathurin, 2015). Death from excessive

alcohol use and ALD is also one of the most common forms of preventable deaths

in the United States (Axley et al., 2019; Witkiewitz et al., 2019). According to the

World Health Organization (WHO), alcohol-related deaths accumulated to 5.3% of

all global deaths in 2016 (WHO, 2018). Studying human ALD in model systems

have been challenging as humans typically exhibit various drinking patterns such

as acute-, chronic-, binge-, and chronic-binge drinking. Additionally, the volume of

alcohol consumed over time may vary between individuals, but generally positively

correlates with disease severity (Ghosh Dastidar et al., 2018). Unlike the human

onset of ALD, *in vivo* models attempt to recapitulate this disease, but often require

a second 'hit' like high fat content in diet or lipopolysaccharide administration

(Ghosh Dastidar et al., 2018; Brandon-Warner et al., 2012).

An emerging concept in alcohol research is that tobacco smoke may enhance liver injury as alcohol and tobacco are often abused together. Several studies suggest that whole tobacco smoke and nicotine exposures are associated with increased serum triglycerides, hepatic steatosis, ROS production, and collagen deposition (Bailey et al., 2009; Lu et al., 2013; Chen et al., 2018). This may have first been indicated in earlier human epidemiology studies where increased cigarette smoking rates was associated with higher alcohol-associated cirrhosis risk (Klatsky and Armstrong, 1992). Recently, our group has shown that chemical exposures can enhance diet-induced obesity models (Wahlang et al., 2013b; Shi et al., 2019b; Jin et al., 2020). It is however not understood if environmental toxicants may promote ALD in a similar fashion as they have demonstrated to in MASLD models.

Previously, PCBs have demonstrated to cause a wide range of adverse health effects across the body including metabolism disruption, cardiovascular, and importantly, liver toxicity (Hardesty et al., 2018; Mesnage et al., 2018; Petriello et al., 2018). One PCB congener, 3,3',4,4',5-Pentachlorobiphenyl (PCB126) is a dioxin-like, coplanar PCB that has also demonstrated carcinogenesis and organ toxicity (IARC, 2016). Previous toxicological studies have also shown PCB126's ability to enhance diet-induced metabolic dysfunction-associated steatohepatitis (MASH) and cardiometabolic disease (Deng et al., 2019; Petriello et al., 2016; Wahlang et al., 2017). Importantly, PCB126 is a metabolism disrupting chemical (MDC) and potent aryl hydrocarbon receptor activator, and studies have demonstrated that AhR activation is likely a primary driver of toxicity and

metabolism disruption (Shi et al., 2019a; Shi et al., 2019b; Wang et al., 2019; Zhang et al., 2012b; Heindel et al., 2017). While some PCBs are considered obesogens, dioxin-like PCBs at high doses, can cause wasting syndrome like lipodystrophy, causing redistribution of lipids from adipose stores to accumulate in the liver. We suspect that PCB126 exposure in conjunction with alcohol feeding will result in enhanced liver steatosis and further disrupt metabolism to hinder liver functionality. The purpose of this study is to develop and characterize a model to investigate how PCB126 may promote dyslipidemia and hepatomegaly in an alcohol feeding model. We aim to assess hepatic steatosis, measures of lipid and carbohydrate metabolism, and albumin levels as a surrogate marker of liver function. This study was originally published by Wiley in the journal of Alcohol: Clinical and Experimental Research (Gripshover et al., 2022).

Materials and Methods

Animals, Diets, and Chemical use

The University of Louisville Institutional Animal Care and Use Committee (IACUC) approved animal use protocols and procedures. Sixty, ten-week-old male C57BL/6J mice were purchased from Jackson Laboratory (strain#: 000664; Bar Harbor, Maine). Five mice per cage were housed in a pathogen-free, temperature controlled (23.9°C) room with a twelve-hour light-dark cycle that is accredited by the Association for Assessment and Accreditation of Laboratory Animal Care (AAALAC). Mice were allowed to acclimate from facility transfer for one week and fed autoclaved laboratory rodent chow diet containing 28.7%, 13.1%, and 58.2% kcal/g of protein, fat, and carbohydrates, respectively (5010; LabDiet, St. Louis,

Missouri) and had ad libitum access to food and water. 3,3',4,4',5-Pentachlorobiphenyl (PCB126) was purchased from AccuStandard (catalog: C-126N-5MG; New Haven, CT). Corn oil vehicle was purchased from Sigma Aldrich (catalog: C8267-500ML). Lieber-DeCarli '82 Shake and Pour ethanol (catalog: F1258SP) and control (catalog: F1259SP) diets were purchased from Bio-Serv (Flemington, NJ). Caloric profile of the ethanol diet contains 355, 135, 359, and 151 kcal/L of ethanol, carbohydrates, fat, and protein, respectively. Caloric profile of the control diet contains 490, 359, and 151 kcal/L of carbohydrates, fat, and protein, respectively. 50 mL glass feeding tubes (catalog: 9019) were employed to facilitate isocaloric ethanol and control diet feeding within rodent cages and were also purchased from Bio-Serv (Flemington, NJ).

Study and Exposure Paradigm

The commonly used chronic-binge (ten-plus-one) rodent alcohol model was employed as a foundational model for the duration of study (Bertola et al., 2013). Rodent cages were divided into four groups: pair-fed+Veh., pair-fed+PCB126, ethanol + vehicle, and ethanol + PCB126. Mice were orally gavaged with either corn oil vehicle or 0.2 mg/kg rodent body weight of PCB126 four days prior to ramp-up ethanol feeding. This dose was selected as a median exposure level based on doses that our research group had previously used to elicit toxicological hepatic effects (Jin et al., 2021; Shi et al., 2019b; Shi et al., 2019a). Two, 50 mL feeding tubes were placed in each rodent cage during ethanol- or pair-feeding. Over the course of five days, ethanol-fed mice were provided the diet in increasing

concentrations of ethanol to acclimate them to the liquid feeding. Pair-fed mice were fed an isocaloric diet where ethanol was substituted with maltose dextrin and fed as described in Bertola et al. (Bertola et al., 2013). Ethanol-fed mice were then maintained on 5.0% ethanol diet for ten days. On the day of the binge, ethanol-fed mice were removed from the housing room at ZT 22 and brought to the euthanasia and tissue collection room. Mice were then administered 5 g/kg ethanol binge beginning at ZT 23 approximately every 8 minutes. Pair-fed mice were orally gavaged nano-pure water instead of the established maltose dextrin binge to avoid carbohydrate intake differences between the two dietary groups. It has previously been shown that maltose dextrin may cause distinct metabolic abnormalities between experimental groups (Soto et al., 2017). Thus, we wanted to control for these differences as ethanol is broken down into acetate and maltose dextrin is broken down into various saccharide molecules. Euthanasia and tissue collection started approximately at ZT 3. The chronic-binge model (Bertola et al., 2013) recommends nine hours post binge for tissue harvest; however, several mice (n=7) in the ethanol + vehicle group experienced premature mortality three hours post binge. To avoid quantitative differences in data within this group, the remaining experimental and control animals were euthanized at a similar time point which was equivalent to approximately three hours post binge. We have reviewed and accounted for the premature mortality in our statistical analysis and no differences between groups were observed. Besides the premature mortality experienced three hours post-binge, one mouse experienced mortality one day prior to planned euthanasia. Body weights were recorded daily during ramp-up ethanol feeding (0%

- 4%) and 5% ethanol feeding. Blood collection from the inferior vena cava was performed followed by euthanasia *via* exsanguination and tissue collection.

Liver Histology

Liver tissues were fixed in 10% neutral buffered formalin for at least 48 hours and then placed in 75% ethanol until tissue processing and paraffin embedding. Tissues were sectioned at 5 μm with Leica Biosystem's Histocore Autocut Automated Rotary Microtome (Leica Biosystem; Deer Park, IL). Tissue sections were stained with hematoxylin (catalog: FS72804; Epredia; Kalamazoo, MI) and eosin (catalog: HT110316-500ML; Sigma Aldrich; St. Louis, MO) (H&E) to assess hepatic morphology. Liver sections were also stained with Naphthol AS-D Chloroacetate-specific esterase purchased from Sigma Aldrich to assess granulocytic leukocyte infiltrates (catalog:91c-1kt; St. Louis, MO). Images were captured using an Aperio GT 450 – Automated, high-capacity pathology slide scanner (Leica Biosystems; Deer Park, IL). H&E and CAE images were captured on Aperio ImageScope software at 10 and 20X magnification, respectively (v12.4.3.5008) (Leica Biosystems Pathology Imaging; Deer Park, IL). CAE scoring was performed where total granulocytes were counted in ten 20X fields of view for five animals per group. Finally, liver sections were also stained according to manufacturer protocol with periodic acid (catalog: P7875-25g) and Schiff reagent (catalog: 3952016-500mL) to determine glycogen content (Sigma Aldrich; St. Louis, MO). All histological staining was performed according to manufacturer's protocol. PAS images were captured at 10X using an Olympus BX43 microscope,

DP74 digital camera, and CellSens software package (Olympus America, Breinigsville, PA, USA). Quantification for positively stained Periodic Acid Schiff (PAS) regions was performed using ImageJ (v1.53k) software (National Institute of Health; Bethesda, MD). To quantify glycogen content, we analyzed up to seven fields of view of all hepatic sections at 10X magnification and percent area was averaged respective to grouping. Finally, Terminal deoxynucleotidyl transferase dUTP nick end labeling (TUNEL) staining was performed to detect hepatocytes undergoing apoptosis. TUNEL staining was accomplished using Apoptag Peroxidase In Situ Apoptosis Detection kit from Sigma Aldrich (catalog: S7100; St. Louis, MO). TUNEL staining was performed according to manufacturer's protocol and up to ten fields of view for each animal at 20X magnification were used to quantify the relative abundance of apoptotic cells. TUNEL positive cell counts were normalized by dividing the number of TUNEL positive cells by the number of fields of view.

Blood Chemistry Analysis

Liver enzymes, triglycerides, glucose, cholesterol, and lipoproteins (HDL, LDL, VLDL) were measured with Lipid Panel Plus diskettes (catalog:400-0030; Abaxis Inc.; Union City, CA) on the Piccolo Xpress Chemistry Analyzer (Abbott; Abbott Park, IL). Plasma adipokines were measured with the Milliplex Map Mouse Adipokine Magnetic Bead Panels (catalog: MADKMAG-71K; EMD Millipore) on a Luminex® 100 system (Luminex Corp.; Austin, TX). Adipokines measured included Insulin, PAI-1, Resistin, and Leptin. Analysis for each assessment was

performed according to the manufacturer's protocol. Plasma albumin levels were measured *via* ELISA from MyBioSource Inc. and performed according to the manufacturer's standard protocol (catalog: MBS564063; San Diego, CA).

Hepatic Triglyceride and Cholesterol Measurement

Hepatic triglycerides and cholesterol were extracted based on the Bligh and Dyer method utilizing a 2:1 chloroform:methanol solution (Bligh and Dyer, 1959). Triglyceride and cholesterol standards were used to generate a standard curve to quantify extracted lipids (catalog: T7531-STD, C7509-STD; Point Scientific; Canton, MI). Extracted lipids were colorimetrically measured with a microplate absorbance reader (BioTek Gen 5; Winsooki, VT).

RT-PCR Analysis

Liver tissues were processed and homogenized in RNA-STAT60, and total RNA was extracted (catalog: CS-502; Tel-test Inc.; Friendswood, TX). RNA quantity and purity was assessed with a Nanodrop OneC spectrometer purchased from ThermoFisher Scientific (catalog: 701-058112; Madison, MI). cDNA was reverse transcribed from 3 µg RNA to yield 60 µl of cDNA using single step cDNA synthesis reagent, QScript (catalog: 95048-500; Quantabio; Beverly, MA). RT-PCR was performed on a CFX384™ Real-Time System (Bio-Rad; Hercules, CA). iTaq Universal Probe Supermix from Bio-Rad was used during RT-PCR set up (catalog: 1725134; Hercules, CA). Relative mRNA expression was calculated based on the 2-ΔΔCt method with Glyceraldehyde-3-Phosphate Dehydrogenase (*Gapdh*) as the

housekeeping gene (catalog: 4351309; Applied Biosystems; Waltham, MA). Fold induction was calculated and normalized to the control group, pair-fed+Veh., which was set to 1. All genes of interest (TaqMan probes) were purchased from ThermoFisher Scientific and are cataloged in Supporting Table S1.

Statistical Analysis

Statistical significance was based on two-way analysis of variance where our two factors were diet (pair-fed v. ethanol-fed) and exposure (vehicle v. PCB126) using GraphPad Prism (v9.2) for Windows unless otherwise noted (GraphPad Software Inc.; La Jolla, CA). Alpha level of 0.05 ($P \leq 0.05$) was used to determine significance. Tukey's post-hoc test was used to compare individual groups for multiple comparison analyses. A P-value table is supplemented with all figures which displays the two-way ANOVA and Tukey's multiple comparisons results to designate significance between our groups. Repeated measures ANOVA test with generalized linear models were used to analyze body weight changes over study days (within-subjects) or irrespective of study days (between-subjects) using SAS (v9.4). Repeated measures ANOVA results are listed in Supporting Tables S2 and S3 for an alpha level set to 0.05.

Results

Ethanol and PCB126 alter Organ and Body Composition

Diet consumption was recorded daily, and a pair-feeding figure is provided in Supporting Figure S1. No major diet intake differences were observed between

dietary groups or due to PCB126 exposure. Initial characterization of the mouse phenotype post PCB126 exposure and ethanol feeding was performed using anthropometric measurements (Figure 1.1). Animal body weight changes were evaluated because the body weight of ethanol-fed mice may initially change during acclimatization to the ethanol diet then stabilize for the duration of the study. Body weight changes were stable in the present study during ethanol acclimatization and feeding, irrespective of PCB126 exposure (Figure 1.1A). A repeated measures ANOVA (RM-ANOVA) was performed to test animal body weight changes over time and if weight changes were an effect due to dietary feeding, exposure, or the combination of feeding and exposure and are listed in Supporting Tables S2 and S3. It was observed that there was a change in mean weight over time (within-subjects) dependent on day, dietary feeding, PCB126 exposure, and combination of day, diet, and PCB126. We also analyzed body weight changes in respect to between-subjects (ignoring time effects) and observed no significant differences between pair-fed v EtOH-fed, vehicle v PCB126, or interacting diet and exposure. Our cumulative results indicate that body weight changes are dependent on time as a factor of day, exposure, and/or diet and not solely due to the feeding or exposure paradigm. Liver-to-body weight ratio was significantly increased due to PCB126 exposure in pair-fed mice (P=0.0004). Ethanol feeding alone significantly increased liver-to-body weight ratio, which was further enhanced in the ethanol + PCB126 group to account for ~6% of body weight (Figure 1.1B). Quantified hepatic triglycerides were significantly increased due to ethanol feeding (P<0.0001) and PCB126 exposure (P<0.0001) (Figure 1.1C). Importantly, hepatic triglycerides

17

were further increased in the ethanol + PCB126 group (74.5 ± 11.5 mg/g liver

weight), which is ~1.4-fold higher than the ethanol + vehicle group (53.1 ± 9.1 mg/g

liver weight) (Figure 1.1C). Furthermore, PCB126 exposure led to decreased white

adipose-to-body weight ratios by approximately 20% in both feeding groups

(Figure 1.1D).

Outcome	EtOH	PCB 126	Interaction	Pair-fed (Veh. vs. PCB 126)	EtOH-fed (Veh. vs. PCB 126)	Veh. (Pair-fed vs. EtOH-fed)	PCB 126 (Pair-fed vs. EtOH-fed)
Liver Weight	<0.0001	<0.0001	0.0122	0.0004	<0.0001	<0.0001	<0.0001
Hepatic TGs	<0.0001	<0.0001	0.0005	n.s.	<0.0001	0.0063	<0.0001
WAT Weight	0.0171	0.0052	n.s.	n.s.	n.s.	n.s.	n.s.
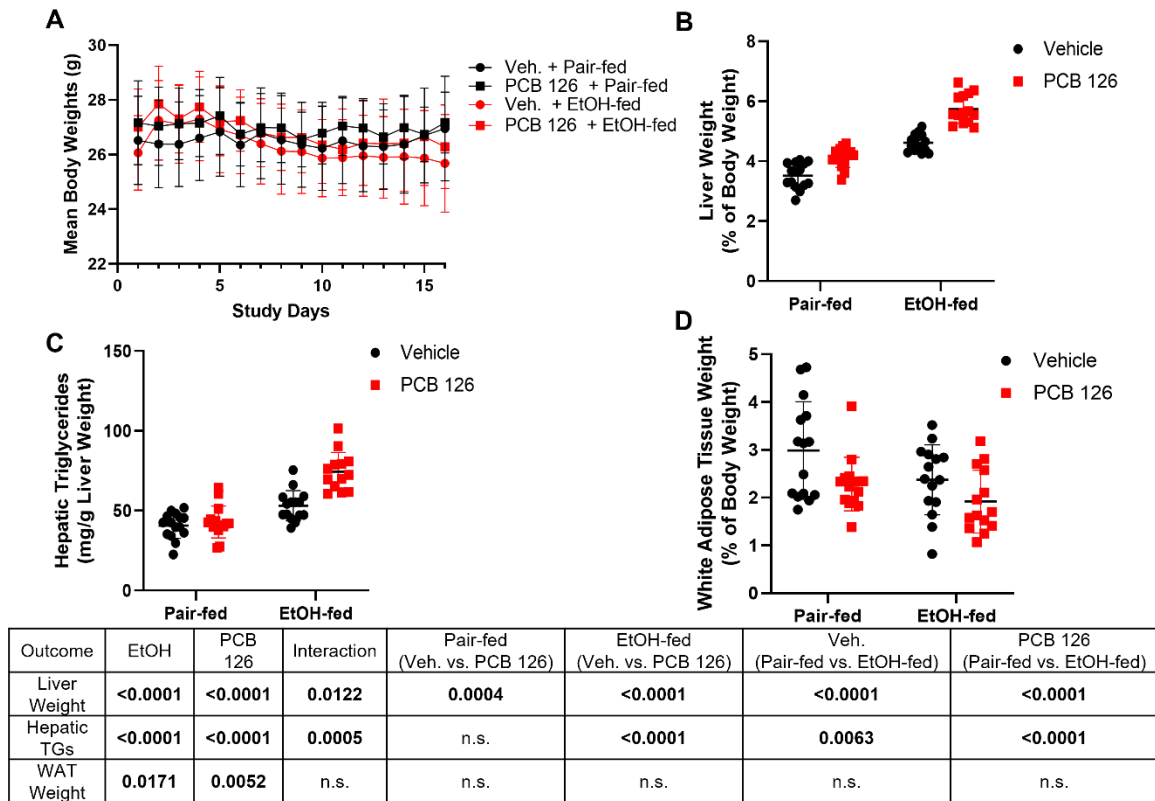
Figure 1.1. Polychlorinated biphenyl 126 and EtOH effects on body composition and hepatic triglycerides. (**A**) Body weights were recorded daily during acclimatization to the alcohol diet and the duration of study. (**B**) After extracting the gallbladder, whole liver weight was recorded. Relative liver weight was calculated based on body weight giving a relative percent of liver to body weight. (**C**) Hepatic triglycerides were isolated from liver tissue and were quantified using a colorimetric assay. (**D**) After isolating the white adipose tissue, it was weighed, and relative white adipose weight was calculated based on body weight to provide a relative percent of white adipose to body weight. Values are represented as mean ± SD with an alpha level set to 0.05. A complete list of P-values, as determined by two-

way ANOVA and Tukey's post-hoc test, is provided in the accompanying table.

EtOH, ethanol; Veh., vehicle; TGs, triglycerides; WAT, white adipose tissue.

PCB126 exacerbated Ethanol-induced Steatosis

Histological staining (H&E) of liver sections demonstrated mild lipid accumulation due to PCB126 exposure in the pair-fed group, while all ethanol-fed mice developed varying degree of steatosis (Figure 1.2A). Importantly, the ethanol + PCB126 group displayed greater lipid droplet formation (steatosis) relative to the ethanol + vehicle group based on masked, qualitative review of all histological images (Figure 1.2A). These results provide evidence for increased lipid accumulation in the liver, indicating developing steatosis.
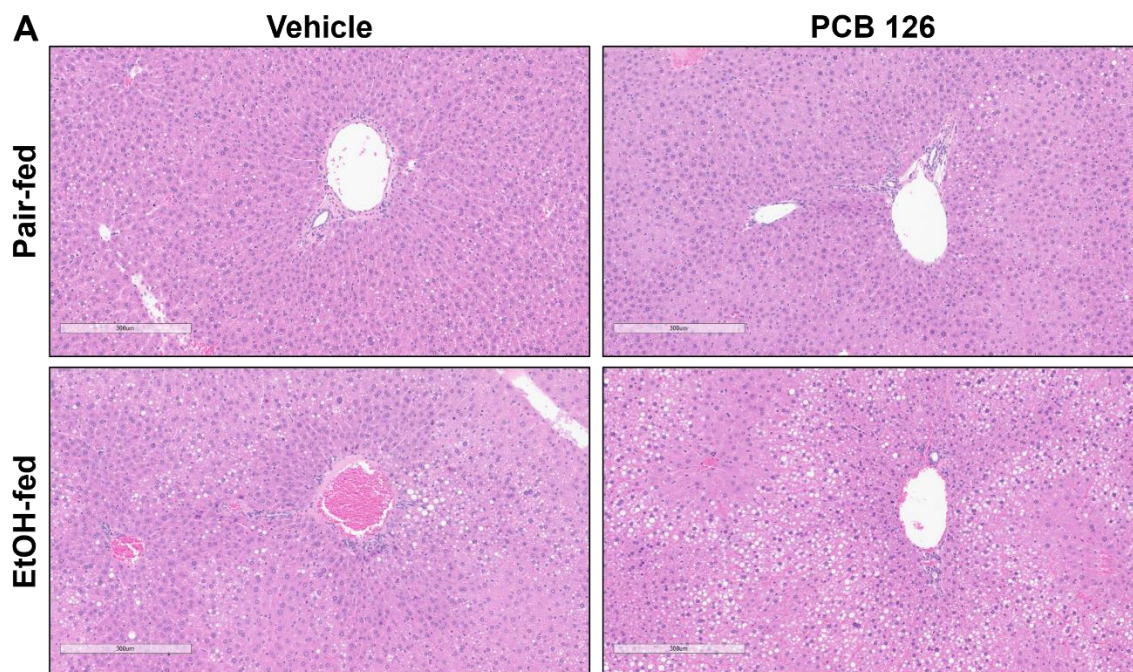
Figure 1.2. Polychlorinated biphenyl 126 and EtOH effects on liver morphology. (**A**) 5μm thin liver sections were analyzed using H&E staining to assess liver morphology and the presence of lipid droplet accumulation. Images were captured at 10X magnification. EtOH, ethanol.

Histological analysis of liver sections by CAE staining indicated granulocyte infiltration responding to stress in the experimental groups (Figure 1.3A). All ethanol-fed mice had varying degrees of positively stained granulocytes in liver tissue. CAE scoring revealed ~2.2-fold increase in granulocytes due to ethanol feeding (Figure 1.3B). Alanine aminotransferase (ALT) and aspartate aminotransferase (AST) levels were not significantly different, likely due to the discussed study limitations and are listed in Supporting Figure S2. Additionally, cytokines/chemokines involved in inflammation and granulocyte trafficking namely tumor necrosis factor-alpha (*Tnfα*), C-X-C Motif Chemokine Ligand 2 (*Cxcl2*), and C-C Motif Chemokine Ligand 2 (*Ccl2*) were examined. However, there were no differences in gene expression for *Cxcl2*, and only a mildly significant increase of expression for *Ccl2* due to ethanol feeding (Supporting Figure S2). *Tnfα* gene expression was increased in mice exposed to PCB126; however, its expression was contradictorily decreased with ethanol feeding (Supporting Figure S2). TUNEL positive cells were counted to be relatively two times higher in ethanol fed mice than pair-fed controls, indicating increased hepatocellular apoptosis (Supporting Figure S3). Markers of endoplasm reticulum (ER) stress and apoptosis were also evaluated by gene expressional changes (Supporting Figure S3). DNA Damage Inducible Transcript 3 (*Chop*) is a gene activated in response to ER stress to induce apoptosis was observed to be increased by ethanol feeding and PCB126 exposure (Supporting Figure S3). Analysis of *Chop* mRNA levels also indicate an interaction effect where the combination of ethanol feeding and PCB126 exposure

increased its abundance up to ~13-fold. Activating Transcription Factor 3 and 4 (*Atf3*, *Atf4*) expression were also evaluated for their role in cellular and ER stress and are listed in Supporting Figure S3. *Atf3* expression was significantly increased by ethanol feeding and PCB126 exposure and robustly increased ~46-fold due to interacting ethanol and PCB126 exposure. *Atf4* mRNA levels were significantly increased due to ethanol feeding but, interestingly, relative mRNA levels were slightly mitigated in the ethanol + PCB126 group.

Outcome	EtOH	PCB 126	Interaction	Pair-fed (Veh. vs. PCB 126)	EtOH-fed (Veh. vs. PCB 126)	Veh. (Pair-fed vs. EtOH-fed)	PCB 126 (Pair-fed vs. EtOH-fed)
CAE Scoring	0.0053	n.s.	n.s.	n.s.	n.s.	n.s.	0.0366
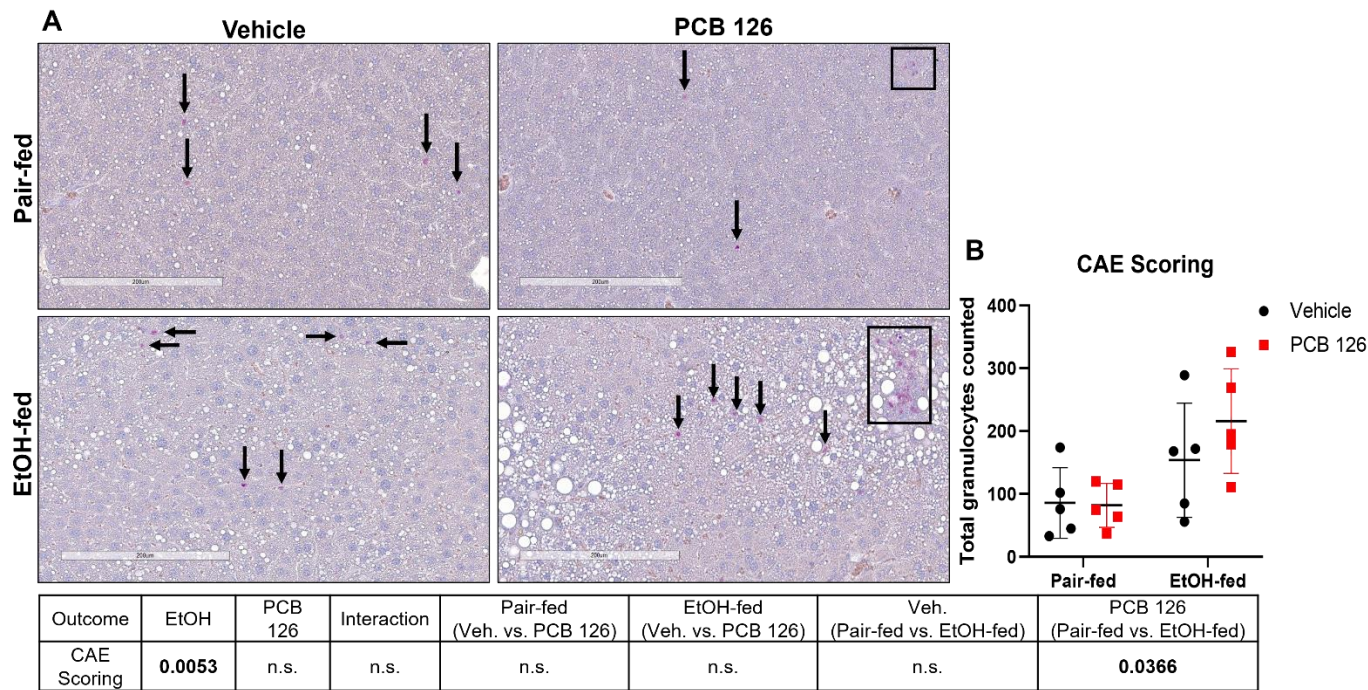
Figure 1.3. Polychlorinated biphenyl 126 and EtOH effects on hepatic inflammation and injury. (**A**) 5µm thin liver sections were analyzed using CAE staining to detect the presence of granulocyte infiltration. (**B**) Total granulocytes were counted in 10 fields of view at 20X magnification for five animals per group. Counted granulocytes were then graphed in the accompanied scatterplot and statistical analysis was performed. Values are represented as mean ± SD with an alpha level set to 0.05. A complete list of P-values, as determined by

two-way ANOVA and Tukey's post-hoc test, is provided in the accompanying table. EtOH, ethanol; Veh.,

vehicle; CAE, chloroacetate esterase.

PCB126 and Ethanol alter Plasma Lipids, Adipokines, Glucose, Insulin, and Albumin

Evaluating the abundance of plasma lipids, adipokines, glucose, insulin, and albumin are important to assess the extent of altered liver function imposed by ethanol feeding or PCB126 exposure and are listed in Table 1.1. Plasma triglycerides were overall significantly increased ~1.7-fold in the ethanol-fed groups compared to pair-fed groups. Interestingly, the ethanol + PCB126 group (42.6 ± 9.8 mg/dL) showed attenuation of plasma triglyceride levels compared to the ethanol-fed group but were still significantly elevated relative to the pair-fed+PCB126 group (26.8 ± 1.9 mg/dL). Plasma cholesterol, high density lipoprotein (HDL), and low density lipoprotein (LDL) were significantly decreased upon PCB126 exposure in pair-fed mice and upon ethanol feeding in the ethanol + vehicle group. Plasma cholesterol, HDL, and LDL were decreased in the ethanol + PCB126 but were not statistically significant. Plasma very low density lipoprotein (VLDL) was significantly elevated in the ethanol-fed mice, but VLDL levels were attenuated in the ethanol + PCB126 group (8.5 ± 2.0 mg/dL), although still significantly higher than pair-fed mice (5.3 ± 0.5 mg/dL). PCB126 exposure significantly decreased Leptin and Resistin levels; however, ethanol only increased Leptin values which were then mitigated in the ethanol + PCB126 group. Plasma levels of plasminogen activating inhibitor 1 (PAI-1) were significantly elevated in the ethanol-fed mice but were not different when accounting for PCB126 exposure, indicating that ethanol feeding may be the dominate driver of this injury marker. Glucose was found to be significantly decreased due to PCB126

and ethanol feeding; notably, there was an interaction in the ethanol + PCB126 group where plasma glucose levels were further decreased by about 22%. Insulin on the other hand, was significantly increased due to ethanol feeding but levels were mitigated due to PCB126 exposure (197.9 ± 68.3 pg/mL) which is concordant with our previous observations in rodent and human epidemiological studies (Clair et al., 2018; Wahlang et al., 2014b; Wahlang et al., 2014a). Plasma albumin was significantly decreased by ethanol feeding and PCB126 exposure. Importantly, the mean albumin concentration in the pair-fed+Veh. group was decreased ~50% from 2.75 g/dL to 1.36 g/dL in the ethanol + PCB126 group.

Table 1.1. Plasma lipids, adipokines, glucose, insulin, and albumin.

Analyte	Pair-Fed		EtOH-Fed	
	Vehicle	PCB126	Vehicle	PCB126
Triglycerides (mg/dL)	32.5 ± 5.7	26.8 ± 1.9	68.7 ± 24.3	42.6 ± 9.8
CHOL (mg/dL)	73.8 ± 15.3	51.9 ± 6.4	56.7 ± 12.5	44.1 ± 8.6
HDL (mg/dL)	56.4 ± 13.3	42.0 ± 3.3	42.2 ± 12.5	31.7 ± 8.3
LDL (mg/dL)	11.0 ± 4.4	6.25 ± 1.7	4.3 ± 1.7	4.8 ± 3.3
VLDL (mg/dL)	6.6 ± 1.2	5.3 ± 0.5	12.2 ± 3.6	8.5 ± 2.0
Leptin (pg/mL)	4350.5 ± 3957.9	1014.7 ± 647.3	6695.9 ± 3769.0	4104.4 ± 2769.5
Resistin (pg/mL)	1296.6 ± 319.5	909.1 ± 318.7	1236.9 ± 447.8	1129.4 ± 337.3
PAI-1 (pg/mL)	1276.1 ± 554.1	1708.8 ± 609.1	2712.8 ± 1056.9	3332.8 ± 1464.4
Glucose (mg/dL)	241.7 ± 59.5	154.2 ± 47.0	123.7 ± 46.3	96.8 ± 26.9
Insulin (pg/mL)	139.3 ± 54.1	108.2 ± 29.9	376.8 ± 172.1	197.9 ± 68.3

Outcome	EtOH	PCB 126	Interaction	Pair-fed (Veh. vs. PCB126)	EtOH-fed (Veh. vs. PCB126)	Veh. (Pair-fed vs. EtOH-fed)	PCB126 (Pair-fed vs. EtOH-fed)
TGs	<0.0001	<0.0001	0.0064	n.s.	0.0001	<0.0001	0.0051
CHOL	0.0012	<0.0001	n.s.	<0.0001	n.s.	0.0207	n.s.
HDL	0.0006	0.0005	n.s.	0.0056	n.s.	0.0363	n.s.
LDL	0.0038	n.s.	n.s.	0.0068	n.s.	0.0225	n.s.
VLDL	<0.0001	0.0002	0.0483	n.s.	0.0016	<0.0001	0.0007
Leptin	0.0044	0.0021	n.s.	0.0333	n.s.	n.s.	n.s.
Resistin	n.s.	0.0190	n.s.	0.0259	n.s.	n.s.	n.s.
PAI-1	<0.0001	n.s.	n.s.	n.s.	n.s.	0.0129	0.0009
Glucose	<0.0001	0.0004	0.0471	<0.0001	n.s.	<0.0001	0.0139
Insulin	<0.0001	0.0001	0.0046	n.s.	0.0001	<0.0001	0.0367

Values are described as mean ± SD for an alpha level of 0.05. A complete list of P-values, as determined by two-way ANOVA and Tukey's post-hoc test, is provided in the accompanying table. EtOH, ethanol; Veh., vehicle; TGs, triglycerides; CHOL, cholesterol.

First, we wanted to briefly evaluate how our exposure paradigm altered albumin's expression, which its related protein is vital to whole organism homeostasis and macromolecule transport. Albumin (*Alb*) gene expression was decreased by ethanol feeding and PCB126 exposure and ~50% in the ethanol + PCB126 group (Figure 1.4A). Transporter genes were first examined in our array of lipid-related genes important to this characterization study. The expression of *Cd36*, fatty acid translocase, was upregulated due to PCB126 exposure and ethanol feeding which was further increased in the ethanol + PCB126 group about 6-fold (Figure 1.4B). The expression of hepatic fatty acid binding protein, *Fabp1*, a cytoplasmic lipid chaperone protein, was downregulated 5-fold due to ethanol feeding (Figure 1.4C). Further, genes involved in lipid synthesis were assessed. Fatty acid synthase (*Fasn*) expression was downregulated 2-fold in both diet groups due to PCB126 exposure (Figure 1.4D). *Scd-1*, a gene involved in synthesizing monounsaturated fatty acids, exhibited decreased expression due to PCB126 in pair-fed mice and ~60% decreased due to ethanol feeding (Figure 1.4E). Additionally, *Srebf1*, a gene involved in the regulation of sterol synthesis was examined. *Srebf1* mRNA level was downregulated in the ethanol + PCB126 group and displayed an interaction effect where its expression was decreased ~40% (Figure 1.4F). We also evaluated genes involved in lipoprotein assembly and export. Apolipoprotein B (*Apob*) is the primary gene encoding for the protein involved in carrying and exporting LDL and VLDL from the liver. *Apob* expression was observed to be increased due to PCB126 exposure in pair-fed mice; however, an interaction effect was noted in the

31

ethanol + PCB126 where *Apob* expression was decreased ~15% (Figure 1.4G). mRNA levels of microsomal triglyceride transfer protein (*Mttp*), which engages in apolipoprotein assembly, were slightly increased due to PCB126 exposure and ethanol feeding (Supporting Figure S4). In addition, genes involved in lipid breakdown were also investigated. *Cpt-1α* and *Cpt-2* are genes that encode fatty acid oxidation transferases that are located at the outer and inner membrane of the mitochondria, respectively. *Cpt-1α* expression was discovered to be significantly increased due to PCB126 exposure in pair-fed mice; however, its expression was decreased about 50% due to ethanol feeding in both ethanol-fed groups (Figure 1.4H). Similarly, *Cpt-2* expression was downregulated in response to ethanol feeding, highlighting decreased lipid oxidation capabilities when mice are consuming an ethanol diet (Supporting Figure S4).

Outcome	EtOH	PCB 126	Interaction	Pair-fed (Veh. vs. PCB 126)	EtOH-fed (Veh. vs. PCB 126)	Veh. (Pair-fed vs. EtOH-fed)	PCB 126 (Pair-fed vs. EtOH-fed)
Alb	0.0006	0.0019	n.s.	n.s.	0.0102	n.s.	0.0055
Cd36	<0.0001	<0.0001	n.s.	<0.0001	<0.0001	<0.0001	<0.0001
Fabp1	<0.0001	n.s.	n.s.	n.s.	n.s.	<0.0001	<0.0001
Fasn	n.s.	<0.0001	n.s.	0.0053	0.0048	n.s.	n.s.
Scd-1	<0.0001	0.0005	0.0012	<0.0001	n.s.	<0.0001	n.s.
Srebf1	<0.0001	0.0427	0.0116	n.s.	0.0095	n.s.	<0.0001
Apob	0.0030	n.s.	<0.0001	0.0422	0.0047	n.s.	<0.0001
Cpt-1α	<0.0001	<0.0001	0.0029	<0.0001	n.s.	<0.0001	<0.0001

Figure 1.4. Hepatic RT-PCR analysis of albumin and lipid metabolism related genes. RT-PCR was performed to measure hepatic mRNA levels of (**A**) *Alb* (**B**) *Cd36*, (**C**) *Fabp1*, (**D**) *Fasn*, (**E**) *Scd-1*, (**F**) *Srebf1*, (**G**) *Apob*, and (**H**) *Cpt-1α*. Values are represented as mean ± SD with an alpha level set to 0.05. A complete list of P-values, as determined by two-way ANOVA and Tukey's post-hoc test, is provided in the accompanying table. EtOH, ethanol; Veh., vehicle; Alb, albumin; Cd36, fatty acid translocase; Fabp1, fatty acid binding protein;

Fasn, fatty acid synthase; Scd-1, stearoyl-CoA desaturase 1; Srebf1, sterol regulatory element binding transcription factor 1; Apob, apolipoprotein b; Cpt-1α, carnitine palmitoyltransferase 1α.

Ethanol and PCB126 deplete Glycogen stores and disrupts Carbohydrate Metabolism

Characterization of additional energy metabolism pathways is important since disrupted metabolism, including carbohydrate metabolism, is often manifested in SLD. It was hypothesized that this model would also impair carbohydrate storage and metabolic activity as both ethanol and PCB126 have independently demonstrated before (Steiner et al., 2015; Wahlang et al., 2017; Zhang et al., 2012b). PAS staining was performed to assess glycogen content, and captured images are displayed in Figure 1.5A. Quantitative assessment demonstrated that glycogen storage was heavily depleted due to PCB126 exposure in pair-fed mice and due to ethanol in alcohol fed mice (Figure 1.5B). The relative abundance of positive staining was found to be decreased about 60% due to PCB126 exposure and ethanol feeding. An interaction effect was observed in the ethanol + PCB126 group where glycogen levels were depleted by an additional 10% relative to the pair-fed+Veh. group (Figure 1.5B). In addition, hepatic expression of various genes involved in glycolysis and gluconeogenesis were evaluated to further identify key mediators that were altered by PCB126 and ethanol feeding. Pyruvate kinase (*Pklr*), the rate-limiting enzyme in glycolysis, expression was decreased due to PCB126 exposure and ethanol feeding and our statistical analysis indicated an interaction in the ethanol + PCB126 group where expression was decreased by ~50% (Figure 1.5C). Phosphoenolpyruvate carboxykinase 1 (*Pck-1*), a gene regulating gluconeogenesis, was downregulated due to ethanol feeding and PCB126 exposure (Figure 1.5D). Interestingly, *Pck-1* expression was

downregulated ~40% due to interacting PCB126 and ethanol (Figure 1.5D). Expression of Glucose-6-phosphatase (*G6pc*), which catalyzes the last step of gluconeogenesis, was overall downregulated ~70% in response to ethanol feeding (Figure 1.5E). We also evaluated glycogen synthase (*Gys2*) mRNA levels and observed a ~60% decrease of expression due to ethanol feeding (Figure 1.5F). Interestingly, *Gys2* expression was moderately increased due to PCB126 exposure and an interaction effect was observed. Finally, glycogen phosphorylase (*Pygl*) expression was unchanged due to ethanol feeding or PCB126 exposure (Figure 1.5G).

Outcome	EtOH	PCB 126	Interaction	Pair-fed (Veh. vs. PCB 126)	EtOH-fed (Veh. vs. PCB 126)	Veh. (Pair-fed vs. EtOH-fed)	PCB 126 (Pair-fed vs. EtOH-fed)
PAS Scoring	0.0001	0.0002	0.0021	<0.0001	n.s.	<0.0001	n.s.
Pklr	0.0052	0.0021	0.0143	0.0009	n.s.	0.0014	n.s.
Pck-1	0.0236	0.0006	0.0119	n.s.	0.0003	n.s.	0.0062
G6pc	<0.0001	n.s.	n.s.	n.s.	n.s.	<0.0001	<0.0001
Gys2	<0.0001	0.0018	0.0423	0.0021	n.s.	<0.0001	<0.0001
Pygl	n.s.	n.s.	n.s.	n.s.	n.s.	n.s.	n.s.
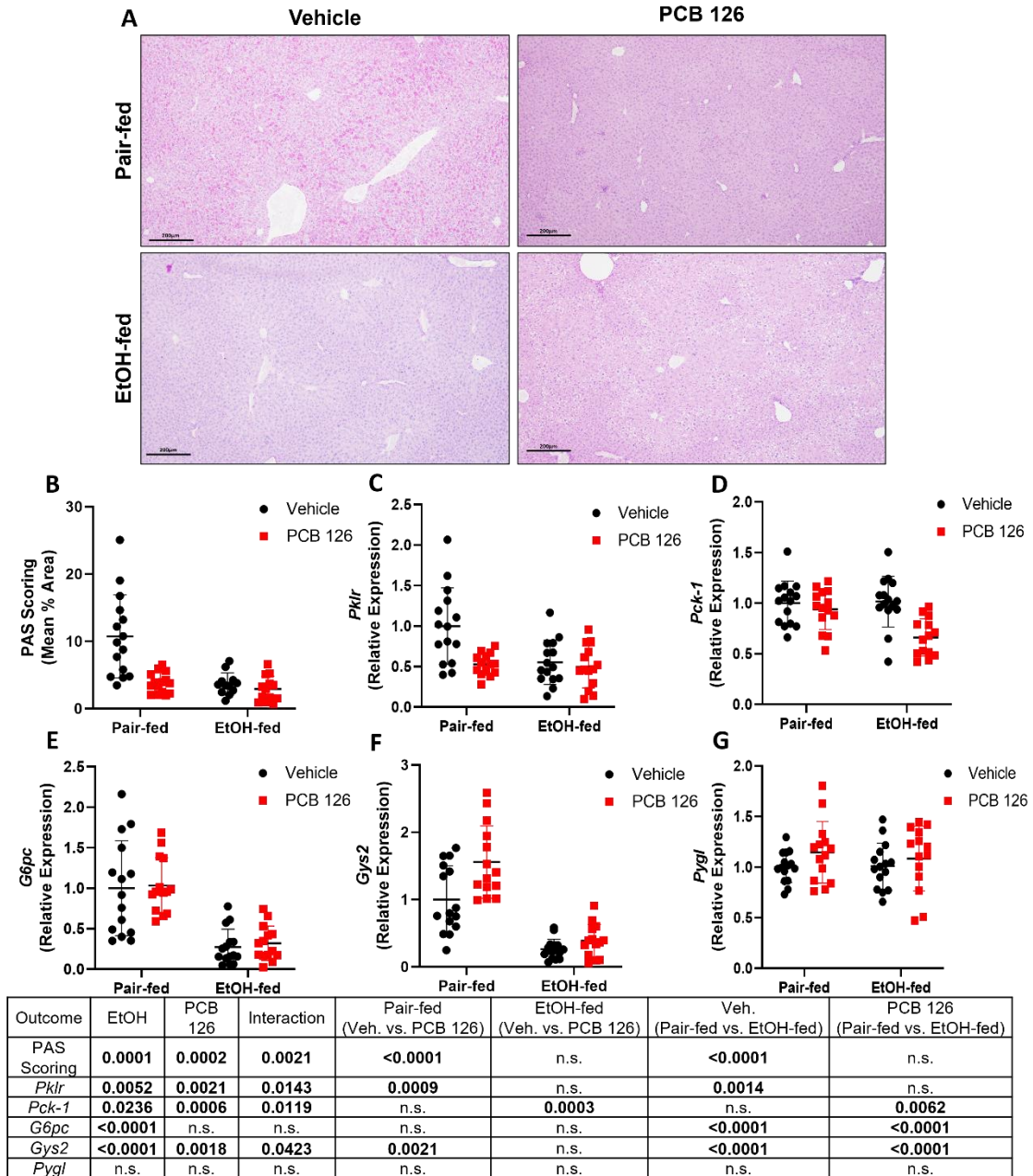
Figure 1.5. Analysis of glycogen content and carbohydrate-related gene expression. (**A**) 5µm thin liver sections were analyzed using PAS staining to detect glycogen presence in hepatic tissue at 10x magnification. (**B**) PAS stain scoring was performed using ImageJ where seven fields per mouse were averaged for all study animals. RT-PCR was performed to measure hepatic mRNA levels of (**C**)

Pklr, (**D**) *Pck-1*, (**E**) *G6pc*, (**F**) *Gys2*, and (**G**) *Pygl*. Values are represented as mean ± SD with an alpha level set to 0.05. A complete list of P-values, as determined by two-way ANOVA and Tukey's post-hoc test, is provided in the accompanying table. EtOH, ethanol; Veh., vehicle; PAS, Periodic Acid Schiff; Pklr, pyruvate kinase L/R; Pck-1, phosphoenolpyruvate carboxykinase 1; G6pc, glucose-6-phosphatase catalytic subunit 1; Gys2, glycogen synthase; Pygl, glycogen phosphorylase.

Ethanol has been shown to perturb hepatic receptor activity such as peroxisomal-proliferator activated receptor's (Ppar's), constitutive androstane receptor (Car), and AhR (Gyamfi and Wan, 2010; Zhang et al., 2012a). In addition, it is well-established that PCBs interact with AhR and other xenobiotic receptors such as Pregnane X Receptor (Pxr) in a dose-dependent manner (Zhang et al., 2012a; Wahlang et al., 2014b). The expression of three hepatic receptors and respective target genes of interest were evaluated in Figure 1.6. *Ahr* expression was significantly increased due to PCB126 exposure and ethanol feeding while its target gene, *Cyp1a2*, was induced 30-fold due to PCB126 exposure in both feeding groups (Figure 1.6A). *Car* expression was significantly elevated due to PCB126 exposure in pair-fed mice but was mitigated in the ethanol + PCB126 mice (Figure 1.6B). *Cyp2b10*, a Car target, expression was found to be significantly induced (~350-fold) due to ethanol feeding alone, highlighting Car's activity in response to ethanol (Figure 1.6B). Finally, *Pparα*'s expression was found to be decreased in response to PCB126 exposure and ethanol feeding; however, the expression of its target gene, *Cyp4a10*, was not perturbed in this model (Figure 1.6C).

Outcome	EtOH	PCB 126	Interaction	Pair-fed (Veh. vs. PCB 126)	EtOH-fed (Veh. vs. PCB 126)	Veh. (Pair-fed vs. EtOH-fed)	PCB 126 (Pair-fed vs. EtOH-fed)
Ahr	<0.0001	0.0098	n.s.	n.s.	n.s.	<0.0001	<0.0001
Cyp1a2	n.s.	<0.0001	n.s.	<0.0001	<0.0001	n.s.	n.s.
Car	n.s.	<0.0001	0.0005	<0.0001	0.0007	n.s.	0.0027
Cyp2b10	<0.0001	n.s.	n.s.	n.s.	n.s.	<0.0001	<0.0001
Pparα	<0.0001	0.0275	n.s.	n.s.	n.s.	<0.0001	<0.0001
Cyp4a10	n.s.	n.s.	n.s.	n.s.	n.s.	n.s.	n.s.
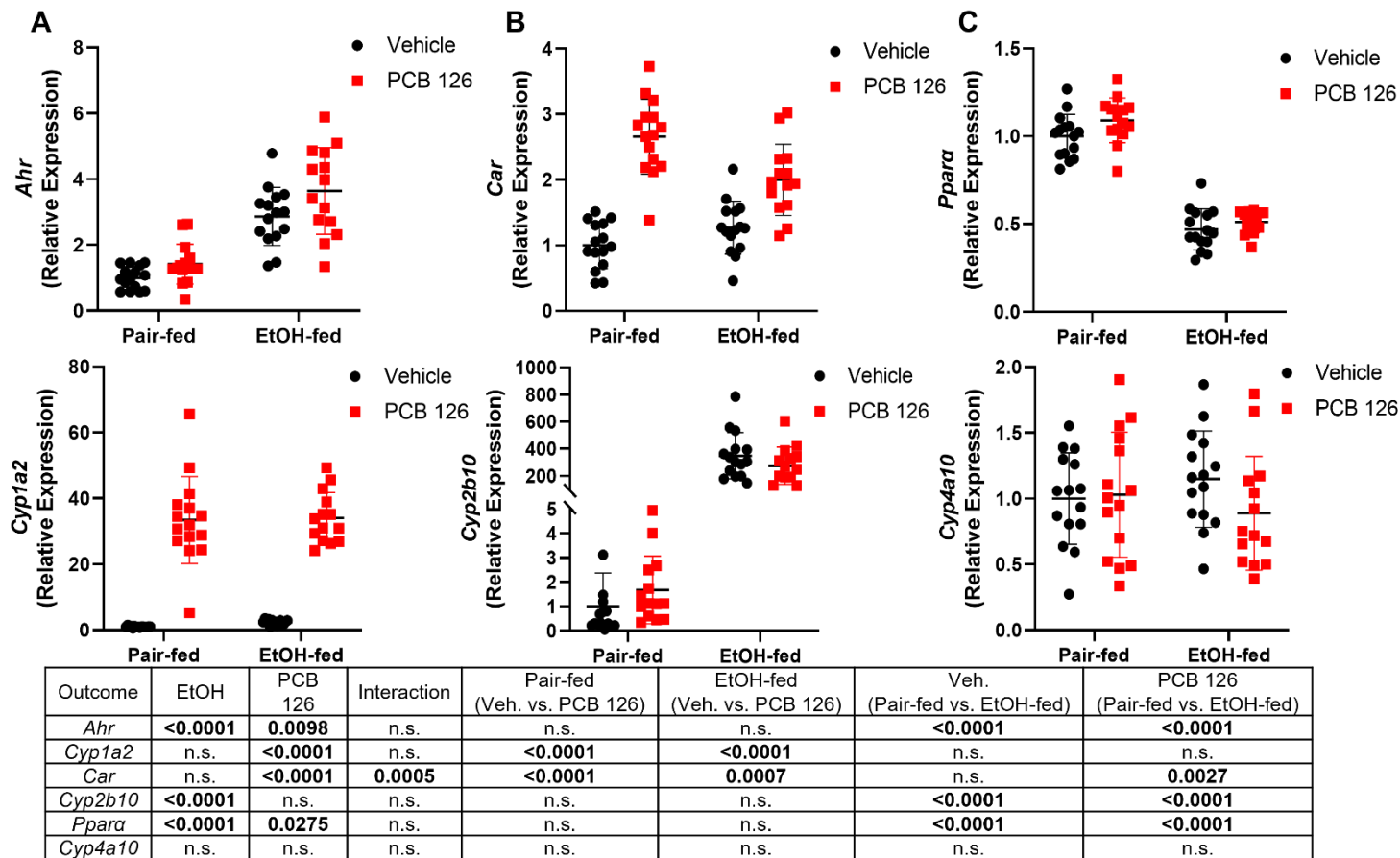
Figure 1.6. Hepatic RT-PCR analysis of hepatic receptors and target genes. RT-PCR was performed to measure hepatic mRNA levels of hepatic receptor *Ahr* and its target gene *Cyp1a2* (**A**), *Car* and its target gene *Cyp2b10* (**B**), *Pparα* and its target gene *Cyp4a10* (**C**). Values are represented as mean ± SD with an alpha level set to 0.05. A complete list of P-values, as determined by two-way ANOVA and Tukey's post-hoc test, is

provided in the accompanying table. EtOH, ethanol; Veh., vehicle; Ahr, aryl hydrocarbon receptor; Cyp1a2, cytochrome P450 family 1, subfamily a, member 2; Car, constitutive androstane receptor; Cyp2b10, cytochrome P450 family 2, subfamily b, polypeptide 10; Pparα, Peroxisomal Proliferator Receptor α; Cyp4a10, cytochrome P450 family 4, subfamily a, polypeptide 10.

Discussion

Although alcohol manufacture and use have thousands of years of history, the scientific understanding of its effects and abuse are relatively recent (Khaderi, 2019). Researchers have attempted to recapitulate human ALD in animal models; however, the full extent of injury and metabolic response is not apparent (Louvet and Mathurin, 2015). A secondary insult, such as high fat supplementation, is generally required to progress rodent ALD pathogenesis to study hepatic injury and metabolic disruption (Brandon-Warner et al., 2012). Toxicological effects of alcohol consumption are well known and characterized in experimental models and human populations (Beier and McClain, 2010; Plaza-Díaz et al., 2020). Similarly, the adverse effects of PCBs are extensively documented, and their mechanism of action have been postulated with high certainty (IARC, 2016; Deng et al., 2019; Wahlang et al., 2017). Importantly, studies have previously demonstrated that obesity and lifestyle factors can impact PCB bodily distribution and enhance disease prognosis (Domazet et al., 2020; Rey-Cadilhac et al., 2020; Wahlang et al., 2019b). For instance, we have previously published that diet, a lifestyle factor, can modify toxicity imposed by environmental pollutants (Jin et al., 2020; Klinge et al., 2021). Overall, this model demonstrated an impact on several major macromolecules including lipids, carbohydrates, and proteins. The key findings from this study revealed that PCB126 exposure and ethanol feeding altered energy metabolism and liver function to worsen ALD endpoints and are illustrated in Figure 1.7.
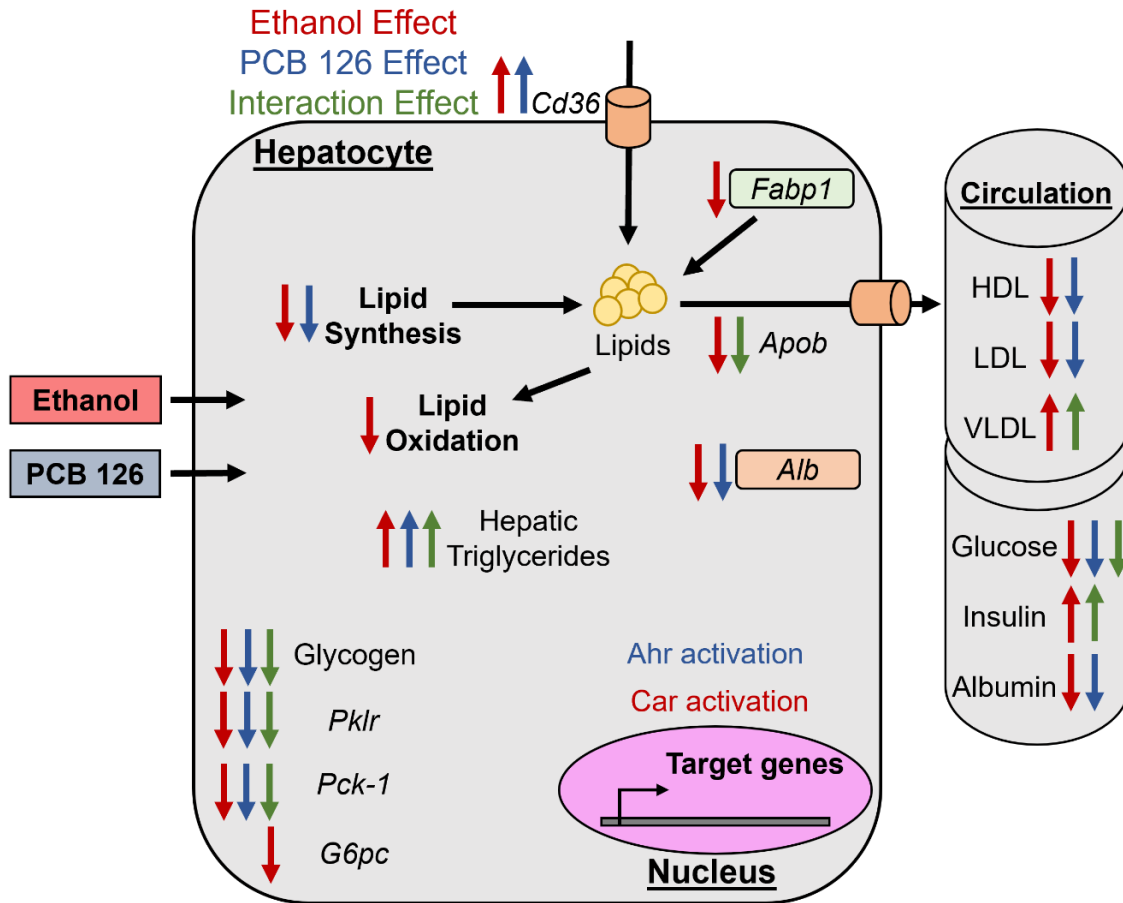
Figure 1.7. Schematic diagram of the major findings in the present study. A schematic diagram outlining the major findings from the present study in terms of hepatic or systemic changes where arrows indicate the increase (↑) or decrease (↓) of expression, processes, or marker levels. Red arrows indicate ethanol effects, blue arrows indicate PCB126 effects, and green indicates an interaction effect (ethanol + PCB126). EtOH, ethanol; Veh., vehicle; Cd36, fatty acid translocase; Fabp1, fatty acid binding protein; Apob, apolipoprotein b; Alb, albumin Pklr, pyruvate kinase L/R; Pck-1, phosphoenolpyruvate carboxykinase 1; G6pc, glucose-6-phosphatase catalytic subunit 1; Ahr, aryl hydrocarbon receptor; Car, constitutive androstane receptor.

A major finding in this study is that steatosis was exacerbated in mice exposed to PCB126 that consumed the ethanol diet. Both PCB126 and ethanol have independently shown to influence lipid storage and drive disease progression along the SLD spectrum to more severe states. Published literature suggests that ethanol promotes steatosis by increasing the ratio of NADH:NAD+ to impede β-oxidation pathways while also impairing Pparα activity, a major lipid metabolism regulator (Lieber, 2004; You and Arteel, 2019). Upon the development of steatosis, sustained alcohol use further disrupts energy metabolism and to promote pathology (Donohue, 2007). PCB126 has also been reported to induce hepatic lipid accumulation and enhance diet-induced steatosis *via* transcriptional reprogramming and altering bodily distribution of lipids (IARC, 2016; Shi et al., 2019b). Contrasting hepatic triglycerides, plasma triglyceride levels were mitigated by PCB126 in ethanol-fed mice, although still statistically higher than controls. PCBs are thought to impede hepatic triglyceride release *via Apob* by disrupting the expression of *Mttp* (Shan et al., 2020). Mttp plays a critical role in lipoprotein assembly; however, Apob's mitigated expression in the ethanol + PCB126 group may explain exacerbated steatosis in these animals. Furthermore, plasma VLDL levels were attenuated by PCB126 in the ethanol-fed mice. These findings are consistent with previously reported PCB126 results in a time course study where plasma triglycerides were elevated 36 hours post PCB126 exposure followed by a gradual decline until the end of study (Gadupudi et al., 2016). PCB's influence on lipid distribution may be an indication as to why hepatic lipid stores of our study

mice were elevated but plasma triglycerides were mitigated at the euthanasia time point.

Previous toxicokinetic studies have alluded that PCBs, due to their high lipophilicity, are concentrated in adipose tissue and redistributed *via* plasma lipids to eventually access the liver and other target organs (ATSDR, 2000). While the mean body weights of our mice were stable during the study, white adipose tissue weight was decreased implying this phenomenon may have occurred in our study animals. Previous studies have implied that wasting syndrome may occur in chronic, high dose PCB exposures. Adipocyte lipolysis is a phenomenon that may have occurred in the current study; however, based on our observed upregulation of *Cd36* and hepatic and plasma triglyceride data, its believed that PCB126 may transcriptionally influence the liver to import more adipose-derived blood lipids to increase steatosis. Overall, at the transcriptional level, our data suggests a potential net accumulation of lipids where lipid import (*Cd36*) was increased, and lipid oxidation (*Cpt-1α* and *Cpt-2*) was decreased in the ethanol + PCB126 group. These expressional changes coupled with increased hepatic triglycerides and liver-to-body weight ratio indicates exacerbated steatosis. Several mechanisms are known to promote steatosis and our data suggests this model recapitulates some of these mechanisms including increased lipid import, reduced lipid oxidation, and reduced lipid clearance (Nassir et al., 2015).

Malnutrition is a major factor in human ALD development where ethanol can directly disrupt glucose homeostasis (Steiner et al., 2015). Poor nutrition due to

alcohol consumption may also be a result of the absence of protein, micronutrients, and vitamins (McClain et al., 2011). PAS scoring indicated that glycogen stores were depleted due to PCB126 exposure and ethanol feeding accompanied by decreased gluconeogenic gene expression (*G6pc* and *Pck-1*) in the ethanol-fed groups. Glycogen synthase (*Gys2*) expression was also decreased due to ethanol feeding; however, the release of glycogen from storage *via Pygl* mRNA analysis was unperturbed. Additionally, *Atf3* and *Atf4* have demonstrated induction in the presence of glucose deprivation and ER stress (Iurlaro et al., 2017; Ku and Cheng, 2020). It may be that carbohydrate metabolism was reprogrammed at the transcriptional level resulting in decreased glucose and glycogen levels observed in the present study to induce *Atf3*, *Atf4*, and *Chop* related apoptosis pathways. The disruption of these hepatic genes with the loss of hepatic glycogen implies that de novo glucose synthesis and storage is disrupted in the liver, but the exact mechanism and contribution to disease development is unclear. It was also noted that the gene expression of *Pklr* was downregulated in the PCB126 exposed and ethanol-fed mice. Taken together, both gluconeogenesis and glycolysis were impeded, signifying disruption of carbohydrate metabolism and depleted glucose. Previous alcohol studies have suggested that ethanol consumption impairs both glycolysis and gluconeogenesis by impacting enzyme transcription and activity (Steiner et al., 2015; Young et al., 2006). With carbohydrate metabolism impaired, a shift from utilizing carbohydrates as a primary energy source to lipids occurs during excess ethanol consumption, which contributes to disease development (Berk et al., 2005). It should be noted that nutritional differences exist where pair-

fed mice receive 490 kcal/L of carbohydrates and ethanol-fed mice receive 135 kcal/L of carbohydrates and 355 kcal/L ethanol. However, previous work has demonstrated that chronic ethanol feeding is responsible for decreased glycogen content rather than dietary carbohydrate intake differences (Van Horn and Cunningham, 1999). Nonetheless, ethanol-fed mice still exhibited decreased glucose levels and glycogen stores even though each dietary group were euthanized after the same amount of time post water or ethanol binge.

Albumin's mRNA and protein levels were decreased ~50% due to ethanol and PCB126 exposure, a finding that is a traditional hallmark of altered liver function and malnutrition in humans (Sun et al., 2019). In the present in vivo model, PCB126 exposure additively decreased albumin with ethanol feeding. The observed albumin reduction appears to be a class effect for dioxin-like molecules as similar results have been published for the prototypical AhR ligand, 2,3,7,8-tetrachlorodibenzo-p-dioxin, in mice fed a standard rodent diet (Nault et al., 2017). However, hepatic albumin protein abundance was increased in vivo in AhR knockout mice fed a control diet in another secondary analysis of our previously published proteomics data (P=0.0006, data not shown) (Jin et al., 2021). While environmental dioxin exposures appear to regulate key liver functions such as albumin production in model systems, more mechanistic and confirmatory human data are required. We postulate this model's toxic mode of action to be attributed to the alteration of liver functionality to induce a metabolic nutritionally deficit state (loss of carbohydrates, reduced lipid oxidation and export, and reduced albumin levels) to overall promote disease status.

Investigating hepatic receptor activation is imperative for identifying the major mode(s) of action of PCB126 and ethanol and how they elicited some of the observed altered molecular processes. PCB126 is considered the most potent dioxin-like PCB congener and demonstrates high affinity binding to AhR (Hestermann et al., 2000; Shi et al., 2019a). The postulated molecular initiating event for PCB126 toxicity begins with its binding and activation of AhR followed by dysregulation of target pathways to induce injury and disease (IARC, 2016; Deng et al., 2019). It has been previously noted that AhR may play a role in not only xenobiotic metabolism, but various energy metabolic pathways (Girer et al., 2020; Tanos et al., 2012). AhR ligand structure and composition are also vital to consider because it has become apparent that specific ligands can also influence what metabolic pathways are acted upon (Safe et al., 2020). The current model demonstrated that PCB126 exposure activated AhR, *via Cyp1a2* induction, and ethanol feeding activated Car, *via Cyp2b10* induction. These perturbations in energy and xenobiotic metabolism suggests that both PCB126 and ethanol may influence different pathways to jointly promote steatosis and immune modulation. Our group has previously demonstrated in an AhR knock-out model that PCB126's effects on the hepatic proteome are AhR dependent (Jin et al., 2021). Moreover, the study described by Jin et al. 2021 demonstrated AhR's critical role in regulating hepatic lipid metabolism. Interestingly the expression of Pparα, a nuclear receptor known to be heavily tied to lipid metabolism, was downregulated in response to ethanol feeding. Ethanol feeding also decreased the expression of other Pparα target genes (*Cpt-1α*, *Cpt-2*, and *Fabp1*). Indeed, the downregulated expression

of *Pparα* and its target genes can potentially influence lipid oxidation and translocation to promote steatosis. Nonetheless, it is known that *Pparα*'s downregulation is a key step in the development and progression of steatosis and possibly fibrosis (Nakajima et al., 2004). Future analyses must confirm these observations as transcriptional modifiers may influence protein activity and abundance.

While this study is novel, in that it is one of few studies to address an alcohol-plus-toxicant model in SLD, it is not without limitations. A major limitation of this study is the mortality experienced prior to the expected euthanasia time point. The chronic-binge model suggests waiting nine hours post-binge to begin euthanasia and tissue collection to obtain peak liver injury enzyme levels. Furthermore, study animals were removed from their housing room approximately two hours (ZT22) before the end of the official 'dark' cycle, which may impact some metabolic endpoints in this study. Nonetheless, pair-fed mice were treated similarly, and we still observed significant differences between ethanol-fed and pair-fed mice. To address these limitations in future studies, mice will be removed from their housing room during the 'light' phase and a more time-controlled period prior to ethanol binge will be introduced to address the mortality issue. Future investigations will also incorporate more specific endpoints pertinent to ALD to better recognize injury mechanisms that PCB126 may interact with. For instance, expression of several intestinal integrity genes was decreased in the current study due to ethanol feeding, but unperturbed due to PCB126 exposure (Supporting Figure S5). Despite these limitations, the characterization of this model is necessary towards future

model designs that are holistic in nature to understand the complex interaction between lifestyle factors and environmental toxicant exposures.

CONCLUSIONS

Environmental pollutant exposures have increasingly been recognized as disease modifiers in MASLD, but almost no data exist for environmental health and ALD. However, as a proof of concept, cigarette smoking has previously been associated with ALD severity (Bailey et al., 2009; Lu et al., 2013). At this point in time, there are no data to suggest that drinkers are exposed to different types of pollutants than non-drinkers. Therefore, we investigated food and water contaminant, PCB126, in ALD based on its human relevance, prior association with MASLD, and the emerging role of its targeted receptor, Ahr, in ALD. In the present model, PCB126 disrupted hepatic intermediary and xenobiotic metabolism. Hepatic lipid, carbohydrate, and protein (albumin) metabolism were impacted in association with hypoglycemia and attenuation of ethanol-induced hypertriglyceridemia. The net impact was worsened steatosis and hepatomegaly with reduced liver glycogen stores. The PCB-exposed ALD liver did not appear capable of making and releasing glucose, albumin, and lipids appropriately, consistent with PCB's previously established role as a metabolism disrupting chemical. We postulate that PCB126 reprogramed intermediary metabolism thereby compounding ethanol-associated malnutrition impacting the liver-adipose and liver-muscle axes. Thus, it appears possible that PCB pollutant exposures could exacerbate the protein-calorie malnutrition associated with ALD, not by impacting food intake, but rather

50

by transcriptional reprograming of systemic energy metabolism. Most importantly, this study suggests a potential role for environmental pollutants as understudied disease modifying factors in ALD. More data on the environmental factors influcencing ALD are required to further understand how toxicants can impact lifestyle related diseases.

CHAPTER III

PCB126 MODIFIES THE MURINE HEPATIC TRANSCRIPTOME AND
METALLOME TO PROMOTE ALCOHOL-ASSOCIATED LIVER DISEASE
PATHOGENESIS

Introduction

In our recent characterization study, we observed that PCB126 reprogrammed
intermediary metabolism to enhance liver disease in a rodent ALD model
(Gripshover et al., 2022). Steatosis, disrupted lipid metabolism, and decreased
plasma glucose and liver glycogen were pronounced in mice that were fed a 5%
EtOH diet and exposed to 0.2 mg/kg PCB126. Furthermore, we observed that
albumin mRNA and plasma protein levels were decreased approximately by half
compared to controls, signifying that liver function was compromised. Neutrophil
infiltration was observed in this model; however, this inflammatory endpoint was
not exacerbated by PCB126. This may be due to the sequence or timing of
exposures or perhaps may be due to AhR activation prior to alcohol feeding. Gene
expression related to endoplasm reticulum stress, *Chop* and *Atf3*, were however
exacerbated ~13-fold and ~46-fold, respectively. The abundance of gene
expression data shown in our characterization study is certainly only a small piece
of the total modified transcriptome.

Previous independent work has demonstrated that PCBs and alcohol consumption can alter the transcriptome. For example, PCB126 globally impacted lipid related genes to favor hepatic accumulation and a steatotic environment (Mesnage et al., 2018; Petri et al., 2022; Nault et al., 2013). Additionally, our collaborators have observed significant alterations to the epitranscriptome due to PCB126 exposure, favoring lipid accumulation (Klinge et al., 2021; Petri et al., 2023). Alcohol studies have demonstrated that the total number of DEGs may positively correlate with disease severity and many DEGs are associated with lipid metabolism, activated immune responses, and cellular injury responses (Yang et al., 2022b; Liu et al., 2019; Cao et al., 2023). While some of these transcriptome responses may be similar, unique expressed genes and enriched pathways are likely to be observed. For instance, in our characterization study (Chapter II), we noted an increase of *Ahr* expression by EtOH, but its target gene *Cyp1a2* was robustly induced by PCB126 (Figure 1.6A). Furthermore, *Car* was induced ~3-fold by PCB126, but its target gene *Cyp2b10* was induced ~300-fold by EtOH (Figure 1.6B). Moreover, *Ppara* mRNA levels were repressed by EtOH, but no exposure paradigm seemed to elicit activation, shown by *Cyp4a10* expression (Figure 1.6C). Indeed, the expression and activation of these critical transcription factors are complex, where receptor crosstalk likely plays a critical role in disease promotion. However, these transcription factors are only a part of the disease network that play into ALD or ALD enhanced by toxicants. Further investigation into our alcohol-plus-toxicant model is warranted to discern global transcriptome alterations that may play into toxicological effects previously observed.

The current study adopts a conventional mRNA sequencing (RNA-Seq) technique to assist in the generation of mechanistic hypotheses related to PCB126's ability to enhance murine ALD. In addition, a major pathology associated with both ALD and dioxin-like exposures are altered essential metal levels (Lai et al., 2010; Zhou et al., 2005; Nicoll et al., 2022). Particularly, the depletion of essential metals like zinc (Zn), selenium (Se), and calcium (Ca) contribute to disease by impacting protein functionality and basic life sustaining functions (Jomova et al., 2022; Baj et al., 2020). Thus, this study also examines the hepatic metallome as they play integral roles in cellular homeostasis and liver disease development. The objective of this study is to elucidate altered genes and enriched gene ontology (GO) processes to explain the results from our initial characterization study (Chapter II). We hypothesize that unique differentially expressed genes (DEGs) and enriched GO processes will be identified that provide insight to how the transcriptome was modified due to the presence of PCB126 in EtOH-fed mice. Furthermore, we hypothesize that PCB126 will further deplete EtOH induced loss of hepatic metal levels. This work is currently under review for publication in *Environmental Health Perspectives* as of November 17, 2023.

Materials and Methods

Animal Study

The University of Louisville Institutional Animal Care and Use Committee (IACUC) approved animal use protocols and procedures. Ten-week-old, male, C57BL/6J mice were purchased from Jackson Laboratory (strain#: 000664; Bar Harbor,

Maine). The current study is an exact repeat in terms of design for scientific rigor and tissue availability for RNA-Seq that is described in our recent published work (Chapter II) (Gripshover et al., 2022). In the current study, we utilized six liver tissues from each of our four groups (pair-fed+Veh., pair-fed+PCB126, EtOH+Veh., and EtOH+PCB126), prioritizing highest quality RNA in terms of optical density ratios (260/280; 260/230) and RNA Integrity Number (RIN). For simplicity, we will refer to our RNA-Seq group comparisons as follows: i) pair-fed+Veh. *vs* pair-fed+PCB126 as *PF(Veh. v PCB126)*, ii) pair-fed+Veh. *vs* EtOH+Veh. as *Veh.(PF v EF)*, iii) pair-fed+PCB126 *vs* EtOH+PCB126 as *PCB126(PF v EF)*, and iv) EtOH+Veh. *vs* EtOH+PCB126 as *EF(Veh. v PCB126)*.

Tissue & Sample Preparation

Hepatic tissues were homogenized in RNA-STAT60, and total RNA was extracted (catalog: CS-502; Tel-test Inc.; Friendswood, TX). RNA samples were then treated with DNase, Amplification Grade I to digest single- and double-stranded DNA species (catalog: 18068015; Invitrogen; Waltham, MA). Finally, RNA samples were treated with RNAClean XP beads at a 1:1 volume ratio to further purify our samples to remove salts, dNTPs, and miscellaneous enzymes that may interfere with sequencing (catalog: A66514; Beckman Coulter Life Sciences; Brea, CA). RNA sample concentration and purity was then assessed with a Nanodrop One[C] spectrometer purchased from ThermoFisher Scientific (catalog: 701-058112; Madison, MI). Initial and final quality control measures included assessing RNA concentration with a Qubit 4 fluorometer (catalog: Q32854; Invitrogen; Waltham,

MA) and RNA integrity with an Agilent 2100 Bioanalyzer (catalog: 5067-4626; Agilent Technologies; Santa Clara, CA). Bioanalyzer quality assessment were performed according to manufacturer's instructions with the Eukaryote Total RNA 6000 Nano electrophoresis kit (catalog: 5067-1511; Agilent Technologies; Santa Clara, CA).

RNA-Seq library preparation & sequencing

RNA-Seq libraries were prepared according to manufacturer's protocols using Illumina's TruSeq Stranded reference guide (document: 100000040498 v00; Illumina; San Diego, CA). Each sample consisted of 300 ng of RNA that was used for poly-A enrichment. First and second strand cDNA synthesis was completed followed by adapter and index ligation. mRNA libraries were prepared with Illumina's stranded mRNA prep ligation for 96 samples (catalog: 20040534; Illumina; San Diego, CA). Amplification of cDNA was performed according to manufacturer's protocol. Library concentrations were assessed using a Qubit 4 fluorometer with dsRNA high sensitivity kit (catalog: Q33231; ThermoFisher; Madison, MI).

Library size and fragment analysis was assessed on Agilent 4159 Tapestation System on a D5000 screen tape (catalog: 5067-5588; Agilent; Santa Clara, CA). Individual samples were then normalized to 10nM prior to pooling and then quantified by Qubit analysis. Pooled libraries and PhiX control were diluted and loaded at 1000pM with 4% PhiX spiked in. Sequencing was performed on Illumina's NextSeq 2000 platform using a P3 100 cycle reagent kit and P3 flow cell.

Read alignment rates for each sample were in a range of 93.46% to 98.17%. Libraries were then sequenced with a single 101 cycle read length with 2 indexes of 8bp each. FASTQ files were generated with BaseSpace DRAGEN analysis (v1.2.1). Raw RNA-Seq data for each sample are available on the Gene Expression Omnibus (GEO) database identified as accession GSE244388.

Computational Downstream Analyses

Sample fragments per kilobase transcript per million mapped reads (FPKM) values were uploaded to web-based interface MetaboAnalyst (v5.0) tool. One factor statistical analysis was used where data was filtered by interquartile range and normalized based on group median. Whole RNA-Seq datasets were uploaded to MetaCore – Integrated pathway analysis for multi-Omics data software (Clarivate; St. Helier, Jersey, United Kingdom). Data was analyzed with MetaCore for network building and pathway analysis where only processes with a false discovery rate (FDR) ≤0.05 were accepted.

RT-PCR Analyses

Liver tissues were homogenized in RNA-STAT60, and total RNA was extracted (catalog: CS-502; Tel-test Inc.; Friendswood, TX). RNA concentration and purity was examined with a Nanodrop One^C spectrometer (catalog: 701-058112; ThermoFisher; Madison, MI). cDNA was reverse transcribed from 3 µg RNA to produce cDNA with QScript, a single-step cDNA synthesis reagent (catalog: 95048-500; Quantabio; Beverly, MA). RT-PCR was performed on a CFX384™

Real-Time platform (Bio-Rad; Hercules, CA). iTaq Universal Probe Supermix was employed during experiment set up (catalog: 1725134; Bio-Rad; Hercules, CA). Relative mRNA expression was calculated using the $2^{-\Delta\Delta Ct}$ method utilizing Glyceraldehyde-3-Phosphate Dehydrogenase (GAPDH) as the housekeeping gene for liver tissues (catalog: 4351309; Applied Biosystems; Waltham, MA). Fold induction was normalized to the control group, pair-fed+Veh., and was set to a value of '1'. TaqMan probes were purchased from ThermoFisher Scientific, and the following list contains probe names and their respective assay ID's: *Abcb10* (Mm 00497926_m1), *Slc46a3* (Mm00503612_m1), *Tuba8* (Mm01184204_m1), and *Ugt1a6b* (Mm07308190_s1).

Western Blot Analysis

Approximately 50-100 mg mouse liver tissue was homogenized in RIPA Buffer (100 mg tissue/0.5 mL RIPA). HALT protease and phosphatase inhibitor cocktail was added to this tissue lysate at 10 uL/mL of RIPA buffer used (catalog: 78443; ThermoFisher Scientific; Madison, MI). Whole protein concentration was assessed by bicinchoninic acid (BCA) protein assay, following manufacturer's protocol (catalog: 23225; ThermoFisher Scientific; Madison, MI). Normalized 50ug protein was loaded and separated on 4-15% Mini-PROTEAN TGX Stain-Free gels (catalog: 4568086; Bio-Rad; Hercules, CA). A total of six protein lysates per group (N=24) were used, where two sets of three protein lysates were loaded onto two different gels in a representative fashion to account for possible running and antibody incubation differences. Separated proteins were then transferred to

polyvinylidene difluoride membranes (catalog: IPVH00010; Millipore Sigma; Burlington, MA), blocked (catalog: 1706404; Bio-Rad; Hercules, CA), and incubated with primary and secondary antibodies. Primary rabbit monoclonal antibodies, phospho-Janus kinase 2 (p-JAK2) (catalog: 3776S), Janus kinase (JAK2) (catalog: 3230S), phospho-signal transducer and activator of transcription 5 (p-STAT5) (catalog: 9359S), signal transducer and activator of transcription 5 (STAT5) (catalog: 94205S), and β-Actin (catalog: 8457S), were purchased from Cell Signaling Technologies (Danvers, MA). Donkey-anti-rabbit secondary antibody was purchased from Jackson ImmunoResearch Laboratories Inc. (catalog: 711-035-152; West Grove, PA). Primary and secondary antibody dilutions were performed according to manufacturer's protocols.

Metals Analysis

Approximately 50 mg of liver tissue were digested in 800 µl of 70% nitric acid (catalog: A509-P500; ThermoFisher Scientific; Madison, MI) and 200 µl of hydrogen peroxide (catalog: 95321; Millipore Sigma; Burlington, MA) for 4 hours at 85°C. Sample homogenates were then cooled to room temperature and diluted to a final concentration of 5% nitric acid with MilliQ DI water. Samples were then filtered by 45 µm filter.

Metal quantification was performed using Agilent 7800 inductively coupled plasma mass spectrometry (ICP-MS) (Agilent Technologies; Japan). This Agilent ICP-MS was optimized with 1 ppb tuning solution and the assay program was tuned by 10 ppb turning solution (catalog: 5188-6564; Agilent Technologies; Santa Clara, CA).

An autosampler SPS 4 was used to load samples. Twenty-five metals calibration standards were purchased from Inorganic Ventures (catalog: IV-STOCK-50; Christiansburg, VA) and serial metal standard dilutions were made with the same acid matrix of samples. Internal standards used were purchased from Agilent (catalog: 5188-6525; Santa Clara, CA) and were mixed with each sample for calibration. Assay program was run on Agilent MassHunter software with He mode and each sample were read three times for a final mean value. Metals that were measured include sodium (Na), potassium (K), magnesium (Mg), calcium (Ca), Iron (Fe), manganese (Mn), cobalt (Co), copper (Cu), zinc (Zn), molybdenum (Mo), and selenium (Se).

Statistical Analyses

Sequenced read quality was assessed using FastQC (v.0.10.1) for each run (Andrews, 2015). Sequences were of good quality and trimming was not necessary. Sequences were directly aligned with *Mus musculus* reference genome assembly (mm39.fa) using STAR (v.2.6) generating alignment files in bam format (Dobin et al., 2013). Differential expression analysis was performed using DESeq2 (Trapnell et al., 2012). DESeq2 was executed in the R programing environment, using a negative binomial regression model to analyze pairwise comparison. Raw read counts were obtained from STAR aligned bam format files using HTSeq (v.0.10.0) (Yu et al., 2012). Raw counts were then normalized using the Relative Log Expression method and filtered to exclude genes with fewer than 10 counts across all samples. Statistical significance was determined by q-values

≤0.05. GO biological processes were generated by the R package clusterProfiler for sets of DEGs in each group comparison.

RT-PCR, western blot, and metals ICP-MS statistical analyses were performed with GraphPad Prism (v.9.5.1) (GraphPad Software Inc.; La Jolla, CA) for Windows using a two-way analysis of variance (two-way ANOVA). Two-way ANOVA was performed where our two factors were diet (pair-fed vs EtOH-fed) and exposure (vehicle vs PCB126). Significance was determined with an alpha level set to 0.05 ($p \le 0.05$). Tukey's post-hoc test was used to compare different groups for multiple comparisons. A p-value table is available for all relevant figures displaying the two-way ANOVA and Tukey's multiple comparison results to designate significance between groups. Western blot band volume intensity was measured by Bio-Rad's Image Lab software (v6.1.0 build 7). After background subtraction, proteins of interest band intensity were divided by their respective β-Actin band intensity for each sample/column.

Results

EtOH alters more DEGs, but PCB126 diversifies DEGs

We first wanted to examine the variance caused by EtOH feeding or PCB126 exposure by principal component analysis (PCA) generated on MetaboAnalyst (Figure 2.1). The two-dimensional PCA plot shows that pair-fed mice exposed to PCB126 are slightly varied compared to pair-fed+Veh. EtOH feeding overall was a major source of variation where EtOH+Veh. and EtOH+PCB126 are two unique populations relative to pair-fed controls. Interestingly, PCB126 exposure causes

some variance in pair-fed mice; however, there is a large degree of variance between the EtOH+Veh. vs EtOH+PCB126. This signifies that PCB126 exposure induces a more distinct transcriptome landscape within EtOH-fed mice, relative to EtOH+Veh.
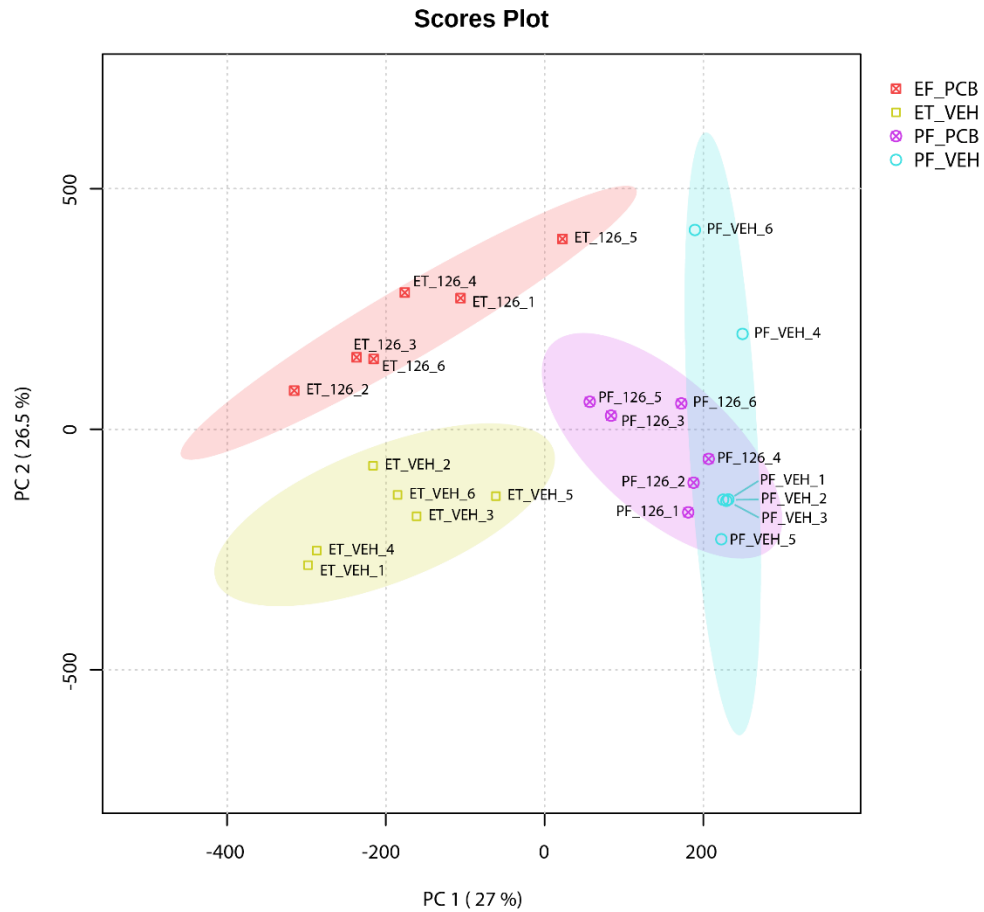
Figure 2.1. PCA plot displaying diverse transcriptome between sample populations. All samples (N=24) were used to generate a scores plot on MetaboAnalyst based on FPKM values, filtered by interquartile range, and normalized based on group median.

Figure 2.2 displays three Venn diagrams of the total, upregulated, and downregulated DEGs for all comparisons. Of our total count of DEGs, the PF(Veh. v PCB126) comparison had 503 DEGs, the Veh.(PF v EF) comparison had 4474 DEGs, the PCB126(PF v EF) comparison had 4832 DEGs, and the EF(Veh. v PCB126) comparison had 907 DEGs. Of the upregulated DEG set, the PF(Veh. v PCB126) comparison had 339 DEGs, the Veh.(PF v EF) comparison had 2231 DEGs, the PCB126(PF v EF) comparison had 2214 DEGs, and the EF(Veh. v PCB126) comparison had 536 DEGs. Of the downregulated DEG set, the PF(Veh. v PCB126) comparison had 164 DEGs, the Veh.(PF v EF) comparison had 2243 DEGs, the PCB126(PF v EF) comparison had 2618 DEGs, and the EF(Veh. v PCB126) comparison had 371 DEGs. These analyses were also performed for EF v PF mice and Veh. v PCB126 exposed mice, regardless of toxicant exposure or diet, and are shown in Supporting Table S4. EF v PF mice had a total of 5919 DEGs and Veh. v PCB126 exposed mice had a total of 449 DEGs. EF v PF mice had 2834 upregulated DEGs and Veh. v PCB126 exposed mice had 278 upregulated DEGs. EF v PF mice had 3085 downregulated DEGs and Veh. v PCB126 exposed mice had 171 downregulated DEGs.

We also wanted to evaluate the top DEGs in terms of significance in our EF(Veh. v PCB126) group. The top 20 up- and downregulated DEGs based on most significant p-values are listed in Supporting Table S5. In our upregulated gene set, cytochrome P450 family 1 subfamily A member 1 and 2 (*Cyp1a1*, *Cyp1a2*) were among the most significantly induced genes, which are canonical AhR targets. Other genes noted in the upregulated gene set include muscle isoform of pyruvate

kinase (*Pkm*), glutathione peroxidase (*Gpx2*), monoamine oxidase A (*Maoa*), and transforming growth factor beta 2 (*Tgfβ2*). In our downregulated gene set, UDP glucuronosyltransferase family 1 member A6b (*Ugt1a6b*) was the most significantly downregulated gene. Other interesting, downregulated genes of note include perilipin 4 (*Plin4*), canonical PXR target cytochrome P450 family 3 subfamily A member 11 (*Cyp3a11*), and lactate dehydrogenase A (*Ldha*).

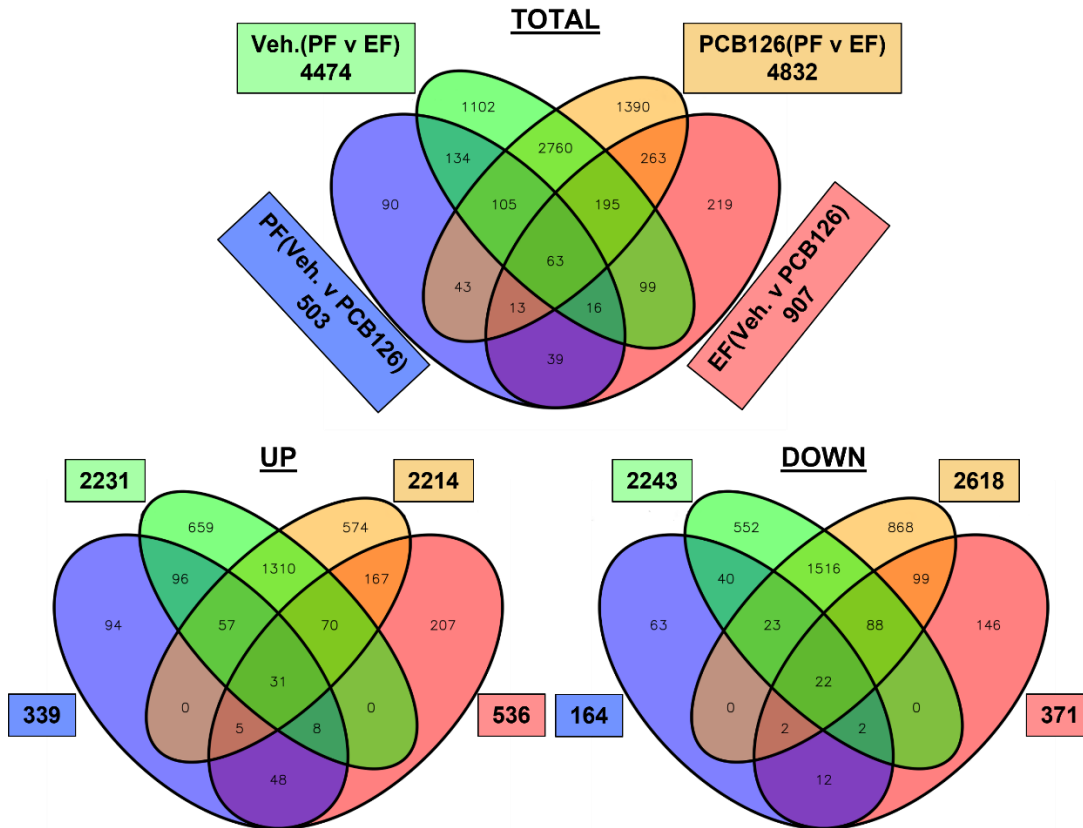Figure 2.2. Venn diagram of the number of DEGs for all group comparisons. DEG count within each group comparison and total number of DEG that are either upregulated, downregulated, or cumulatively differentially expressed. The four group comparisons are labeled by color where: pair-fed+Veh. VS pair-fed+PCB126 is blue; pair-fed+Veh. VS EtOH+Veh. is green; pair-fed+PCB126 VS EtOH+PCB126 is orange; EtOH+Veh. VS EtOH+PCB126 is red.

RT-PCR analyses confirm RNA-Seq observations

Four specific genes were chosen from RNA-Seq analyses to be validated due to differing effects from either EtOH or PCB126 on that specific gene (e.g., upregulation from PCB126 only). Figure 2.3 displays gene expression of ATP binding cassette subfamily B member 10 (*Abcb10*), UDP glucuronosyltransferase 1 family, polypeptide A6B (*Ugt1a6b*), solute carrier family 46, member 3 (*Slc46a3*), and Tubulin, alpha 8 (*Tuba8*). *Abcb10* is a multidrug resistant mitochondrial transporter, and its expression was found to be downregulated ~50% by EtOH feeding (Figure 2.3A). *Ugt1a6b* is a phase II enzyme part of the glucuronidation process, and its expression was non-significantly elevated due to PCB126 exposure in pair-fed mice. Interestingly, we noted a significant interaction effect where PCB126 exposure in EtOH-fed mice downregulated *Ugt1a6b*'s expression ~60% (Figure 2.3B). *Slc46a3* is a lysosomal transporter involved in the distribution of small molecules and catabolites, and its expression was found to be increased by PCB126 10-fold in pair-fed mice. We noted an interaction effect in EtOH-fed mice, where PCB126's induction of *Slc46a3* was mitigated to approximately 5-fold, likely due to ethanol feeding (Figure 2.3C). Finally, *Tuba8*, a non-canonical alpha-tubulin molecule involved in microtubule formation and signaling, was upregulated 25-fold in pair-fed mice; however, our analyses indicate an interaction where *Tuba8* was upregulated 60-fold by PCB126 exposure in EtOH-fed mice (Figure 2.3D).

Outcome	EtOH	PCB 126	Interaction	Pair-fed (Veh. vs. PCB 126)	EtOH-fed (Veh. vs. PCB 126)	Veh. (Pair-fed vs. EtOH-fed)	PCB 126 (Pair-fed vs. EtOH-fed)
Abcb10	<0.0001	n.s.	n.s.	n.s.	n.s.	<0.0001	<0.0001
Ugt1a6b	<0.0001	<0.0001	0.0001	n.s.	<0.0001	n.s.	<0.0001
Slc46a3	<0.0001	<0.0001	<0.0001	<0.0001	<0.0001	n.s.	<0.0001
Tuba8	<0.0001	<0.0001	0.0016	<0.0001	<0.0001	n.s.	<0.0001
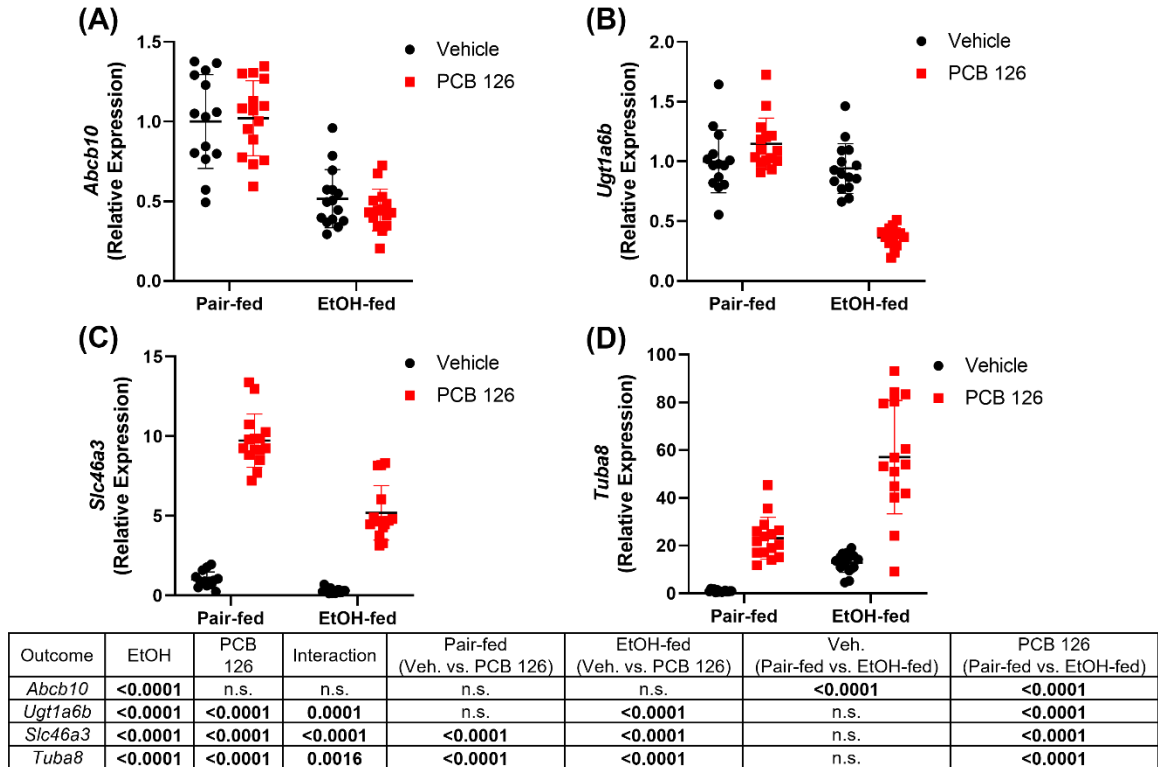
Figure 2.3. Validation of hepatic DEGs found in RNA-Seq analyses by RT-PCR. RT-PCR analysis was performed to measure mRNA transcripts of (A) *Abcb10,* (B) *Ugt1a6b*, (C) *Slc46a3*, and (D) *Tuba8*. Values are represented as mean ± SD with an alpha level set to 0.05. A complete list of p-values, as determined by two-way ANOVA and Tukey's post-hoc test, is provided in the accompanying table. Abcb10, ATP binding cassette subfamily B member 10; Ugt1a6b, UDP glucuronosyltransferase 1 family, polypeptide A6B; Slc46a3, solute carrier family 46, member 3; Tuba8, tubulin, alpha 8.

Peptidyl-Tyrosine Modifications the most significant GO Processes

We examined enriched GO processes *via* the clusterProfiler R package to gather connections between gene expression/products and reported biological observations. Figure 2.4 displays the top 20 GO processes for the EF(Veh. v PCB126) comparison. The top annotated term in this list is "peptidyl-tyrosine modifications". This GO term is further down the gene ontology tree, which then branches into various modifications such as acetylation, methylation, dehydrogenation, phosphorylation, etc. The third, fifth, and sixth, annotated GO terms are also related to this term and are listed as positive regulation of peptidyl-tyrosine phosphorylation, regulation of peptidyl-tyrosine phosphorylation, and peptidyl-tyrosine phosphorylation, respectively. Other annotated terms within this comparison included xenobiotic metabolic process, regulation of endocytosis, or those related to immune cell regulation.

Top 20 GO Processes
EF(Veh. v PCB126)

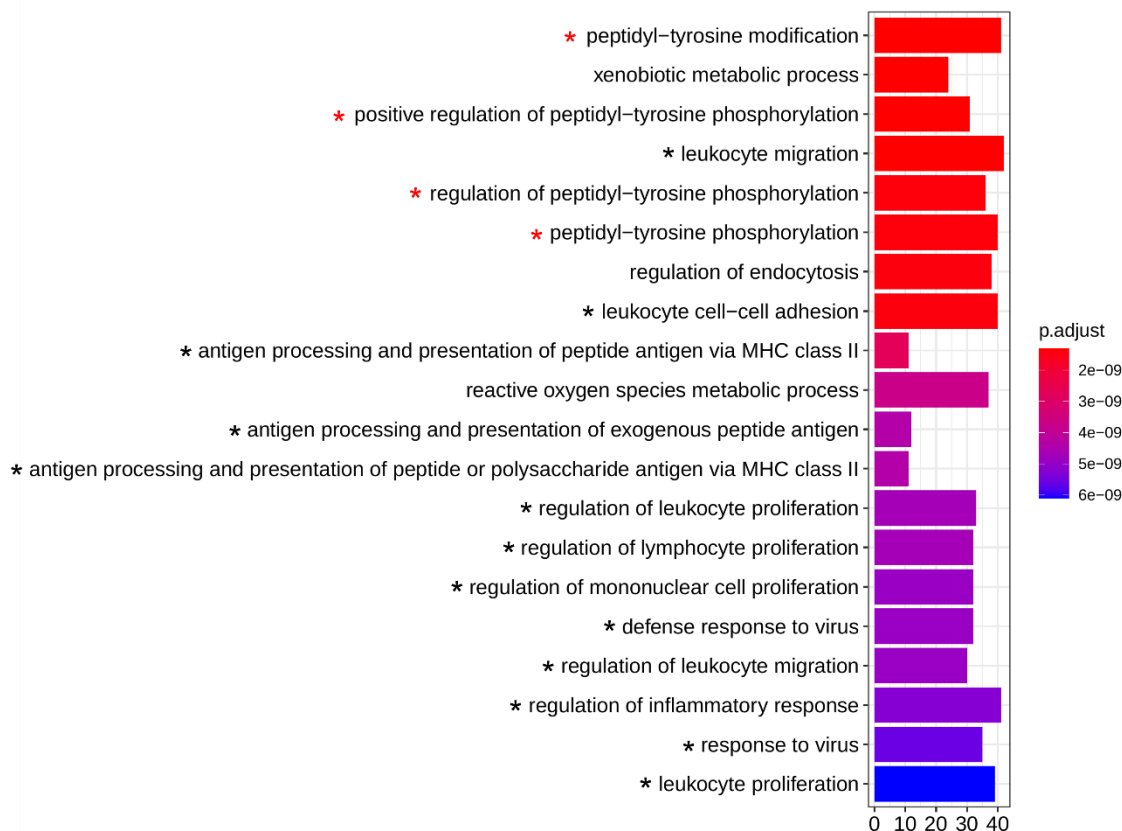Figure 2.4. Top 20 GO biological processes of the EF(Veh. v PCB126) comparison. Biological GO processes were determined by R package clusterProfiler where DESeq2 differential expression analysis results were implemented for this pairwise comparison. Red '*' signifies that GO term falls under peptidyl-tyrosine modification branch of GO tree. Black '*' signifies that GO term is affiliated with an immunological process.

Next, we further investigated the top GO process term "peptidyl-tyrosine modifications" and its affiliated terms found in Figure 2.4 by MetaCore software analysis. A network was built around the GO process term "peptidyl-tyrosine modifications" and is placed in Supporting Figure S6. Several observations were noted such as the high induction of *Atf3*, which was retrospectively confirmed in our characterization study (Chapter II). Other observations include a mainly downregulation of mitogen activated protein kinase (MAPK) genes, and the induction of several nuclear factor κ B (NFκB) subunit genes. We also observed differential expression in genes involving the JAK-STAT pathway.

Studies have implicated that there may be an underlying relationship between the progression of SLD and altered JAK-STAT signaling axis (Rosenfeld et al., 2007; Brooks and Waters, 2010). Therefore, we wanted to evaluate how our exposure model may have altered the phosphorylation of these two critical proteins. Figure 2.5 displays representative western blot images and their respective quantitative bar graphs. We observed in our two-way ANOVA analyses that EtOH feeding alone had significant effects where JAK2 (Figure 2.5A, Figure 2.5C), STAT5 (Figure 2.5B, Figure 2.5D), and their respective phosphorylated counterparts were decreased, except for p-JAK2/JAK2 ratio. We observed a significant interaction effect where PCB126 decreased p-JAK2 in EtOH-fed mice (Figure 2.5A). EtOH feeding alone mildly increases the p-JAK2/JAK2 ratio, although this effect was not statistically significant. However, PCB126 exposure seems to mitigate the p-

JAK2/JAK2 ratio, down to pair-fed ratio levels. This signifies that PCB126 may be

altering this signaling axis at the p-JAK2 level to impair signaling.
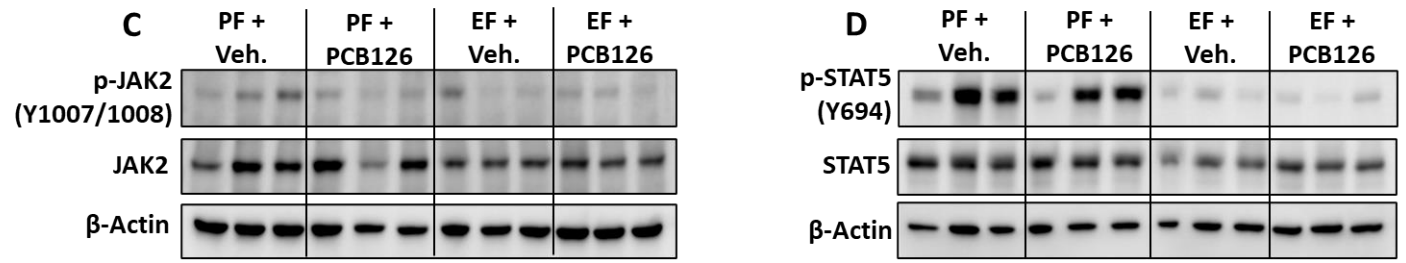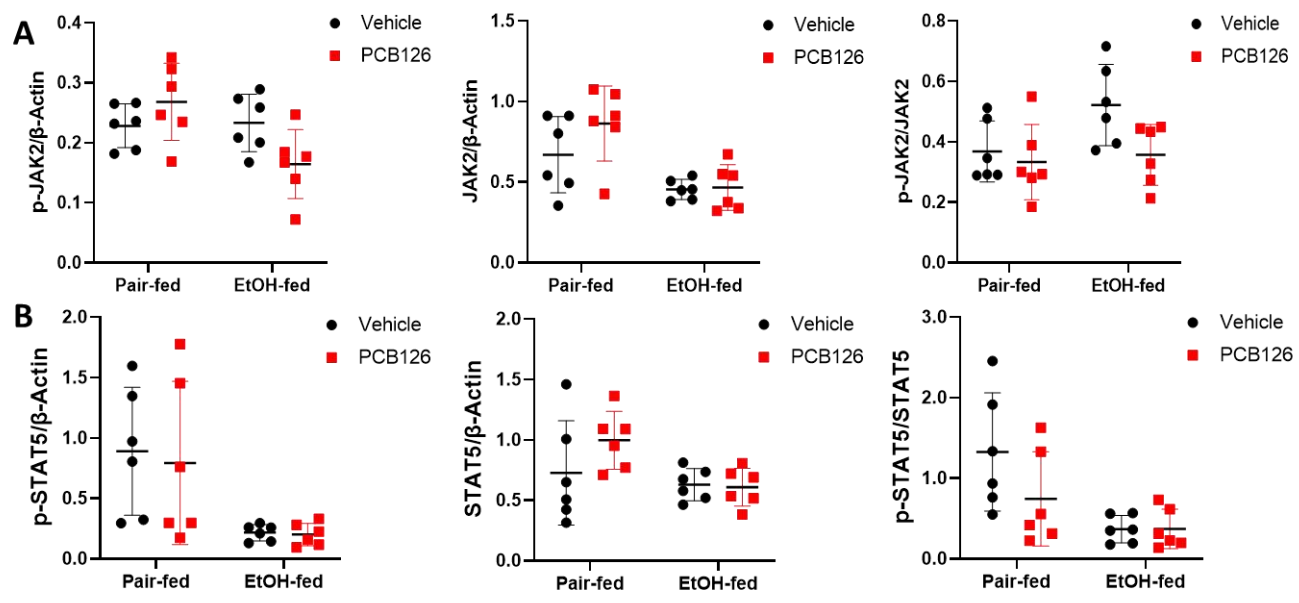
Outcome	EtOH	PCB 126	Interaction	Pair-fed (Veh. vs. PCB 126)	EtOH-fed (Veh. vs. PCB 126)	Veh. (Pair-fed vs. EtOH-fed)	PCB 126 (Pair-fed vs. EtOH-fed)
p-JAK2	**0.0319**	n.s.	**0.0199**	n.s.	n.s.	n.s.	**0.0133**
JAK2	**0.0006**	n.s.	n.s.	n.s.	n.s.	n.s.	**0.0064**
p-JAK2/JAK2	n.s.	**0.0480**	n.s.	n.s.	n.s.	n.s.	n.s.
p-STAT5	**0.0019**	n.s.	n.s.	n.s.	n.s.	n.s.	n.s.
STAT5	**0.0383**	n.s.	n.s.	n.s.	n.s.	n.s.	n.s.
p-STAT5/STAT5	**0.0035**	n.s.	n.s.	n.s.	n.s.	**0.0151**	n.s.

Figure 2.5. Western blot analysis of p-JAK2, JAK2, p-STAT5, and STAT5. Quantitative and qualitative western blot analysis of p-JAK2, JAK2, and p-JAK2/JAK2 ratio (**A**/**C**) and p-STAT5, STAT5, and p-STAT5/STAT5 ratio (**B**/**D**). A complete list of P-values, as determined by two-way ANOVA and Tukey's post-hoc test, is provided in the accompanying table. EtOH, ethanol; Veh., vehicle; p-JAK2, phosphorylated Janus kinase 2; JAK2, Janus kinase; p-STAT5, phosphorylated signal transducer and activator of transcription 5; STAT5, signal transducer and activator of transcription 5.

PCB126 Further Reduces Essential Metal levels in EtOH-fed Mice

MetaCore analyses revealed that several GO Molecular Function processes contained 'ion binding', 'metal ion binding', 'transition metal ion binding', and 'zinc ion binding' were highly significant (Supporting Table S6). Essential metals play a vital role in normal physiological functions within the cell. Specifically, various metals act in catalytic functions, protein stabilization, redox transition, and participating in membrane potential (Jomova et al., 2022). Other enriched GO Molecular Functions of note include 'protein binding', 'binding', ' catalytic activity', and 'enzyme binding'. Thus, we wanted to assess how our model impacted hepatic essential metal levels (Table 2.1). Overall, EtOH-fed mice exposed to vehicle exhibited a significant decrease in K, Mg, Co, Cu, Zn, Mo, and Se. EtOH feeding did however significantly increase Na ~40% and Mn ~20% relative to the pair-fed+Veh. group. PCB126 significantly decreased hepatic K, Mg, Co, and Zn levels in pair-fed mice. By our statistical analysis, the only essential metal to display an interaction event was Na, where EtOH elevated levels to 1062.54 µg/g liver from 758.07 µg/g liver, and PCB126 mitigated these levels down to 767.34 µg/g liver (p=0.0049). Importantly, metals that were further reduced by PCB126 in EtOH-fed mice were Mg (p=0.0066), Co (p<0.0001), and Zn (p=0.0036). Finally, the most dramatic change is observed when comparing the pair-fed+Veh. v the EtOH+PCB126 group where all metals were significantly reduced in a range from 31.9% to 49.2%, except for Mn which was significantly increased by 25.1%, Fe and Na were not statistically significant (Supporting Figure S7).

Table 2.1. ICP-MS analysis of hepatic metal levels.

Group Mean of Metals (µg/g liver)				
Metal	PF+Veh.	PF+PCB126	EF+Veh.	EF+PCB126
Sodium (Na)	758.07±112.37	777.36±148.46	1062.54±217.16	767.34±281.80
Potassium (K)	3229.24±222.32	2877.95±217.17	2204.14±378.59	2102.22±351.40
Magnesium (Mg)	273.90±16.08	244.24±14.44	195.16±27.36	168.71±21.82
Calcium (Ca)	21.18±6.59	17.03±5.48	17.34±7.92	13.48±9.36
Iron (Fe)	83.35±11.06	87.79±22.85	81.82±16.59	70.48±9.27
Manganese (Mn)	1.15±0.138	1.34±0.153	1.40±0.315	1.45±0.262
Cobalt (Co)	0.05±0.006	0.04±0.004	0.04±0.008	0.02±0.004
Copper (Cu)	6.62±0.889	6.30±0.712	4.93±1.23	4.34±0.647
Zinc (Zn)	32.42±3.35	28.46±2.89	25.71±5.48	20.76±3.18
Molybdenum (Mo)	0.80±0.108	0.81±0.095	0.49±0.114	0.47±0.066
Selenium (Se)	1.29±0.160	1.17±0.138	0.99±0.261	0.88±0.150

Outcome	EtOH	PCB 126	Interaction	Pair-fed (Veh. vs. PCB 126)	EtOH-fed (Veh. vs. PCB 126)	Veh. (Pair-fed vs. EtOH-fed)	PCB 126 (Pair-fed vs. EtOH-fed)
Na	0.0081	0.0128	0.0049	n.s.	0.0015	0.0010	n.s.
K	<0.0001	0.0068	n.s.	0.0163	n.s.	<0.0001	<0.0001
Mg	<0.0001	<0.0001	n.s.	0.0019	0.0066	<0.0001	<0.0001
Ca	0.0095	0.0060	n.s.	n.s.	n.s.	n.s.	n.s.
Fe	0.0303	n.s.	n.s.	n.s.	n.s.	n.s.	n.s.
Mn	0.0072	n.s.	n.s.	n.s.	n.s.	0.0367	n.s.
Co	<0.0001	<0.0001	n.s.	0.0020	<0.0001	0.0012	<0.0001
Cu	<0.0001	n.s.	n.s.	n.s.	n.s.	<0.0001	<0.0001
Zn	<0.0001	<0.0001	n.s.	0.0069	0.0036	<0.0001	<0.0001
Mo	<0.0001	n.s.	n.s.	n.s.	n.s.	<0.0001	<0.0001
Se	<0.0001	0.0222	n.s.	n.s.	n.s.	0.0004	0.0005

Values are represented as group means (µg metal/g liver) ±SD with an alpha level set to 0.05. A complete list of *p*-values, as determined by two-way ANOVA and Tukey's post-hoc test, is provided in the accompanying table. Na, sodium; K, potassium; Mg, magnesium; Ca, calcium; Fe, Iron; Mn, manganese; Co, cobalt; Cu, copper; Zn, zinc; Mo, molybdenum; Se, selenium.

Discussion

With increasing research providing convincing evidence on the negative impact of environmental pollutants on MASLD, it is pertinent to examine toxicant effects in alcohol-associated liver pathology. Excessive alcohol consumption has been shown to impact a wealth of molecules such as nucleic acids, proteins, cofactors, and micronutrients (Beier et al., 2011; Medici and Halsted, 2013; He et al., 2022; Hardesty et al., 2022). Thus, it was no major surprise to find that EtOH feeding caused more total DEGs and acted on more GO processes relative to PCB126 exposure. While PCB126 did cause specific variations in DEGs and enriched GO processes, this exposure was a single moderate to high dose at the beginning of study to mimic a lifetime of human exposures and activate the murine AhR. PCBs have shown to impact similar genes, but not previously in the context of EtOH co-exposure. Thus, this study is innovative in that toxicant effects in the context of ALD have not been previously studied and the concomitant effect on the transcriptome and metallome are unknown for these types of exposures.

The PCA plot (Figure 2.1) indicated that our pair-fed+PCB126 group only slightly deviated in terms of variance from the pair-fed+Veh. group by increasing along the y-axis. This would corroborate with our findings in Figure 2.2, where there are only 503 DEGs in the total count in the PF(Veh. v PCB126) comparison. While this total DEG count is seemingly a high number, it is relatively the smallest change respective to all other group comparisons. Importantly, the EtOH+PCB126 group is completely unique in variance relative to all other comparisons, including the

EtOH-fed+Veh. group. While EtOH feeding seems to be the foremost driver of toxicity, this is signifying that the transcriptome is significantly altered with respect to PCB126 exposure in EtOH-fed mice. These transcriptional changes induced by PCB126 in EtOH-fed mice, in part, may explain some of the phenotypes observed in our characterization study (Chapter II). For instance, relative liver weight (Figure 1.1B), quantified hepatic triglycerides (Figure 1.1C), and increased *Cd36* expression (Figure 1.4B), were exacerbated due to PCB126 exposure. Based on previous and current findings however, these phenomena may be due to an additive effect on the transcriptome to enhance liver disease between the chosen model toxicant and EtOH. This does not imply that other chemical exposures may not synergistically enhance ALD, but toxicokinetics of pollutants must be considered when developing future alcohol-plus-toxicant models or importantly, human epidemiology studies. For example, in a model we previously performed, EtOH feeding significantly altered the distribution and bioavailability of perfluorooctane sulfonate (PFOS) (data not shown). For the current study, the dioxin-like PCB utilized can freely diffuse through the plasma membrane, negating this altered kinetic effect (Alvarado et al., 2023).

Out of the top six enriched GO processes found in our EF(Veh. v PCB126) comparison, four of these processes consisted of 'peptidyl-tyrosine modifications' (Figure 2.4). Being that peptidyl-tyrosine modifications are the among most significant processes, we decided to investigate phosphorylation in the context of signaling. Previously, our group performed phosphoproteomics on mouse livers that were exposed to Aroclor 1260 (Hardesty et al., 2019a). This study

demonstrated that Aroclor 1260, a non-dioxin like PCB mixture, reduced hepatic phospho-peptide levels by ~25%. Though, PCB126 is a dioxin-like congener, we hypothesize a similar reduction of phospho-peptides would occur. Additionally, our group has demonstrated that PCB126 and PCB153 have putative bindings sites on the epidermal growth factor receptor (EGFR), a receptor tyrosine kinase (Hardesty et al., 2018). Further, Gadupudi et al. demonstrates reduced phosphorylation of hepatic cAMP response element-binding protein (CREB) due to PCB126 exposure (Gadupudi et al., 2018). Other molecular actions PCB126 exposure may have on phosphorylation is the reduction of kinase availability or limiting the production of ATP. Our group's previous proteomics study demonstrated that PCB126 downregulates various kinase's expression (Jin et al., 2020). Another study demonstrated that dioxin reduces hepatic mitochondrial ATP levels by approximately 60% (Aluru et al., 2017). PCB126 is the most potent, dioxin-like PCB congener, as its toxic equivalency factor (TEF) to dioxin is equal to 0.1 and may have a similar impact (Van den Berg et al., 2006).

With regards to activity, many kinases are influenced by metals through direct binding or altered extracellular composition (Jomova et al., 2022). Divalent cations such as Mg and Ca have shown to participate in phosphoryl transfer and stabilization of protein kinase A (Knape et al., 2015). Our ICP-MS results depict that Mg was significantly decreased by EtOH and PCB126 in all comparisons and while Ca was not significant, levels were still trending down. Besides kinase activity, a prominent and well known metalloprotein are zinc-finger proteins. Zn is capable of forming bonds with amino acid residues to form stable tertiary

complexes, which is necessary for an abundance of molecular functions (Rakhra and Rakhra, 2021). For example, zinc fingers contribute to an array of processes from cell differentiation to intermediary metabolism regulation (Cassandri et al., 2017; Liu et al., 2017). Additionally, zinc fingers are also known to play diverse functions in the development of liver disease (Li et al., 2020). Specifically, Zn deficiency has shown to promote alcohol induced liver injury, whereas zinc supplementation attenuates injury (Zhong et al., 2013; Zhou et al., 2005). Our study demonstrated that Zn was depleted by EtOH and was further reduced by PCB126 exposure (Table 2.1). Notably, both transcriptomic and metallomic investigations similarly converged on the loss of essential metals, and thus metal binding. Further studies are needed to understand how PCB126 augments EtOH-mediated zinc depletion.

JAK-STAT signaling was highlighted in our GO processes, thus we performed western blotting and confirmed altered phosphorylation levels. Our western blot statistical analysis revealed a significant interaction effect where PCB126 exposure decreased the phosphorylation of JAK2 in EtOH fed mice (Figure 2.5). The ratio of p-JAK2/JAK signifies that p-JAK2 may usually be more prevalent in EtOH feeding; however, PCB126 decreased its abundance, implying that signaling may be disrupted or unable to compensate. Meanwhile, p-STAT5 and STAT5 levels were overall decreased only by EtOH feeding. Previously, studies have shown that disruption of the growth hormone (GH)-JAK2-STAT5 signaling axis may contribute to steatosis and SLD development (Mueller et al., 2012; Kaltenecker et al., 2019). Activation of this signaling axis typically results in the

expression of various genes involved in growth, cell survival, and importantly, regulation of lipid and carbohydrate metabolism. The impaired phosphorylation of JAK2 by PCB126 and STAT5 by EtOH would align with our previous data where lipid retention and defective carbohydrate metabolism was prevalent. However, the disruption of one signaling axis is likely not the only contributing factor to enhanced dyslipidemia, steatosis, and glycogen depletion. Future investigations are required to expand on this signaling axis as other proteins certainly interact with up- and downstream effectors that modulate metabolism.

One canonical target of the GH-JAK2-STAT5 pathway is insulin like growth factor 1 (IGF1), which is largely involved in a feedback regulation of GH but also influences metabolism (Al-Samerria and Radovick, 2021). We found that the expression of *Igf1* was significantly decreased due to EtOH feeding only (Supporting Figure S8). The loss of *Igf1* further signifies the disruption of the GH-JAK2-STAT5 signaling pathway, but importantly is implicated in malnutrition and increased blood insulin (Kasprzak, 2021; Yakar et al., 2001). We observed a similar phenotype in our characterization model (Chapter II), where plasma insulin was increased 3-fold by EtOH feeding alone but was mitigated to about 2-fold by PCB126 exposure in EtOH-fed mice (Gripshover et al., 2022).

Furthermore, a major nuclear receptor and master metabolism regulator is hepatocyte nuclear factor 4 alpha (HNF4α). This transcription factor is known to interact with a wealth of other proteins including PPARα, FXR, FABP1, and even STAT5 (Lu, 2016). HNF4α is largely considered to be decreased from chronic

alcohol use and promotes disease progression (Argemi et al., 2022; Xu et al., 2016; Shirpoor et al., 2018). In contrast, our group has previously demonstrated that PCBs downregulate *Hnf4α* expression, which also exhibits sexually dimorphic responses to these pollutants (Hardesty et al., 2019b; Wahlang et al., 2019c). Contradictorily, our RT-PCR analyses indicate that *Hnf4α* expression is increased about 2-fold solely due to EtOH feeding (Supporting Figure S8). Furthermore, HNF4α may positively regulate albumin's expression after binding to the *Alb* enhancer region; however, albumin's secretion from the liver depends on its phosphorylation status (Yang et al., 2022a; Argemi et al., 2022; Feng et al., 2022). We observed a reduction of albumin liver mRNA and plasma protein (Chapter II); therefore, we must assess hepatic albumin protein in future experiments. Indeed, there must be differential effects by PCB126 and EtOH that jointly disrupt intermediary metabolism and growth signaling mechanisms.

In addition to these three key mechanistic players identified by our approaches, another key mechanism pertinent to this model are differential AhR activation by EtOH and PCB126. AhR is readily activated by dioxin-like species, like PCB126, shown by prototypical target gene induction, *Cyp1a1* and *Cyp1a2*. AhR is not only involved in detoxification processes, but also play important endogenous roles that are ligand specific (Murray and Perdew, 2020; Jin et al., 2021; Tanos et al., 2012; Nguyen et al., 2013; Safe et al., 2020). Interestingly, we observed that EtOH feeding alone significantly induced *Cyp1a1* ~4-fold and *Cyp1a2* ~2.5-fold compared to pair-fed+Veh. control (Supporting Figure S9). EtOH has previously shown to influence AhR activities related to autophagy, hepatic stellate cell

activation, and interact with the microbiome (Kim et al., 2022; Zhang et al., 2012a; Qian et al., 2022). AhR activation by EtOH may be an indirect protective effect that stem from EtOH's ability to dysregulate metabolites and induce oxidative stress responses (Dong et al., 2021). Other studies have demonstrated that AhR activating gut-derived indole metabolites are protective for the liver in ALD (Kouno et al., 2023). One endpoint we did not study in this model is intestinal dysbiosis by EtOH, a clinical hallmark of ALD. Therefore, AhR activation by EtOH in the current model may be intestinal-mediated feedback signaling to the liver to modulate disease pathogenesis. Overall, AhR activation by both PCB126 and EtOH followed by their respective dysregulation of signaling needs to be further studied. An interesting effect AhR may have on the aforementioned GH-JAK2-STAT5 signaling axis is that AhR activation leads to a suppression of growth hormone receptor (*Ghr*) and *Jak2* expression, which are both regulated by HNF4α (Nukaya et al., 2004; Nault et al., 2017).

While this study is unique in that it is investigating interactions of EtOH feeding and pollutant exposure, we must report its limitations. Besides the limitations stated in our characterization study (Chapter II), RNA-Seq and our other described methods have clear pitfalls. First, total RNA was extracted by the commonly used phenol-chloroform extraction method, resulting in possible sample contamination with various salts, dNTPs, and phenol and thus inaccurate sequencing. However, we performed DNase digestion and XP bead cleaning of samples to minimize contaminates, which are explained in the *Materials and Methods* section of this chapter. Future RNA-Seq endeavors will utilize spin column methods of RNA

extraction. Furthermore, quality assessment of reads sequenced ranged from ~6 million to 133 million with alignment rates between 93% to 98%. Lower aligned reads (6 to 22 million) were most frequently found throughout all EtOH-fed mice, but the lower alignment rates (93% to 95%) were found among the pair-fed mice. This could introduce sample bias or undetected genes by means of inadequate rRNA depletion. Additionally, our MetaCore analyses could be skewed in that MetaCore is a database consisting of inputted data from other pre-existing RNA-Seq studies. As this study is novel in the context of model design and the absence of previously sequenced data pertaining to this model, MetaCore is thus only applicable in a sense that it is suggestive to activated pathways and gene expression.

Conclusion

While public knowledge is becoming increasingly aware of environmental exposure threats, it is simultaneously becoming important to acknowledge lifestyle interactions. Researchers are currently developing human exposome studies to incorporate and consider interactions between pollutant exposures and alcohol consumption. While this study does not contain human data, our multi-omics approach suggests that hepatic phospho-proteins and metal levels are subject to enhanced modification by PCB126 in the context of ALD. Furthermore, recent research has indicated that AhR likely participates in more homeostatic maintenance functions than previously thought. AhR certainly has ligand specific effects, and its importance in ALD pathology warrants additional studies. The

84

present study's multi-omics approach demonstrated a significant alteration of the transcriptomic landscape and further reduction of hepatic essential metals by PCB126. RNA-Seq analyses and western blotting suggest that phosphorylation may also be impacted in this rodent ALD model by PCB126. Enriched transcripts influenced by our exposure paradigm may be attempting to promote modifications at the protein level or are dysregulating kinase or phosphatase activities. Future studies will need to elucidate changes to the phosphoproteome to better understand how excessive alcohol feeding with and without PCB126 exposure alters these effector proteins. Finally, therapeutic studies are warranted to determine if dietary supplementation with depleted trace metals attenuates liver disease in co-exposed mice by balancing essential metal homeostasis.

CHAPTER IV

POLYCHLORINATED BIPHENYL 126 MODIFIES THE HEPATIC
PHOSPHOPROTEOME IN A RODENT ALCOHOL MODEL

Introduction

It is well understood that the liver is a primary toxicological target from a plethora of biological and chemical xenobiotics. Liver disease often manifests along a spectrum of disease states known as steatotic liver disease (SLD). Obesity, excessive alcohol consumption, genetic predisposition, and environmental pollutant exposure are all important risk factors that influence SLD initiation and progression to more severe disease states (Al-Dayyat et al., 2018; Altamirano and Bataller, 2011; Eslam et al., 2018; Wahlang et al., 2013a). Our group has characterized several experimental models that relate to how toxicant exposure can enhance MASLD (Wahlang et al., 2013b; Shi et al., 2019a; Hardesty et al., 2019a; Jin et al., 2020). This exacerbation and metabolic modification effect by environmental toxicants has also been described in human epidemiology studies (Cave et al., 2011; Bassler et al., 2019; Cave et al., 2022; Clair et al., 2018; Werder et al., 2020; Lee et al., 2003). It is not understood how toxicants may modify or enhance another arm of the SLD spectrum, alcohol-associated liver disease (ALD); however, research has demonstrated that cigarette smoking increases cirrhosis development risk with excessive alcohol consumption (Klatsky and Armstrong, 1992; Liu et al., 2009; Dam et al., 2013).

Previously, our group demonstrated that environmental toxicant, polychlorinated biphenyl (PCB) 126, can promote ALD pathogenesis by disrupting intermediary metabolism to enhance steatosis and dyslipidemia (Gripshover et al., 2022). This study was followed by two 'Omics methods to investigate how the transcriptome and metallome may be uniquely modified by PCB126 exposure in EtOH-fed mice. We discovered that PCB126 uniquely modified the transcriptome and 'peptidyl-tyrosine modifications' are the most significant GO biological processes that were detected in our dataset. We also observed depletion of essential metals and enriched GO molecular function processes indicated a loss of metal, ion, and zinc binding. MetaCore analyses suggested several pathways that were acted on, including the JAK-STAT pathway, which has previously been attributed to worsened liver disease (Kaltenecker et al., 2019; Nault et al., 2017). Our group has previously observed that PCBs decrease phospho-peptide levels, alter kinase levels, and has an overall negative effect on protein levels, all of which likely impact signaling (Hardesty et al., 2019a; Jin et al., 2020). Meanwhile, alcohol has shown to have a modulatory effect on protein phosphorylation, but predominately decreases protein levels, likely through damaging the ER and other vital organelles (Singh et al., 2022; Steiner and Lang, 2014; Ji, 2012).

In the current study, we seek to take a comparative, label-free phosphoproteomics approach to better understand how phosphorylation events are altered by our exposure model. We hypothesize that phosphorylated amino acids are significantly decreased by EtOH feeding and further decreased with PCB126 exposure, highlighting the loss of signaling mechanisms. Additionally, we suspect

that differentially impacted phospho-peptides will implicate altered signaling that may play, in part, to altered metabolic phenotype observed in our previous studies.

Materials and Methods

Animal Study

Animal use protocols and procedures were approved by the University of Louisville Institutional Animal Care and Use Committee (IACUC) prior to study initiation. This study utilized tissues harvested from the repeat EtOH+PCB126 model described in Chapter III.

Tissue & Sample Preparation

Liver tissues were harvested during euthanasia and tissue collection and then snap frozen in liquid nitrogen. Samples were then archived in the -80°C freezer until use. For this study, six liver tissues were used from each of our four groups, where diet and exposure status are in a two-by-two array (pair-fed+Veh., pair-fed+PCB126, EtOH+Veh., and EtOH+PCB126). Archived tissues were removed from the -80°C freezer and weighed, then immediately placed in 2% SDS RIPA buffer containing 10uL HALT protease and phosphatase inhibitors per mL of RIPA used (catalog: 78443; ThermoFisher Scientific; Madison, MI). Tissues were then homogenized in this solution followed by rocking at 4°C for 30 minutes. Sample lysates were then centrifuged at 13,000g for 30 minutes at 4°C. Supernatant was collected and protein concentrations were measured by bicinchoninic acid (BCA) protein assay, following manufacturer's protocol (catalog: 23225; ThermoFisher

Scientific; Madison, MI). Lysates were then normalized to 400 ug protein for phospho-peptide preparation.

Phospho-peptide Sample Preparation

Protein lysates were trypsinized at a 1:20 (enzyme:sample) ratio and prepared following ProtiFi's S-Trap™ mini spin column digestion protocol (website: https://files.protifi.com/protocols/s-trap-mini-long-4-1.pdf; ProtiFi; Fairport, NY). Phospho-peptides were enriched with MagReSyn's titanium ion - immobilized metal affinity chromatography (Ti-IMAC) microparticles following ReSyn Biosciences MagReSyn's Ti-IMAC protocol (Bekker-Jensen et al., 2020). Samples were then purified using C18 PROTO™ 300 angstrom Ultra MicroSpin columns. Eluate was frozen at -80°C then dried under a SpeedVac. Dried eluate residue was then stored at -80°C prior to peptide concentration assessment.

Liquid Chromatography for Phospho-peptide Separation

Samples were diluted to 0.05 µg/µl with 2% (v/v) acetonitrile and 0.1% (v/v) formic acid and 4 µl were used for liquid chromatography. Columns used were a 75µm x 15cm, 3µm, 100 angstrom PepMap™ RSLC C18 EASY-spray separating column at 40°C and a 300µm x 5mm, 5µm PepMap™ Neo C18 trap cartridge at 30°C (ThermoFisher Scientific; Madison, MI). A Dionex Ultimate3000 RSLC nano system was used with solvents A) 0.1% (v/v) formic acid in LCMS grade water and B) 0.1% formic acid in LCMS grade acetonitrile. Separation was achieved at 200 nl/min with a 5-minute linear gradient from 5% solvent B to 7.5% solvent B followed

by a 90-minute linear gradient from 7.5% solvent B to 35% solvent B. An EASY-spray source was used to position the separating column emitter 1mm from the ion transfer capillary of the mass spectrometer, which was set to 320°C and 1.8kV.

Mass Spectrometry

After liquid chromatography separation, an Orbitrap Exploris 480 mass spectrometer was used to analyze eluate. Full MS – ddMS2 method with a 3 second cycle time was generated in Xcalibur (v4.5.445.18) operating in positive polarity (ThermoFisher Scientific; Madison, MI). Scan event one of this method attained an MS1 scan for 60,000 resolution, normalized AGC target of 100%, for a scan range of 350 – 1400 m/z. Scan event two obtained dd-MS2 scans for 7,500 resolution and normalized AGC target of 50%, on ions with charged states from 2-6 and a minimum intensity of 8,000 until cycle time completion.

Raw LCMS Data Curation and Analysis

RAW data files were separately searched in PeaksXpro (Bioinformatics Solutions Inc.; Waterloo, ON, Canada) using Denovo, PeaksDB, and PeaksPTM algorithms against the UniprotKB *Mus musculus* canonical protein sequences (proteomics ID: UP000000589) downloaded March 17, 2023. Initially, specified enzyme was semi-specific trypsin with Carbamidomethyl set as a fixed modification and Oxidation and Phosphorylation as variable modifications. Fragment tolerance was 0.02Da and parent tolerance was 15 ppm. Label Free Quantification algorithm was then used with PeaksPTM results utilizing a mass error tolerance of 10 ppm and

90

retention time shift tolerance of 6-minutes. Peptides were accepted at a 1% FDR threshold for consideration by the Label Free Quantification algorithm. A peptide.csv file was exported from this algorithm for data maintenance and curation in Microsoft Excel. One sample part of the EtOH+PCB126 group (EF_PCB3) was determined to be an outlier from overlaid MS total ion current (TIC) traces and was removed from our downstream analyses.

Western Blot Analysis

Approximately 50-100 mg mouse liver tissue was homogenized in RIPA Buffer (100 mg tissue/0.5 mL RIPA). HALT protease and phosphatase inhibitor cocktail was added to this tissue lysate at 10 uL/mL of RIPA buffer used (catalog: 78443; ThermoFisher Scientific; Madison, MI). Whole protein concentration was assessed by bicinchoninic acid (BCA) protein assay, following manufacturer's protocol (catalog: 23225; ThermoFisher Scientific; Madison, MI). Normalized 50ug protein was loaded and separated on 4-15% Mini-PROTEAN TGX Stain-Free gels (catalog: 4568086; Bio-Rad; Hercules, CA). A total of six protein lysates per group (N=24) were used, where two sets of three protein lysates were loaded onto two different gels in a representative fashion to account for possible running and antibody incubation differences. Separated proteins were then transferred to polyvinylidene difluoride membranes (catalog: IPVH00010; Millipore Sigma; Burlington, MA), blocked (catalog: 1706404; Bio-Rad; Hercules, CA), and incubated with primary and secondary antibodies. Primary rabbit monoclonal antibodies PGRMC1 (catalog: 13856S) and β-Actin (catalog: 8457S), were

purchased from Cell Signaling Technologies (Danvers, MA). Donkey-anti-rabbit secondary antibody was purchased from Jackson ImmunoResearch Laboratories Inc. (catalog: 711-035-152; West Grove, PA). Primary and secondary antibody dilutions were performed according to manufacturer's protocols.

Computational and Statistical Analyses

Mass spectral readouts (peptide area) normalized by TIC were uploaded onto the web-based interface MetaboAnalyst (v5.0) R tool. One factor statistical analysis was used where data was filtered by interquartile range at 60% and normalized based on group median. Significant results were then imported into the STRING database to assess functional and physical relationships between proteins (Szklarczyk et al., 2019).

Bio-Rad's Image lab software (v.6.1.0 build 7) was used to assess band intensity. After background subtraction, proteins of interest band intensity were divided by their respective β-Actin band intensity for each sample/column. GraphPad Prism (v.10.0.2) (GraphPad Software Inc.; La Jolla, CA) was employed on Windows using a two-way analysis of variance (two-way ANOVA). Two-way ANOVA was performed where our two factors were diet (pair-fed vs EtOH-fed) and exposure (vehicle vs PCB126). Significance was determined with an alpha level set to 0.05 ($p \leq 0.05$). Tukey's post-hoc test was used to compare different groups for multiple comparisons. A *p*-value table is available for all relevant figures displaying the two-way ANOVA and Tukey's multiple comparison results to designate significance between groups.

Results

Phospho-peptides were primarily altered by EtOH feeding

First, we wanted to characterize the global impact of EtOH and PCB126 on detected phospho-peptides (Table 3.1). After filtering mass spectral data for peptides that contained at least one phosphorylated amino acid, a total of 8550 peptides were detected for 2306 unique proteins. The pair-fed+Veh. group had the highest total count and group averaged phospho-peptides in terms of detection. PCB126 non-significantly decreased these amounts within the pair-fed group. EtOH feeding alone decreased phospho-peptide detection more compared to pair-fed+PCB126, relative to the pair-fed+Veh. group. Finally, the EtOH+PCB126 group had the lowest detection of peptides compared to all other groups. It should be noted that this group contained a significant outlier (EF_PCB3) and may be enhancing the magnitude of phospho-peptide loss. After removing this outlier, the average phospho-peptide detection rates were still lower than all other groups. Independently, EtOH (p=0.0054) and PCB126 (p=0.0168) had significant effects; however, an interaction effect was determined not significant, and our multiple comparisons test for the EF(Veh. v PCB126) comparison was only trending significance (p=0.0899).

Table 3.1. Dataset characterization of detected phospho-peptides for each sample in our four respective groups.

Phospho-peptide Dataset Characteristics				
Sample	PF+Veh.	PF+PCB126	EF+Veh.	EF+PCB126
1	5308	4909	4835	3921
2	5224	5038	4914	4568
3	4832	4662	4845	2232*
4	4700	4871	4583	4427
5	4996	4730	4901	4393
6	4625	4497	4313	4503
Sum phospho-peptides detected	29685	28707	28391	24044 (21812*)
Average phospho-peptides detected	4947.5	4784.5	4731.8	4007 (4362*)
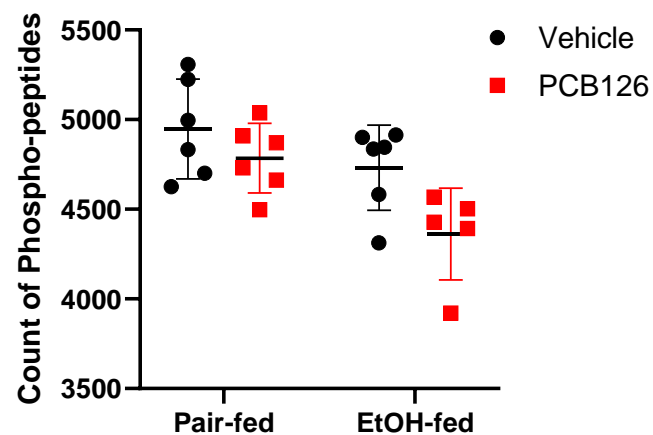
Outcome	EtOH	PCB 126	Interaction	Pair-fed (Veh. vs. PCB 126)	EtOH-fed (Veh. vs. PCB 126)	Veh. (Pair-fed vs. EtOH-fed)	PCB 126 (Pair-fed vs. EtOH-fed)
Count of P-peptides	0.0054	0.0168	ns	ns	ns	ns	0.0444

Peptide areas normalized by TIC were counted if the detectable reading provided a value greater than '0'.

Asterisk (*) designates the consideration of significant outlier EF_PCB3, the sum and average phospho-

peptide detected rows are provided with and without (*) the outlier present. The following figure depicts each detected phospho-peptide, where values are expressed as mean±SD with an alpha level set to 0.05. A complete list of p-values, as determined by two-way ANOVA and Tukey's post-hoc test, is provided in the accompanying table.

Further, we wanted to test our groups global variation in altered phospho-peptides by partial least square discriminate analysis (PLSDA) (Figure 3.1). We observed an overlap between both pair-fed groups with some mild deviation due to PCB126 exposure. EtOH-fed groups were spread out along component 1, more in the negative x-axis direction. Additionally, the EtOH+PCB126 group is slightly diversified from the EtOH+Veh. where samples spread across component 1 away from all other groups. While most EtOH+PCB126 samples are outside of the standard deviation area of all other groups, only one sample was notably varied away from controls (EF_PCB1). Based on mass spectral analyses, the EF_PCB1 sample is not a significant outlier. Overall, EtOH feeding primarily drove differences observed in phospho-peptide levels; however, minor variances were noted from PCB126 exposure by the standard deviation areas.

The MetaboAnalyst R tool is also capable of revealing important features, or peptides that may be driving distinct variations in the PLSDA plot. The highest variable importance in projection (VIP) value pertains to a peptide contained in the progesterone receptor membrane component 1 (PGRC1) protein. Additionally, the second and thirteenth peptide with highest VIP score are also other peptides belonging to PGRMC1. Other interesting peptides of note include fetuin-A (FETUA), a hepatocyte derived glycoprotein upregulated in hepatic steatosis and metabolic syndrome; and heat shock protein 90 A and B (HS90A, HS90B), chaperones known for their stabilizing role in AhR signaling (Dogru et al., 2021; Larigot et al., 2018). Calnexin (CALX), another chaperone, specifically affiliated

with misfolded glycoproteins, appears three times in this important feature list (Cameron et al., 2009).
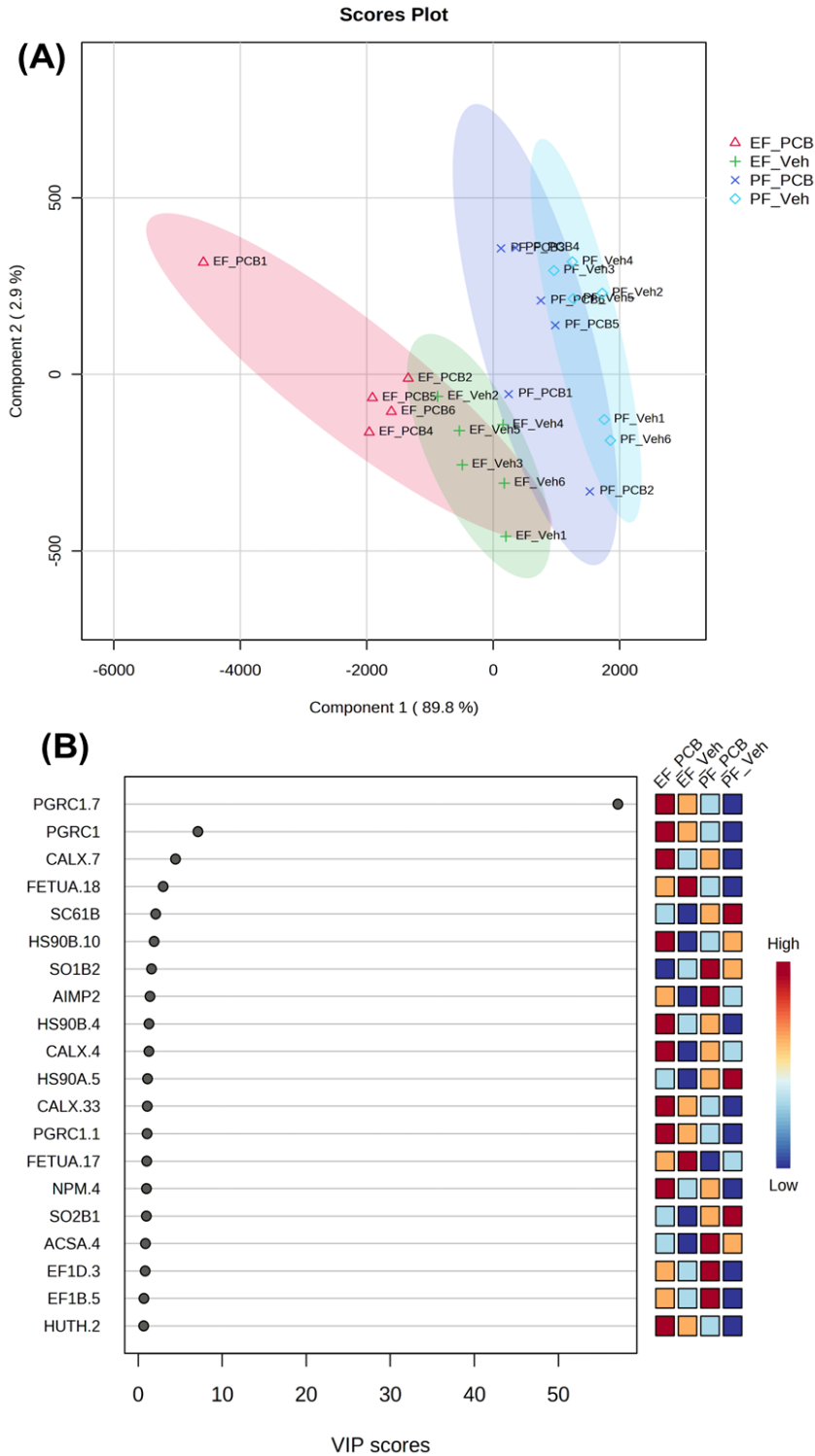
Figure 3.1. Descriptive modeling of PCB126 and EtOH effects on the phosphoproteome. (A) Partial Least Squares Discriminate Analysis (PLSDA) plot

for all samples, excluding outlier EF_PCB3 (N=23) based on peptide area values, normalized by TIC. When imported into MetaboAnalyst, data were filtered by interquartile range for 60% peptides, and normalized based on group median. (B) The top 20 important features identified by PLSDA via MetaboAnalyst are listed where peptides are designated along the y-axis, different identified peptides of the same protein are listed with ".#" following the protein name.

A heatmap was constructed to display the top 50 hierarchical clustered phospho-peptides (Figure 3.2). As alluded to in the previous section, most phospho-peptides are altered by EtOH feeding. Figure 3.2 shows a stark contrast between the top 16 phospho-peptides that were decreased and the bottom 34 that were primarily increased by EtOH feeding. A phospho-peptide belonging to STAT5 (STA5B), which was depicted as decreased protein expression in Chapter III, is also found in this heatmap. Only few phospho-peptides found in the pair-fed group were substantially altered by PCB126 exposure. For instance, two echinoderm microtubule-associated protein-like 4 (EMAL4) phospho-peptides and Proline-rich and coiled-coil-containing protein 2A (PRC2A.10) phospho-peptide were differentially expressed in pair-fed mice. Others that were increased by PCB126 in pair-fed mice, albeit minor, were two glutathione S-Transferase P (GSTP1) phospho-peptides; although, they were decreased with EtOH feeding. Importantly, 12 phospho-peptides were highly differentiated by PCB126, specifically only in EtOH-fed mice. Of note, four PGRC1 phospho-peptides detected were increased by PCB126 in EtOH-fed mice. Other phospho-peptides that were increased include NADPH quinone dehydrogenase 1 (NQO1) and cytochrome P450 family 3, subfamily A, polypeptide 13 (CP3AD). EtOH had the dominant impact on altering most phospho-peptide levels, but PCB126 specifically increased 10 phospho-peptides and decreased 2 phospho-peptides in EtOH-fed mice.
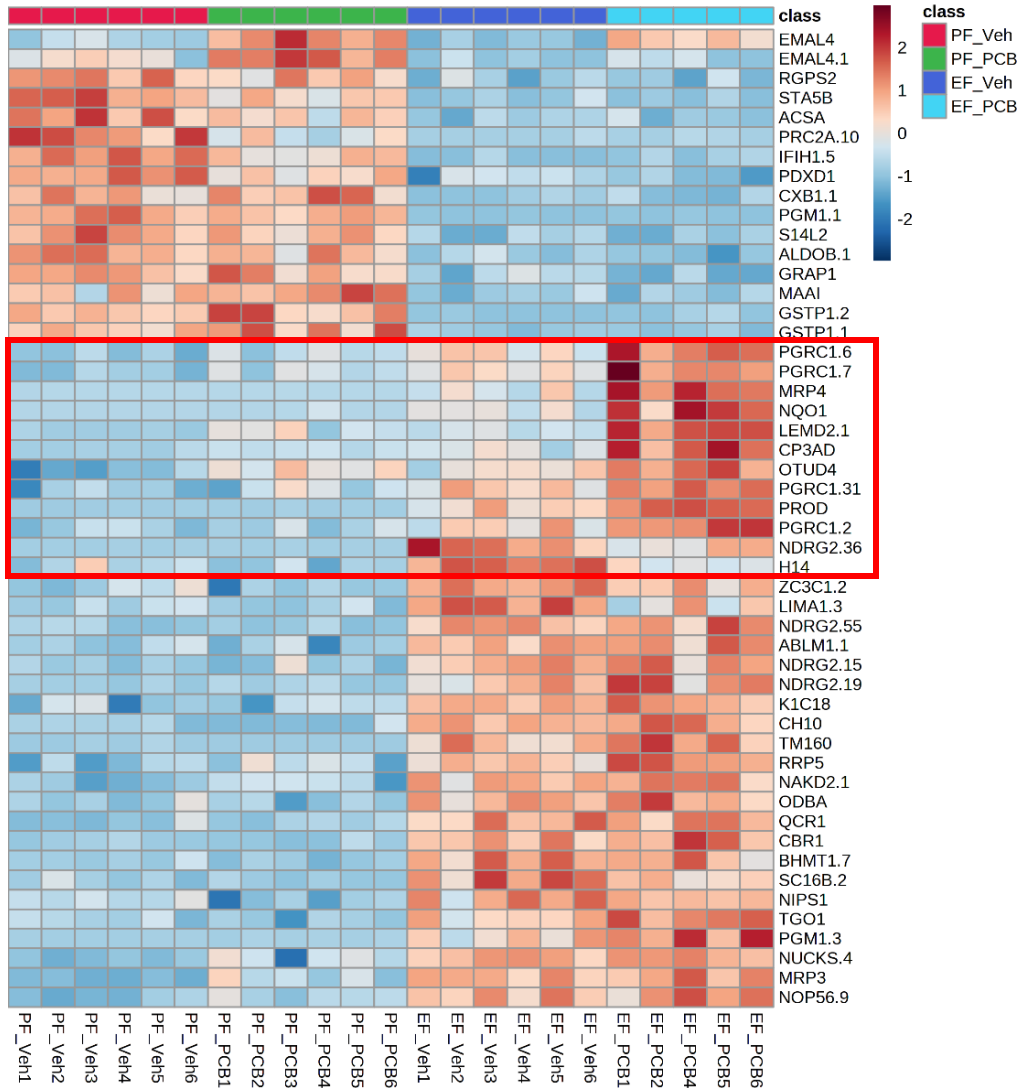
Figure 3.2. MetaboAnalyst Heatmap displaying the top 50 clustered peptides. When imported into MetaboAnalyst, data were filtered by interquartile range for 60% peptides, and normalized based on group median. Different identified peptides of the same protein are listed with ".#" following the protein name. All samples except outlier 'EF_PCB3' were included (N=23).

After filtering our data to just the EtOH-fed groups, we imported this dataset into MetaboAnalyst to evaluate top up- and downregulated phospho-peptides. A volcano plot was generated by t-test for the EF(Veh. v PCB126) comparison for a p-value cutoff of 0.05 (Supporting Figure S10). All significant hits were then uploaded to the STRING database according to increasing or decreasing in abundance. Figure 3.3 displays two networks built around the increasing or decreasing phospho-peptides to elucidate clustered peptides that were impacted by PCB126 in EtOH-fed mice. Unsurprisingly, a network was built around CYP1A2 interacting with various proteins involved in detoxification and oxidative stress. This was not unsuspected as CYP1A2 is a major canonical target of dioxin-like induced AhR activation. Among these top increasing phospho-peptides, it was discovered that PGRMC1 (PGRC1) interacts with CYP1A2, cytochrome b5 type a (CYB5A), epoxide hydrolase 1(EPHX1), and SERPINE1 mRNA binding protein 1 (SERBP1).

Among the decreasing phospho-peptides, GYS2 is present which was confirmed at the expression level in Chapter II. Interestingly, other proteins that are involved in intermediary metabolism are present, i) pyruvate carboxylase (PCX), ii) 3-Hydroxy-3-Methylglutaryl-CoA Synthase 1 & 2 (HMGCS1, HMGCS2), and iii) citrate synthase (CS). Several other proteins in this network are involved with cellular adhesion, migration, and cytoskeletal rearrangement. The bottom unconnected, decreasing network, consists of proteins involved in RNA splicing and processing.
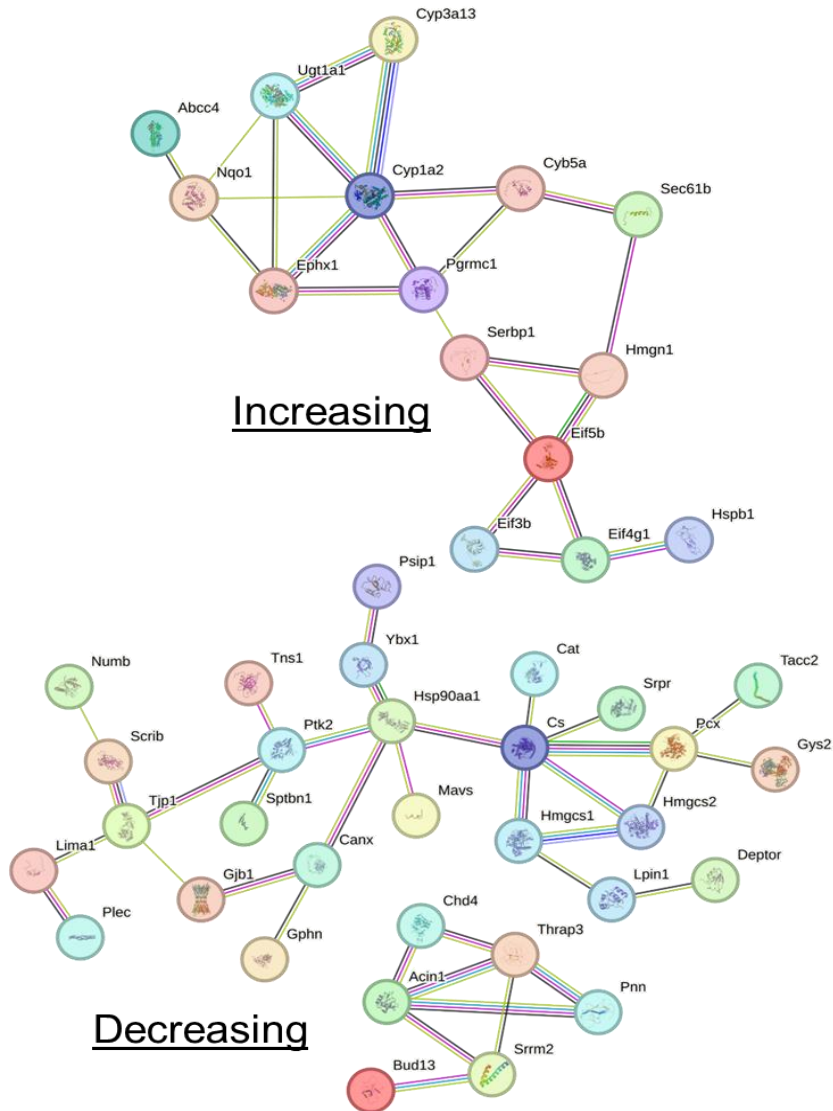
<u>Figure 3.3.</u> Significant, increasing and decreasing clustered phospho-peptides. Phospho-peptides were sorted by fold change that were determined from MetaboAnalyst volcano plot for the EF(Veh. v PCB126) comparison. Top increasing or decreasing phospho-peptides were uploaded into String database for functional protein interaction network generation.

EtOH feeding Increased PGRMC1 expression where PCB126 Promoted its Phosphorylation at S181

PGRMC1 is consistently a top hit in our analyses; thus, we decided to perform western blotting to examine how our model may have modified its abundance (Figure 3.4). We found that overall EtOH feeding increased PGRMC1 abundance while PCB126 had no significant effect. Additionally, we assessed the most prominent phospho-peptide corresponding to this protein, PGRMC1.7, which amino acid sequence presents the phosphorylated serine 181 (S181) residue (EGEEPTVYS(+79.97)DDEEPKDETAR). It was observed that PGRMC1.7 peptide area was significantly increased by EtOH ($p < 0.001$) and PCB126 ($p = 0.0064$). PCB126 significantly enhanced the phosphorylation of PGRMC1.7 in EtOH-fed mice compared to vehicle control; however, this result was not a significant interaction effect.

Outcome	EtOH	PCB 126	Interaction	Pair-fed (Veh. vs. PCB 126)	EtOH-fed (Veh. vs. PCB 126)	Veh. (Pair-fed vs. EtOH-fed)	PCB 126 (Pair-fed vs. EtOH-fed)
PGRMC1	<0.0001	ns	ns	ns	ns	<0.0001	0.0058
PGRMC1.7 peptide	<0.0001	0.0064	ns	0.0299	0.0299	<0.0001	<0.0001
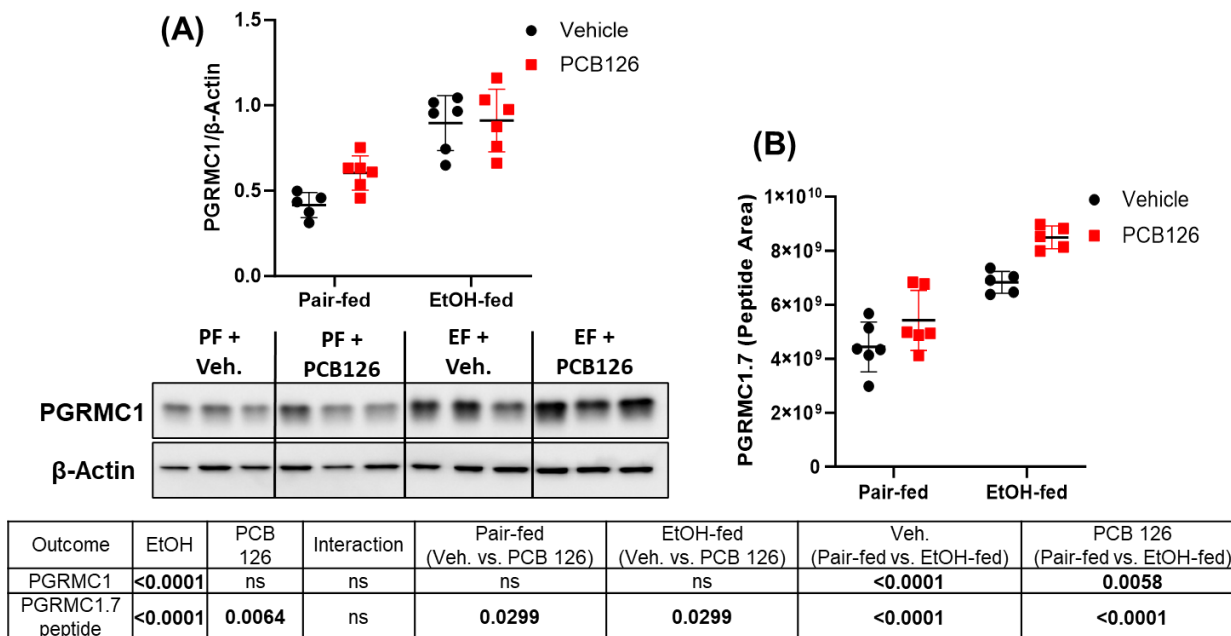
Figure 3.4. Hepatic western blot and phospho-peptide area were analyzed to evaluate the abundance of PGRMC1. (A) Pixel volume intensity graph and respective western blot image for PGRMC1 is displayed. Normalization was performed by dividing PGRMC1 intensity with respective β-Actin intensity. (B) PGRMC1.7 (peptide 7) peptide was exported from our TIC normalized dataset. Individual sample peptide areas were placed into GraphPad prism where we calculated significant differences by two-way ANOVA and Tukey's post-hoc test. Values are represented as mean±SD with an alpha level set to 0.05. A complete list of p-values, as

determined by two-way ANOVA and Tukey's post-hoc test, is provided in the accompanying table. PGRMC1,

progesterone receptor membrane component 1.

Discussion

The present study conducted a comparative phosphoproteomics approach to understand if PCB126 promoted the loss of phosphorylation in EtOH-fed mice. It was observed that total phospho-peptide levels were significantly decreased by EtOH feeding and only trending decreased by PCB126 exposure. While our analyses suggest only trending interaction effects by EtOH+PCB126, there is currently not enough evidence to propose that PCB126 significantly promotes EtOH-induced loss of phosphorylation. However, based on the mean counts and clustering of samples, approximately 700 phospho-peptides less were detected in the EtOH+PCB126 group compared to EtOH+Veh. (Table 3.1). The global effects by which this model acts on the phosphoproteome are affected more by EtOH feeding whereas, specific phospho-peptides were impacted by PCB126 exposure. Figure 3.1 PLSDA plot displays more robust separation of groups by EtOH feeding and only minor shifts in the standard deviation area by PCB126 exposure. It may be that PCB126 limited the phosphorylation of peptides as previously alluded to, but it is just as likely that protein synthesis is reduced (Hardesty et al., 2022; Hardesty et al., 2019a). This is evident in Chapter II where albumin, a protein synthesized in the liver and the most abundant protein in circulation, is severely decreased in the EtOH+PCB126 group relative to controls (Sun et al., 2019). It is known that albumin secretion is mediated by phosphorylation, but interestingly, our data depicts that albumin is more highly phosphorylated in the EtOH+PCB126 group compared to all other groups (data not shown). Inspecting the total proteome

is indeed critical to understanding how our model impacted proteins translation and their respective modifications.

Nevertheless, some important features were observed in this label free quantitative approach. Foremost, our MetaboAnalyst assessment illustrated that PGRMC1 phospho-peptides were more abundant in EtOH+PCB126 groups than all other groups. PGRMC1 is a multifunctional receptor that binds and associates with various of other molecules including several cytochrome P450's and EGFR (McGuire et al., 2021; Lee et al., 2021). This non-canonical progesterone receptor protein has been implicated in steroid signaling, autophagy, and cell cycle regulation (Sabbir, 2019). Recently, PGRMC1 has also been observed to take part in various metabolic signaling pathways including carbohydrate and lipid metabolism (Kaia et al., 2018; Thejer et al., 2020). While this protein was the most prominent 'Important Feature' detected by the PLSDA plot, it may have an underappreciated role in dysfunctional metabolic-associated liver pathology.

Published studies have illustrated that PGRMC1 may play a protective role against hepatic steatosis and oxidative stress by regulating lipogenesis and limiting acetaldehyde levels (Lee et al., 2018; Jo et al., 2023). Interestingly, PGRMC1 has also been linked to glucose regulation where progesterone and the insulin receptor interact with PGRMC1 to influence glycolysis and gluconeogenesis (Lee et al., 2020; Thejer et al., 2020). The specific S181 residue that was more highly phosphorylated in our data resides on the C-terminal end and is highly conserved between species (Hehenberger et al., 2020). Several studies have identified

casein kinase 2 (CK2) as a major kinase that phosphorylates PGRMC1 at S181, which may have negative consequences at other phospho-sites, such as tyrosine 180 (Y180) (Hehenberger et al., 2020; Cahill et al., 2016). However, studies using CK2 knockdown models demonstrated that S181 phosphorylation status was not affected, so other kinases likely phosphorylate this site (Franchin et al., 2018). According to Massachusetts Institute of Technology Scansite 4.0 predictive web-based tool, there are at least six kinases that interact with Y180, including PI3KR1 (p85 subunit), and two kinases that interact with S181 (Obenauer et al., 2003) (Supporting Table S7). One phosphoproteomic study showed that mitogen-activated protein kinase 14 (MAPK14/p38) phosphorylates PGRMC1 at this site, where p38 may be acting in concert with PGRMC1 to mediate oxidative stress responses (Knight et al., 2012; Feng et al., 2019).

Both PGRMC1 Y180 and S181 reside in a Src homology 2 (SH2) binding domain, and our data suggests that S181 is highly phosphorylated, but Y180 was not (data not shown). Y180 is an upstream, regulatory motif in metabolism regulation which interacts with the phosphoinositide 3-kinase (PI3K) and protein kinase B (AKT) pathway (Bashar et al., 2019; Willibald et al., 2017; Cahill and Neubauer, 2021). The phosphorylation of S181 could be sterically hindering the activity of Y180 and preventing regulatory PI3K/AKT signaling. Curiously, another study has demonstrated that PGRMC1 may be an upstream regulator of JAK2 expression, albeit in neuronal tissue (Adams, 2015). However, more work is required to understand the specific regulatory action of PGRMC1 on the array of pathways it acts on.

PGRMC1 has gained more attention in breast cancer research where most studies are implicating its targetable therapeutic role (Pedroza et al., 2020; Zhang et al., 2022). PGRMC1's role in altering metabolism may lie in its upstream interactions with insulin receptor, EGFR, or glucagon-like peptide-1 receptor (GLP1R) to impact downstream PI3K-AKT signaling (Pedroza et al., 2020; Zhang et al., 2022; Cao et al., 2021; Zhang et al., 2014). Importantly, the carbohydrate metabolic disturbances noted in Chapter II could be a result from PGRMC1 dysregulation *via* PI3K-AKT pathway. Cao et. al. notes that overexpression of PGRMC1 led to decreased glucose and glucagon levels followed by decreased gluconeogenesis and increased glycogenesis (Cao et al., 2021).

Our label-free quantitative approach showed that AKT phosphorylation is primarily decreased only by EtOH-feeding but GSK3 is decreased by PCB126 in EtOH-fed mice (Supporting Figure S11). Decreased GSK3 phosphorylation would promote its activation and therefore deactivate GYS2 by phosphorylation; However, our data shows that GYS2 is highly under phosphorylated in the EtOH+PCB126 group, which promotes glycogen synthesis (Supporting Figure S11). Differential upstream insulin signaling likely contributes to the phenotypic differences observed in Chapter II, where glycogen synthesis is promoted but either i) cannot sufficiently compensate for glycogen loss or ii) EtOH-induced decreased mRNA is limiting GYS2 synthesis. We noted another kinase from Figure 3.2 involved in glucose regulation, phosphoglucomutase 1 (PGM1) (Supporting Figure S11). PGM1 lost phosphorylation in response to PCB126 exposure but more severely in EtOH-fed mice. An interaction effect was observed where phospho-peptide levels were

further reduced by PCB126 in EtOH-fed mice. PGM1 can be phosphorylated by glucose 1,6-bisphosphate in the presence of magnesium (Stiers et al., 2016). EtOH and PCB126's decrease of PGM1 phosphorylation and hepatic magnesium (Chapter III) likely contributes to dysfunctional carbohydrate metabolism where glucose 1,6-bisphosphate is a major regulator (Neumann et al., 2022; Carreras et al., 1986).

While this study builds on our novel model and contributes to our ongoing hypotheses, we must be transparent and report the study limitation. Foremost, a major limitation is that our 'Omics analysis only evaluated phosphorylated peptides and not the total proteome. This is a limitation because it is likely that protein translation was globally impacted, making it difficult to interpret whether only phospho-protein levels or total proteins levels were impacted by our exposure paradigm. Certainly, future investigations will need to incorporate the total proteome to understand how this model impacted proteins on the total and post-translational level. Nevertheless, this comparative phosphoproteomic approach was used for each group comparison and gave us insight to our hypothesis, developed in Chapter III. Additionally, this study utilized data from label-free protein quantification. While label-free quantification has inherent advantages, it is limited based on mass spectral reliability and possible issues with sequence coverage and comparing samples within a single group. Finally, much of our analyses rely on curated data from online databases. While these online tools are certainly useful, they rely on previously performed experiments and little to no studies have been performed evaluating PCB effects in EtOH-fed mice.

Conclusion

While we observed an overall loss of phospho-peptides by EtOH feeding, these levels were not significantly reduced by PCB126, by statistical interaction. However, it was revealed that mean phospho-peptide levels were numerically reduced by PCB126 in EtOH-fed mice. PGRMC1 phospho-peptide containing S181 was a consistent top feature in our analysis, where previous research has shown this post-translational status to regulate various metabolic pathways including glycolysis and gluconeogenesis. Carbohydrate metabolism is heavily regulated by reversible phosphorylation of proteins, and the dysregulation of these proteins by altered phosphorylation status indeed contributes to metabolic disruption. Additionally, several key enzymes in carbohydrate metabolism rely on metals as a binding cofactor to mediate phosphoryl transfer, and we found that several of these metals were depleted (Chapter III). As observed in Chapter II, glycogen stores were significantly reduced in EtOH+PCB126 mice, and curiously, key enzyme transcripts that regulate glycolysis and gluconeogenesis were primarily decreased. Additional studies are warranted to elucidate altered phospho-PGRMC1 effects on downstream pathways involved in cell survival and energy metabolism.

CHAPTER V

MAJOR FINDINGS AND COMPREHENSIVE CONCLUSIONS

Dissertation Objective and Specific Aims

Various POPs have demonstrated to induce significant organ injury and disease,
particularly the liver as it is a primary toxicological target. These chemicals are
often thermodynamically stable and resistant to degradation. Thus, their
persistence results in inevitable human exposures and likely interacts with lifestyle
factors that ultimately influence health and wellbeing. Nutrition is one substantial
factor in daily human life, and our group has previously demonstrated that POPs
can enhance diet-induced liver dysfunction. A major lifestyle factor in question that
has shown to induce liver injury and disease is excessive alcohol consumption.
Alcohol beverages have coexisted with humans for thousands of years, but the
total understanding of their toxic effects and ability to be modified by external
factors remain to be elucidated. Therefore, we developed a toxicant exposure
model in the context of ALD to study this interaction pathogenesis. As a human
relevant POP and evidence suggests it enhances diet-induced metabolic
dysfunction, PCB126 was chosen as the model toxicant. The alcohol feeding
component of this model was largely based on the commonly used chronic-binge
model which mimics human alcohol-associated hepatitis pathology (Bertola et al.,
2013). The 0.2 mg/kg PCB126 dose selected was a moderate to high

dose relative to human exposures. However, the reason this PCB126 dose was chosen was to ensure sufficient AhR activation, as mouse and human activity vary. Our overall objective was to characterize the rodent hepatic phenotype and identify mechanisms in which alcohol and PCB126 interact through to promote liver disease pathology. To achieve these objectives, we proposed the following Specific Aims for this dissertation project:

1. Develop a rodent alcohol-plus-toxicant model and characterize the hepatic phenotype

2. Perform multiple high throughput 'Omics analyses to suggest mechanisms of action for interacting alcohol and toxicant

> 2a. Following model completion and characterization, RNA sequencing and proteomic approaches will be implemented to identify key genes, proteins, and enriched pathways that are unique in our alcohol-plus-toxicant group

> 2b. Perform validation measures by molecular biology techniques in concert with Aim 2a by evaluating suggested transcripts and proteins

A wealth of previous studies has focused on specific toxicants or mixtures to assess their relative toxicity by both toxicokinetics and -dynamics parameters. More recently, lifestyle factors that certainly influence health and wellbeing are being incorporated into laboratory model systems. This dissertation project sought to examine how our chemical exposures may enhance or modify the development of ALD, which has previously been under explored. Our proof-of-concept studies

have demonstrated that toxicants, in general, may promote ALD pathogenesis. While much of our data suggested that PCB126 acted in an additive manner to ALD toxicity, some endpoints likely are synergistic in nature. For example, measures of hepatic steatosis (liver weight, hepatic triglycerides, H&E staining), lipid metabolism (*Srebf1*, *Apob*), and carbohydrate metabolism (plasma glucose, PAS staining, *Pck-1*, *Pklr*) displayed a statistical interaction with greater magnitude of change.

Major Findings

Studies discussed in Chapter II, III, and IV concentrated on addressing Specific Aims 1 and 2, respectively. The major findings of each experiment are outlined in the proceeding paragraphs.

Chapter II Major Findings

After surveying the literature, we observed that no studies have been conducted that address toxicant effects in alcohol models. Additionally, we determined that the chronic-binge (ten-plus-one) model would be a sufficient foundation for the alcohol component of this project. This was primarily to compare experimental results to other published studies while also considering feasibility. After designing the parameters of the study, we performed the model as planned followed by humane rodent euthanasia and tissue collection for our subsequent analyses.

Foremost, we observed that hepatomegaly and steatosis were enhanced in EtOH+PCB126 mice. We also observed that hepatic triglycerides were further

increased by PCB126 in EtOH-fed mice. Mean body weights were overall stable throughout the study; however, white adipose tissue was significantly decreased by PCB126 in both feeding groups. Regarding hepatic functionality, albumin is a critical protein that accounts for most of the protein content found in circulation. We found that EtOH alone significantly decreased plasma albumin and hepatic albumin mRNA levels ~40% and ~20%, respectively. Importantly, when comparing our control group to the EtOH+PCB126 group, these levels were further reduced to ~50%. While an interaction effect was only nearing significance, a 50% decrease of circulating albumin is a major indicator of liver dysfunction and/or malnutrition.

Dyslipidemia and altered lipid metabolism were our primary endpoint of study as they contribute to SLD development. It was observed that plasma triglycerides and VLDL were increased while HDL was decreased in our EtOH+PCB126 group, signifying dyslipidemia. Relative transcript levels of lipid related genes suggested an overall promotion of hepatic lipids, indicating altered metabolism. Because intermediary metabolism is often dysregulated by excessive alcohol consumption and dioxin-like exposures, we sought to also characterize carbohydrate metabolism. Chiefly, hepatic glycogen and plasma glucose were significantly decreased by our exposure paradigm, while plasma insulin was differentially impacted by alcohol and PCB126. mRNA levels of carbohydrate related genes were generally decreased by alcohol and were significantly modified by PCB126 exposure. Finally, we observed that AhR was activated by PCB126 exposure, while CAR was activated by alcohol feeding. In a reverse manner however, AhR

expression was increased by alcohol whereas CAR expression was increase by PCB126.

Chapter III Major Findings

Upon the completion of our characterization model, we noted the substantial differential effect that alcohol and/or PCB126 on mRNA transcripts. Therefore, we wanted to take a global approach to assessing these changes and performed RNA-Seq to suggest potential mechanisms. Foremost, we observed that the EtOH-fed group had a completely unique population in terms of variance compared to controls. PCB126 significantly altered this variance further to be different from both EtOH-fed and pair-fed groups, signifying a highly modified transcriptome. In concordance with our characterization study, chronic alcohol feeding seems to dominate in terms of transcriptional alterations to the transcriptomic landscape. We observed that the total number of transcript changes were more numerous due to alcohol feeding rather PCB126 exposure. Interestingly, the EF(Veh. v PCB126) comparison had almost double the transcriptomic changes than the PF(Veh. v PCB126) comparison, suggesting underlying interaction events during transcription. Furthermore, our top enriched GO processes indicated that peptidyl tyrosine modifications are most significant in our EF(Veh. v PCB126) comparison. The transcriptome may be uniquely altered to support the modification, primarily phosphorylation, of tyrosine. Our western blot analyses indicated that p-JAK2 was significantly decreased in our EtOH+PCB126 group relative to EtOH+Veh. While our study focused on the JAK-STAT pathway, JAK2 is known to act on other

pathways such as PI3K/AKT and MAPK (Pandey et al., 2022). In addition, the RNA-Seq enriched GO Molecular function analyses revealed several metal or ion bonding that was decreased. Thus, we performed metallomics to quantify hepatic essential metals. We found that most metals were decreased by EtOH feeding; however importantly, we found that critical metals, potassium, magnesium, cobalt, and zinc were further decreased by PCB126 in EtOH-fed mice. Indeed, the loss of these critical micronutrient metals likely promote ALD pathogenesis and decreased liver function.

Chapter IV Major Findings

We found that while phospho-peptide levels were decreased in our EtOH-fed groups, PCB126 did not significantly reduce total phospho-peptide count. Interestingly, the mean phospho-peptide count of the EtOH+PCB126 group was lower, although only trending. After evaluating the phosphoproteome's important features, clustered phospho-peptide heatmap, and volcano plot, a consistent feature that stood out was a PGRMC1 peptide that contained a phosphorylated serine (S181). Phospho-S181 was more pronounced by EtOH feeding in general; however, our statistical analyses revealed that PCB126 further increased this phosphorylation event (p=0.0299). While the phosphorylating kinase is currently unclear, the increased phosphorylation status may be sterically hindering normal signaling mechanisms (Thejer et al., 2020; Cahill et al., 2016). Specifically, by inhibiting Y180 phosphoacceptor residue which is required to promote PI3K/AKT signaling. Interestingly, EtOH feeding increased PGRMC1 protein abundance

while PCB126 increased its phosphorylation, likely through altered kinase or phosphatase activity. PGRMC1 is known to influence signaling that can feed into cell survival and intermediary metabolism regulation (Cao et al., 2021). With upstream disruption of PGRMC1 phosphorylation, the proper utilization of glycogen and production of glucose could be impaired, promoting disease severity. Glycogen storage is critical to maintaining proper energy (ATP) production, and if depleted, can promote non-optimal energy production through alternative mechanisms. For example, excessive lipid oxidation may result in toxic aldehyde generation which can react with proteins and nucleic acids to promote disease. Additionally, many catalytic processes, including phosphorylation, require the use of metals as a cofactor. In Chapter III, we demonstrated that metals (magnesium, cobalt, and zinc), were further reduced by PCB126 exposure in EtOH-fed mice. Taken together, modification of phospho-peptides and metal levels can further enhance disease status as these functional molecules are critical to maintain proper signaling.

Strengths of this Dissertation

This dissertation is innovative in that it developed and characterized a novel rodent alcohol model that considers concomitant toxicant exposure. While our studies only performed a single exposure prior to alcohol feeding, the sequence and number of exposures can certainly be modified for future studies. Collectively, our data demonstrates that PCBs can act as a modifying factor in ALD pathogenesis and can be used as a template for future investigations. Additionally, the studies

performed were robust in statistical power where fifteen mice per group were utilized during the study period, and up to six mice per group for our 'Omics approaches. Another strength of this dissertation is our suggestion of a particular mechanism by dysregulated signaling. While more work needs to be done to elucidate these specific interaction mechanisms, enhanced disrupted signaling is likely a key event that contributes to disease.

Another strength of this project resides in the reproducibility of our results. We performed this model twice, once to collect tissue for the characterization study, and again for our 'Omics approaches. Relative organ weights, transcription factor activation, and plasma lipid measures were reproducible or trending towards similar results. Furthermore, many of our results coincide with previously published alcohol or PCB126 studies, such as AhR activation, glycogen depletion, and hepatic steatosis. Therefore, our studies and findings are robust.

Limitations of this Dissertation

Despite the mentioned strengths of this dissertation, we must report the major limitations of our studies. Foremost, this project currently lacks human relevance as there have been minimal reports of enhanced liver disease in human populations due to interacting alcohol consumption and toxicant exposure (Mastrangelo et al., 2004). However, at the completion of this dissertation, institutions are beginning to develop exposome research that are focused within human ALD populations. Human relevant data will be produced over the next few years concerning the impact of the exposome in those who excessively consume

alcohol. Another major limitation of this model is consistent with the limitations of the standard chronic-binge (ten-plus-one) alcohol model. The acuteness of study, grams of ethanol consumed, and limited inflammatory effects are vastly different compared to human behavioral patterns and pathology. It is of great interest to perform a similar study but in a more chronic model, where altered metabolic phenotype and hepatitis are more prevalent (Ghosh Dastidar et al., 2018). It is currently unclear what effects PCB126 may have in ALD over a longer study duration or if repeated dosing could more greatly exacerbate the observed effects.

This dissertation is also limited by the absence of microbiome and robust intestinal data. It is becoming increasingly apparent that the gut microbiome and altered intestinal absorption play a significant role in ALD pathology. Future studies need to pay closer attention to these alterations as PCB126 may be enhancing ALD *via* modified gut microbiome or further limiting nutrient reabsorption in the intestine. Furthermore, while PCBs are still being detected in human populations, average blood concentrations have been trending down over the past few decades (Raffetti et al., 2017; LaKind et al., 2009; Lin et al., 2018). Nevertheless, PCBs even at lower levels, bioaccumulate with repeated exposures which can result in toxicity.

Finally, a major limitation of this work is sexually dimorphism biases, as female rodents were not utilized in our studies. ALD is typically reported more highly in male populations due to consumption patterns; however, females are more sensitive to developing this disease. Metabolic detoxification by of ethanol differs between sexes resulting in varying toxicological consequences. Additionally,

STAT5 has been considered to influence 'feminization' or 'masculinization' of the liver and may be involved in sexually dimorphic responses to disease progression (Lau-Corona et al., 2022). These differences along with protein expression and hormone secretion patterns certainly are expected to alter disease phenotype and progression. Future models will need to incorporate female mice as research are lacking in sexually dimorphic responses to toxic stimuli.

Future Directions

While this dissertation clearly has its limitations, another major strength of this work is the great potential for future experiments to follow observations outlined in Chapter II-IV. First, it is of great interest to investigate other toxicants in this model to study differential effects. For example, we are recently repeated the first version of this model where we investigated PFOS exposure with concomitant alcohol feeding (Gripshover, 2021). While we expect some different phenotypic results, we are primarily interested in how alcohol may differentially impact PFOS tissue partitioning between the blood, liver, intestine, kidney, urine, and stool. Preliminary analyses suggest that mRNA levels of key hepatic transporters are heavily decreased with EtOH feeding which may be impacting PFOS distribution (data not shown). Additionally, while there appears to be global disruption of protein phosphorylation in the liver, specific pathways must be further investigated to elucidate a mechanism. Specifically, the regulatory actions PGRMC1 has with its binding partners to influence metabolism.

Concerning mechanisms, a major endpoint of study was the promotion of hepatic steatosis and disrupted carbohydrate metabolism. Future investigations will need to examine these alterations more closely and discern how PCB126 alters the metabolic landscape within ALD. An interesting theory is that extensive damage was done to the mitochondria, limiting regenerative turn over. Upon accounting for injury (e.g., refolding proteins or cellular proliferation), glucose use for repair combined with typical cellular energy requirements exceeds the amount that was stored in the form of glycogen and thus resulting in low circulating glucose and hepatic glycogen. Furthermore, we found that relative WAT weight (Figure 1.1D) was significantly decreased by PCB126 exposure, which could suggest that alternative oxidation pathways were activated to promote non-optimal energy generation. This would be a major, clinically relevant observation as hospitalized ALD patients often have depleted glycogen stores. PCB126 may be promoting this deprivation by negatively reprograming energy metabolism and limiting compensatory mechanisms that may not be an issue under typical ALD pathogenesis. Indeed, mitochondrial injury must be investigated in future studies to appreciate the dual toxicity by alcohol and PCB126 on proper energy use and turn over.

Finally, AhR activation likely plays a crucial role in PCB126's promotion of this disease. Our data suggests that both PCB126 and alcohol activated AhR (Figure 1.6 & Supporting Figure S9). The distinct ligand activation of AhR likely leads to specific effects that alter pathways that may be unique to either ligand or a combination of both (Kim et al., 2022; Zhang et al., 2012b). Thus, an AhR ablation

study would be an important future direction that could assist in the discovery of specific effects of PCB126 in alcohol models (Jin et al., 2021).

Conclusions

Altogether, this dissertation project demonstrated that PCB126 reprograms intermediary metabolism in ALD to modify liver disease pathogenesis. Our three 'Omics study results suggest that these landscapes are, in part, globally changed by alcohol feeding, and uniquely modified by PCB126 exposure. Transcription and protein phosphorylation are two conserved molecular actions that are critical to cellular homeostasis, and this model demonstrated to cause aberrations in both events. Additionally, hepatic metals were decreased with EtOH feeding, and important functional metals were further reduced by PCB126. Our exposure paradigm is indeed causing vital changes at the mRNA and protein level to promote the disease characterized in Chapter II. This work overall suggests that environmental pollutants can promote alcohol-induced liver pathology, an interaction that may explain exacerbated promotion of pathology in some individuals. Human ALD development and rate of progression clinical cases may be unique, and our work demonstrates that pollutant exposure may modify these disease parameters. More work is required to understand the combinatorial effect of alcohol and toxicants, and studies are underway to confirm these events in human populations.

REFERENCES

Adams, H. 2015. *Regulation of Jak1 and Jak2 Synthesis through Non-Classical Progestin Receptors.* University of Massachusetts Amherst.

Adams, L. A. & Ratziu, V. 2015. Non-alcoholic fatty liver - perhaps not so benign. *J Hepatol,* 62(5), pp 1002-4.

Al-Dayyat, H. M., Rayyan, Y. M. & Tayyem, R. F. 2018. Non-alcoholic fatty liver disease and associated dietary and lifestyle risk factors. *Diabetes Metab Syndr,* 12(4), pp 569-575.

Al-Eryani, L., Wahlang, B., Falkner, K. C., Guardiola, J. J., Clair, H. B., Prough, R. A. & Cave, M. 2015. Identification of Environmental Chemicals Associated with the Development of Toxicant-associated Fatty Liver Disease in Rodents. *Toxicologic pathology,* 43(4), pp 482-497.

Al-Samerria, S. & Radovick, S. 2021. The Role of Insulin-like Growth Factor-1 (IGF-1) in the Control of Neuroendocrine Regulation of Growth. *Cells,* 10(10), pp.

Altamirano, J. & Bataller, R. 2011. Alcoholic liver disease: pathogenesis and new targets for therapy. *Nature Reviews Gastroenterology & Hepatology,* 8(9), pp 491-501.

Aluru, N., Karchner, S. I. & Glazer, L. 2017. Early Life Exposure to Low Levels of AHR Agonist PCB126 (3,3',4,4',5-Pentachlorobiphenyl) Reprograms Gene Expression in Adult Brain. *Toxicol Sci,* 160(2), pp 386-397.

Alvarado, R., Cárdenas, G., Nogueira, J. J., Ramos-Berdullas, N. & Mandado, M. 2023. On the Permeation of Polychlorinated Dibenzodioxins and Dibenzofurans

through Lipid Membranes: Classical MD and Hybrid QM/MM-EDA Analysis. *Membranes* [Online], 13.

Andrews, S. 2015. *FastQC: A Quality Control Tool for High Throughput Sequence Data* [Online]. Available: http://www.bioinformatics.babraham.ac.uk/projects/fastqc/.

Argemi, J., Kedia, K., Gritsenko, M. A., Clemente-Sanchez, A., Asghar, A., Herranz, J. M., Liu, Z.-X., Atkinson, S. R., Smith, R. D., Norden-Krichmar, T. M., Day, L. Z., Stolz, A., Tayek, J. A., Bataller, R., Morgan, T. R. & Jacobs, J. M. 2022. Integrated Transcriptomic and Proteomic Analysis Identifies Plasma Biomarkers of Hepatocellular Failure in Alcohol-Associated Hepatitis. *The American Journal of Pathology,* 192(12)**,** pp 1658-1669.

ATSDR. 2000. *Public Health Statement Polychlorinated Biphenyls (PCBS)* [Online]. Available: https://wwwn.cdc.gov/TSP/PHS/PHS.aspx?phsid=139&toxid=26 [Accessed 07/12/2022.

Axley, P. D., Richardson, C. T. & Singal, A. K. 2019. Epidemiology of Alcohol Consumption and Societal Burden of Alcoholism and Alcoholic Liver Disease. *Clin Liver Dis,* 23(1)**,** pp 39-50.

Bailey, S. M., Mantena, S. K., Millender-Swain, T., Cakir, Y., Jhala, N. C., Chhieng, D., Pinkerton, K. E. & Ballinger, S. W. 2009. Ethanol and tobacco smoke increase hepatic steatosis and hypoxia in the hypercholesterolemic apoE(-/-) mouse: implications for a "multihit" hypothesis of fatty liver disease. *Free Radic Biol Med,* 46(7)**,** pp 928-38.

Baj, J., Flieger, W., Teresiński, G., Buszewicz, G., Sitarz, R., Forma, A., Karakuła, K. & Maciejewski, R. 2020. Magnesium, Calcium, Potassium, Sodium, Phosphorus, Selenium, Zinc, and Chromium Levels in Alcohol Use Disorder: A Review. *J Clin Med,* 9(6)**,** pp.

Bashar, M. T., Partho, P. A., Amandeep, K., Sarah, L. T., Ashleigh Van, O., Ishith, S., Marina, P., Kate, M. H., Megan, P., Perlita, P., Jalal, A. J., Thiri, Z., Dana, P., Marina, L., Michael, P., Juan, C. C., Lynne, T., Mitra, J., Alexander, C. J., Craig,

P. C., Tara, L. R., Simon, J. K., Ross, D. H., Ellis, P., Mark, P. M., Elizabeth, J. N., Tanja, N. F., Hans, N., Ewa, M. G., Leslie, A. W. & Michael, A. C. 2019. PGRMC1 phosphorylation status and cell plasticity 1: glucose metabolism, mitochondria, and mouse xenograft tumorigenesis. *bioRxiv,* 737718.

Bassler, J., Ducatman, A., Elliott, M., Wen, S., Wahlang, B., Barnett, J. & Cave, M. C. 2019. Environmental perfluoroalkyl acid exposures are associated with liver disease characterized by apoptosis and altered serum adipocytokines. *Environmental Pollution,* 247(1055-1063.

Beier, J. I., Arteel, G. E. & McClain, C. J. 2011. Advances in alcoholic liver disease. *Current gastroenterology reports,* 13(1)**,** pp 56-64.

Beier, J. I. & McClain, C. J. 2010. Mechanisms and cell signaling in alcoholic liver disease. *Biological chemistry,* 391(11)**,** pp 1249-1264.

Bekker-Jensen, D. B., Bernhardt, O. M., Hogrebe, A., Martinez-Val, A., Verbeke, L., Gandhi, T., Kelstrup, C. D., Reiter, L. & Olsen, J. V. 2020. Rapid and site-specific deep phosphoproteome profiling by data-independent acquisition without the need for spectral libraries. *Nat Commun,* 11(1)**,** pp 787.

Berk, P. D., Zhou, S. & Bradbury, M. W. 2005. Increased hepatocellular uptake of long chain fatty acids occurs by different mechanisms in fatty livers due to obesity or excess ethanol use, contributing to development of steatohepatitis in both settings. *Transactions of the American Clinical and Climatological Association,* 116(335-345.

Bertola, A., Mathews, S., Ki, S. H., Wang, H. & Gao, B. 2013. Mouse model of chronic and binge ethanol feeding (the NIAAA model). *Nature protocols,* 8(3)**,** pp 627-637.

Bligh, E. G. & Dyer, W. J. 1959. A rapid method of total lipid extraction and purification. *Can J Biochem Physiol,* 37(8)**,** pp 911-7.

Brandon-Warner, E., Schrum, L. W., Schmidt, C. M. & McKillop, I. H. 2012. Rodent models of alcoholic liver disease: of mice and men. *Alcohol (Fayetteville, N.Y.),* 46(8)**,** pp 715-725.

Brooks, A. J. & Waters, M. J. 2010. The growth hormone receptor: mechanism of activation and clinical implications. *Nat Rev Endocrinol,* 6(9)**,** pp 515-25.

Cahill, M. A., Jazayeri, J. A., Kovacevic, Z. & Richardson, D. R. 2016. PGRMC1 regulation by phosphorylation: potential new insights in controlling biological activity. *Oncotarget,* 7(32)**,** pp 50822-50827.

Cahill, M. A. & Neubauer, H. 2021. PGRMC Proteins Are Coming of Age: A Special Issue on the Role of PGRMC1 and PGRMC2 in Metabolism and Cancer Biology. *Cancers (Basel),* 13(3)**,** pp.

Cameron, P. H., Chevet, E., Pluquet, O., Thomas, D. Y. & Bergeron, J. J. 2009. Calnexin phosphorylation attenuates the release of partially misfolded alpha1-antitrypsin to the secretory pathway. *J Biol Chem,* 284(50)**,** pp 34570-9.

Cao, L., Wu, D., Qin, L., Tan, D., Fan, Q., Jia, X., Yang, M., Zhou, T., Feng, C., Lu, Y. & He, Y. 2023. Single-Cell RNA Transcriptome Profiling of Liver Cells of Short-Term Alcoholic Liver Injury in Mice. *Int J Mol Sci,* 24(5)**,** pp.

Cao, T., Chen, Q., Zhang, B., Wu, X., Zeng, C., Zhang, S. & Cai, H. 2021. Clozapine Induced Disturbances in Hepatic Glucose Metabolism: The Potential Role of PGRMC1 Signaling. *Front Endocrinol (Lausanne),* 12(727371.

Carpenter, D. O. 2006. Polychlorinated biphenyls (PCBs): routes of exposure and effects on human health. *Rev Environ Health,* 21(1)**,** pp 1-23.

Carreras, J., Bartrons, R., Climent, F. & Cusso, R. 1986. Bisphosphorylated metabolites of glycerate, glucose, and fructose: functions, metabolism and molecular pathology. *Clin Biochem,* 19(6)**,** pp 348-58.

Cassandri, M., Smirnov, A., Novelli, F., Pitolli, C., Agostini, M., Malewicz, M., Melino, G. & Raschellà, G. 2017. Zinc-finger proteins in health and disease. *Cell Death Discovery,* 3(1)**,** pp 17071.

Cave, M., Falkner, K. C., Henry, L., Costello, B., Gregory, B. & McClain, C. J. 2011. Serum cytokeratin 18 and cytokine elevations suggest a high prevalence of occupational liver disease in highly exposed elastomer/polymer workers. *J Occup Environ Med,* 53(10)**,** pp 1128-33.

Cave, M., Falkner, K. C., Ray, M., Joshi-Barve, S., Brock, G., Khan, R., Bon Homme, M. & McClain, C. J. 2010. Toxicant-associated steatohepatitis in vinyl chloride workers. *Hepatology (Baltimore, Md.),* 51(2)**,** pp 474-481.

Cave, M. C., Pinkston, C. M., Rai, S. N., Wahlang, B., Pavuk, M., Head, K. Z., Carswell, G. K., Nelson, G. M., Klinge, C. M., Bell, D. A., Birnbaum, L. S. & Chorley, B. N. 2022. Circulating MicroRNAs, Polychlorinated Biphenyls, and Environmental Liver Disease in the Anniston Community Health Survey. *Environmental health perspectives,* 130(1)**,** pp 17003-17003.

Cheemerla, S. & Balakrishnan, M. 2021. Global Epidemiology of Chronic Liver Disease. *Clin Liver Dis (Hoboken),* 17(5)**,** pp 365-370.

Chen, X., Owoseni, E., Salamat, J., Cederbaum, A. I. & Lu, Y. 2018. Nicotine enhances alcoholic fatty liver in mice: Role of CYP2A5. *Arch Biochem Biophys,* 657(65-73.

Clair, H. B., Pinkston, C. M., Rai, S. N., Pavuk, M., Dutton, N. D., Brock, G. N., Prough, R. A., Falkner, K. C., McClain, C. J. & Cave, M. C. 2018. Liver Disease in a Residential Cohort With Elevated Polychlorinated Biphenyl Exposures. *Toxicological sciences : an official journal of the Society of Toxicology,* 164(1)**,** pp 39-49.

Crabb, D. W., Im, G. Y., Szabo, G., Mellinger, J. L. & Lucey, M. R. 2020. Diagnosis and Treatment of Alcohol-Associated Liver Diseases: 2019 Practice Guidance From

the American Association for the Study of Liver Diseases. *Hepatology,* 71(1)**,** pp 306-333.

Dam, M. K., Flensborg-Madsen, T., Eliasen, M., Becker, U. & Tolstrup, J. S. 2013. Smoking and risk of liver cirrhosis: a population-based cohort study. *Scand J Gastroenterol,* 48(5)**,** pp 585-91.

Deng, P., Barney, J., Petriello, M. C., Morris, A. J., Wahlang, B. & Hennig, B. 2019. Hepatic metabolomics reveals that liver injury increases PCB 126-induced oxidative stress and metabolic dysfunction. *Chemosphere,* 217(140-149.

Dobin, A., Davis, C. A., Schlesinger, F., Drenkow, J., Zaleski, C., Jha, S., Batut, P., Chaisson, M. & Gingeras, T. R. 2013. STAR: ultrafast universal RNA-seq aligner. *Bioinformatics,* 29(1)**,** pp 15-21.

Dogru, T., Kirik, A., Gurel, H., Rizvi, A. A., Rizzo, M. & Sonmez, A. 2021. The Evolving Role of Fetuin-A in Nonalcoholic Fatty Liver Disease: An Overview from Liver to the Heart. *Int J Mol Sci,* 22(12)**,** pp.

Domazet, S. L., Grøntved, A., Jensen, T. K., Wedderkopp, N. & Andersen, L. B. 2020. Higher circulating plasma polychlorinated biphenyls (PCBs) in fit and lean children: The European youth heart study. *Environment International,* 136(105481.

Dong, H., Hao, L., Zhang, W., Zhong, W., Guo, W., Yue, R., Sun, X. & Zhou, Z. 2021. Activation of AhR-NQO1 Signaling Pathway Protects Against Alcohol-Induced Liver Injury by Improving Redox Balance. *Cellular and Molecular Gastroenterology and Hepatology,* 12(3)**,** pp 793-811.

Donohue, T. M., Jr. 2007. Alcohol-induced steatosis in liver cells. *World journal of gastroenterology,* 13(37)**,** pp 4974-4978.

Dyson, J. K., Anstee, Q. M. & McPherson, S. 2014. Non-alcoholic fatty liver disease: a practical approach to diagnosis and staging. *Frontline Gastroenterol,* 5(3)**,** pp 211-218.

El-Zayadi, A. R. 2008. Hepatic steatosis: a benign disease or a silent killer. *World J Gastroenterol,* 14(26)**,** pp 4120-6.

EPA. 2022. *What are PCB's?* [Online]. Available: https://www3.epa.gov/region1/eco/uep/pcb.html.

Eslam, M., Valenti, L. & Romeo, S. 2018. Genetics and epigenetics of NAFLD and NASH: Clinical impact. *Journal of Hepatology,* 68(2)**,** pp 268-279.

Feng, L., Allen, T. K., Marinello, W. P. & Murtha, A. P. 2019. Roles of Progesterone Receptor Membrane Component 1 in Oxidative Stress-Induced Aging in Chorion Cells. *Reprod Sci,* 26(3)**,** pp 394-403.

Feng, R., Kan, K., Sticht, C., Li, Y., Wang, S., Liu, H., Shao, C., Munker, S., Niess, H., Wang, S., Meyer, C., Liebe, R., Ebert, M. P., Dooley, S., Ding, H. & Weng, H. 2022. A hierarchical regulatory network ensures stable albumin transcription under various pathophysiological conditions. *Hepatology,* 76(6)**,** pp 1673-1689.

Franchin, C., Borgo, C., Cesaro, L., Zaramella, S., Vilardell, J., Salvi, M., Arrigoni, G. & Pinna, L. A. 2018. Re-evaluation of protein kinase CK2 pleiotropy: new insights provided by a phosphoproteomics analysis of CK2 knockout cells. *Cell Mol Life Sci,* 75(11)**,** pp 2011-2026.

Gadupudi, G. S., Elser, B. A., Sandgruber, F. A., Li, X., Gibson-Corley, K. N. & Robertson, L. W. 2018. PCB126 Inhibits the Activation of AMPK-CREB Signal Transduction Required for Energy Sensing in Liver. *Toxicol Sci,* 163(2)**,** pp 440-453.

Gadupudi, G. S., Klaren, W. D., Olivier, A. K., Klingelhutz, A. J. & Robertson, L. W. 2016. PCB126-Induced Disruption in Gluconeogenesis and Fatty Acid Oxidation Precedes Fatty Liver in Male Rats. *Toxicological Sciences,* 149(1)**,** pp 98-110.

Ghosh Dastidar, S., Warner, J. B., Warner, D. R., McClain, C. J. & Kirpich, I. A. 2018. Rodent Models of Alcoholic Liver Disease: Role of Binge Ethanol Administration. *Biomolecules,* 8(1)**,** pp.

Girer, N. G., Tomlinson, C. R. & Elferink, C. J. 2020. The Aryl Hydrocarbon Receptor in Energy Balance: The Road from Dioxin-Induced Wasting Syndrome to Combating Obesity with Ahr Ligands. *Int J Mol Sci,* 22(1)**,** pp.

Glass, L. M., Hunt, C. M., Fuchs, M. & Su, G. L. 2019. Comorbidities and Nonalcoholic Fatty Liver Disease: The Chicken, the Egg, or Both? *Federal practitioner : for the health care professionals of the VA, DoD, and PHS,* 36(2)**,** pp 64-71.

Gripshover, T. C. 2021. *Investigating the effects of Perfluorooctanoic Sulfonate (PFOS) and ethanol on fatty liver disease using a modified NIAAA model.* University of Louisville.

Gripshover, T. C., Wahlang, B., Head, K. Z., Young, J. L., Luo, J., Mustafa, M. T., Kirpich, I. A. & Cave, M. C. 2022. The environmental pollutant, polychlorinated biphenyl 126, alters liver function in a rodent model of alcohol-associated liver disease. *Alcohol Clin Exp Res.*

Gyamfi, M. A. & Wan, Y.-J. Y. 2010. Pathogenesis of alcoholic liver disease: the role of nuclear receptors. *Experimental biology and medicine (Maywood, N.J.),* 235(5)**,** pp 547-560.

Hardesty, J., Day, L., Warner, J., Warner, D., Gritsenko, M., Asghar, A., Stolz, A., Morgan, T., McClain, C., Jacobs, J. & Kirpich, I. 2022. Hepatic Protein and Phosphoprotein Signatures of Alcohol-Associated Cirrhosis and Hepatitis. *Am J Pathol,* 192(7)**,** pp 1066-1082.

Hardesty, J. E., Al-Eryani, L., Wahlang, B., Falkner, K. C., Shi, H., Jin, J., Vivace, B. J., Ceresa, B. P., Prough, R. A. & Cave, M. C. 2018. Epidermal Growth Factor Receptor Signaling Disruption by Endocrine and Metabolic Disrupting Chemicals. *Toxicol Sci,* 162(2), pp 622-634.

Hardesty, J. E., Wahlang, B., Falkner, K. C., Shi, H., Jin, J., Wilkey, D., Merchant, M., Watson, C., Prough, R. A. & Cave, M. C. 2019a. Hepatic signalling disruption by pollutant Polychlorinated biphenyls in steatohepatitis. *Cell Signal,* 53(132-139.

Hardesty, J. E., Wahlang, B., Falkner, K. C., Shi, H., Jin, J., Zhou, Y., Wilkey, D. W., Merchant, M. L., Watson, C. T., Feng, W., Morris, A. J., Hennig, B., Prough, R. A. & Cave, M. C. 2019b. Proteomic Analysis Reveals Novel Mechanisms by Which Polychlorinated Biphenyls Compromise the Liver Promoting Diet-Induced Steatohepatitis. *Journal of Proteome Research,* 18(4), pp 1582-1594.

He, L., Vatsalya, V., Ma, X., Klinge, C. M., Cave, M. C., Feng, W., McClain, C. J. & Zhang, X. 2022. Metabolic Analysis of Nucleosides/Bases in the Urine and Serum of Patients with Alcohol-Associated Liver Disease. *Metabolites,* 12(12), pp.

Hehenberger, E., Eitel, M., Fortunato, S. A. V., Miller, D. J., Keeling, P. J. & Cahill, M. A. 2020. Early eukaryotic origins and metazoan elaboration of MAPR family proteins. *Molecular Phylogenetics and Evolution,* 148(106814.

Heindel, J. J., Blumberg, B., Cave, M., Machtinger, R., Mantovani, A., Mendez, M. A., Nadal, A., Palanza, P., Panzica, G., Sargis, R., Vandenberg, L. N. & vom Saal, F. 2017. Metabolism disrupting chemicals and metabolic disorders. *Reproductive Toxicology,* 68(3-33.

Hestermann, E. V., Stegeman, J. J. & Hahn, M. E. 2000. Relative Contributions of Affinity and Intrinsic Efficacy to Aryl Hydrocarbon Receptor Ligand Potency. *Toxicology and Applied Pharmacology,* 168(2), pp 160-172.

Heyens, L. J. M., Busschots, D., Koek, G. H., Robaeys, G. & Francque, S. 2021. Liver Fibrosis in Non-alcoholic Fatty Liver Disease: From Liver Biopsy to Non-invasive Biomarkers in Diagnosis and Treatment. *Front Med (Lausanne),* 8(615978.

Hirode, G., Saab, S. & Wong, R. J. 2020a. Trends in the Burden of Chronic Liver Disease Among Hospitalized US Adults. *JAMA Network Open,* 3(4)**,** pp e201997-e201997.

Hirode, G., Saab, S. & Wong, R. J. 2020b. Trends in the Burden of Chronic Liver Disease Among Hospitalized US Adults. *JAMA Netw Open,* 3(4)**,** pp e201997.

IARC 2016. Polychlorinated Biphenyls and Polybrominated Biphenyls. *IARC Monogr Eval Carcinog Risks Hum,* 107(9-500.

Iurlaro, R., Püschel, F., León-Annicchiarico, C. L., O'Connor, H., Martin, S. J., Palou-Gramón, D., Lucendo, E. & Muñoz-Pinedo, C. 2017. Glucose Deprivation Induces ATF4-Mediated Apoptosis through TRAIL Death Receptors. *Mol Cell Biol,* 37(10)**,** pp.

Ji, C. 2012. Mechanisms of alcohol-induced endoplasmic reticulum stress and organ injuries. *Biochem Res Int,* 2012(216450.

Jin, J., Wahlang, B., Shi, H., Hardesty, J. E., Falkner, K. C., Head, K. Z., Srivastava, S., Merchant, M. L., Rai, S. N., Cave, M. C. & Prough, R. A. 2020. Dioxin-like and non-dioxin-like PCBs differentially regulate the hepatic proteome and modify diet-induced nonalcoholic fatty liver disease severity. *Med Chem Res,* 29(1247-1263.

Jin, J., Wahlang, B., Thapa, M., Head, K. Z., Hardesty, J. E., Srivastava, S., Merchant, M. L., Rai, S. N., Prough, R. A. & Cave, M. C. 2021. Proteomics and metabolic phenotyping define principal roles for the aryl hydrocarbon receptor in mouse liver. *Acta pharmaceutica Sinica. B,* 11(12)**,** pp 3806-3819.

Jo, S. L., Baek, I. J., Ko, J. W., Kwun, H. J., Shin, H. J. & Hong, E. J. 2023. Hepatic progesterone receptor membrane component 1 attenuates ethanol-induced liver injury by reducing acetaldehyde production and oxidative stress. *Am J Physiol Gastrointest Liver Physiol,* 324(6)**,** pp G442-g451.

Jomova, K., Makova, M., Alomar, S. Y., Alwasel, S. H., Nepovimova, E., Kuca, K., Rhodes, C. J. & Valko, M. 2022. Essential metals in health and disease. *Chem Biol Interact,* 367(110173.

Kaia, K. H., Katie, A., Hilaree, F., Olivier, T. & Rolf, J. C. 2018. Insulin Receptor Plasma Membrane Levels Increased by the Progesterone Receptor Membrane Component 1. *Molecular Pharmacology,* 94(1)**,** pp 665.

Kaltenecker, D., Themanns, M., Mueller, K. M., Spirk, K., Suske, T., Merkel, O., Kenner, L., Luís, A., Kozlov, A., Haybaeck, J., Müller, M., Han, X. & Moriggl, R. 2019. Hepatic growth hormone - JAK2 - STAT5 signalling: Metabolic function, non-alcoholic fatty liver disease and hepatocellular carcinoma progression. *Cytokine,* 124(154569.

Kasprzak, A. 2021. Insulin-Like Growth Factor 1 (IGF-1) Signaling in Glucose Metabolism in Colorectal Cancer. *Int J Mol Sci,* 22(12)**,** pp.

Khaderi, S. A. 2019. Introduction: Alcohol and Alcoholism. *Clin Liver Dis,* 23(1)**,** pp 1-10.

Kim, Y. S., Ko, B., Kim, D. J., Tak, J., Han, C. Y., Cho, J. Y., Kim, W. & Kim, S. G. 2022. Induction of the hepatic aryl hydrocarbon receptor by alcohol dysregulates autophagy and phospholipid metabolism via PPP2R2D. *Nat Commun,* 13(1)**,** pp 6080.

Klatsky, A. L. & Armstrong, M. A. 1992. Alcohol, smoking, coffee, and cirrhosis. *Am J Epidemiol,* 136(10)**,** pp 1248-57.

Klinge, C. M., Piell, K. M., Petri, B. J., He, L., Zhang, X., Pan, J., Rai, S. N., Andreeva, K., Rouchka, E. C., Wahlang, B., Beier, J. I. & Cave, M. C. 2021. Combined exposure to polychlorinated biphenyls and high-fat diet modifies the global epitranscriptomic landscape in mouse liver. *Environ Epigenet,* 7(1)**,** pp dvab008.

Knape, M. J., Ahuja, L. G., Bertinetti, D., Burghardt, N. C., Zimmermann, B., Taylor, S. S. & Herberg, F. W. 2015. Divalent Metal Ions Mg²⁺ and Ca²⁺ Have Distinct Effects on Protein Kinase A Activity and Regulation. *ACS Chem Biol,* 10(10)**,** pp 2303-15.

Knight, J. D., Tian, R., Lee, R. E., Wang, F., Beauvais, A., Zou, H., Megeney, L. A., Gingras, A. C., Pawson, T., Figeys, D. & Kothary, R. 2012. A novel whole-cell lysate kinase assay identifies substrates of the p38 MAPK in differentiating myoblasts. *Skelet Muscle,* 2(5.

Kouno, T., Zeng, S., Wang, Y., Duan, Y., Lang, S., Gao, B., Hartmann, P., Cabré, N., Llorente, C., Galbert, C., Emond, P., Sokol, H., James, M., Chao, C. C., Gao, J. R., Perreault, M., Hava, D. L. & Schnabl, B. 2023. Engineered bacteria producing aryl-hydrocarbon receptor agonists protect against ethanol-induced liver disease in mice. *Alcohol Clin Exp Res (Hoboken),* 47(5)**,** pp 856-867.

Ku, H.-C. & Cheng, C.-F. 2020. Master Regulator Activating Transcription Factor 3 (ATF3) in Metabolic Homeostasis and Cancer. *Frontiers in Endocrinology,* 11(

Lai, I., Chai, Y., Simmons, D., Luthe, G., Coleman, M. C., Spitz, D., Haschek, W. M., Ludewig, G. & Robertson, L. W. 2010. Acute toxicity of 3,3',4,4',5-pentachlorobiphenyl (PCB 126) in male Sprague-Dawley rats: effects on hepatic oxidative stress, glutathione and metals status. *Environ Int,* 36(8)**,** pp 918-23.

LaKind, J. S., Hays, S. M., Aylward, L. L. & Naiman, D. Q. 2009. Perspective on serum dioxin levels in the United States: an evaluation of the NHANES data. *J Expo Sci Environ Epidemiol,* 19(4)**,** pp 435-41.

Larigot, L., Juricek, L., Dairou, J. & Coumoul, X. 2018. AhR signaling pathways and regulatory functions. *Biochim Open,* 7(1-9.

Lau-Corona, D., Ma, H., Vergato, C., Sarmento-Cabral, A., Del Rio-Moreno, M., Kineman, R. D. & Waxman, D. J. 2022. Constitutively Active STAT5b Feminizes Mouse Liver Gene Expression. *Endocrinology,* 163(5)**,** pp.

Le, M. H., Yeo, Y. H., Zou, B., Barnet, S., Henry, L., Cheung, R. & Nguyen, M. H. 2022. Forecasted 2040 global prevalence of nonalcoholic fatty liver disease using hierarchical bayesian approach. *Clin Mol Hepatol,* 28(4)**,** pp 841-850.

Lee, L. J. H., Chung, C. W., Ma, Y. C., Wang, G. S., Chen, P. C., Hwang, Y. H. & Wang, J. D. 2003. Increased mortality odds ratio of male liver cancer in a community contaminated by chlorinated hydrocarbons in groundwater. *Occupational and Environmental Medicine,* 60(5)**,** pp 364.

Lee, S. R., Choi, W. Y., Heo, J. H., Huh, J., Kim, G., Lee, K. P., Kwun, H. J., Shin, H. J., Baek, I. J. & Hong, E. J. 2020. Progesterone increases blood glucose via hepatic progesterone receptor membrane component 1 under limited or impaired action of insulin. *Sci Rep,* 10(1)**,** pp 16316.

Lee, S. R., Kwon, S. W., Kaya, P., Lee, Y. H., Lee, J. G., Kim, G., Lee, G. S., Baek, I. J. & Hong, E. J. 2018. Loss of progesterone receptor membrane component 1 promotes hepatic steatosis via the induced de novo lipogenesis. *Sci Rep,* 8(1)**,** pp 15711.

Lee, S. R., Lee, J. G., Heo, J. H., Jo, S. L., Ryu, J., Kim, G., Yon, J. M., Lee, M. S., Lee, G. S., An, B. S., Shin, H. J., Woo, D. C., Baek, I. J. & Hong, E. J. 2021. Loss of PGRMC1 Delays the Progression of Hepatocellular Carcinoma via Suppression of Pro-Inflammatory Immune Responses. *Cancers (Basel),* 13(10)**,** pp.

Li, G., Ma, X. & Xu, L. 2020. The roles of zinc finger proteins in non-alcoholic fatty liver disease. *Liver Research,* 4(1)**,** pp 35-39.

Lieber, C. S. 2004. Alcoholic fatty liver: its pathogenesis and mechanism of progression to inflammation and fibrosis. *Alcohol,* 34(1)**,** pp 9-19.

Lin, M., Ma, Y., Yuan, H., Luo, X., Wang, Q., Liu, A., Wang, Y. & Jin, J. 2018. Temporal trends in dioxin-like polychlorinated biphenyl concentrations in serum from the general population of Shandong Province, China: A longitudinal study from 2011 to 2017. *Environmental Pollution,* 243(59-65.

Liu, B., Balkwill, A., Roddam, A., Brown, A. & Beral, V. 2009. Separate and joint effects of alcohol and smoking on the risks of cirrhosis and gallbladder disease in middle-aged women. *Am J Epidemiol,* 169(2)**,** pp 153-60.

Liu, G., Zhou, L., Zhang, H., Chen, R., Zhang, Y., Li, L., Lu, J.-Y., Jiang, H., Liu, D., Qi, S., Jiang, Y.-M., Yin, K., Xie, Z., Shi, Y., Liu, Y., Cao, X., Chen, Y.-X., Zou, D. & Zhang, W. J. 2017. Regulation of hepatic lipogenesis by the zinc finger protein Zbtb20. *Nature Communications,* 8(1)**,** pp 14824.

Liu, H., Liu, H., Zhu, L., Zhang, Z., Zheng, X., Liu, J. & Fu, X. 2019. Comparative Transcriptome Analyses Provide Potential Insights into the Molecular Mechanisms of Astaxanthin in the Protection against Alcoholic Liver Disease in Mice. *Mar Drugs,* 17(3)**,** pp.

Louvet, A. & Mathurin, P. 2015. Alcoholic liver disease: mechanisms of injury and targeted treatment. *Nature Reviews Gastroenterology & Hepatology,* 12(4)**,** pp 231-242.

Lu, H. 2016. Crosstalk of HNF4α with extracellular and intracellular signaling pathways in the regulation of hepatic metabolism of drugs and lipids. *Acta Pharm Sin B,* 6(5)**,** pp 393-408.

Lu, Y., Ward, S. C. & Cederbaum, A. I. 2013. Nicotine enhances ethanol-induced fat accumulation and collagen deposition but not inflammation in mouse liver. *Alcohol,* 47(5)**,** pp 353-7.

Mandrekar, P. & Szabo, G. 2009. Signalling pathways in alcohol-induced liver inflammation. *J Hepatol,* 50(6)**,** pp 1258-66.

Markowitz, G. & Rosner, D. 2018. Monsanto, PCBs, and the creation of a "world-wide ecological problem". *Journal of Public Health Policy,* 39(4)**,** pp 463-540.

Mastrangelo, G., Fedeli, U., Fadda, E., Valentini, F., Agnesi, R., Magarotto, G., Marchì, T., Buda, A., Pinzani, M. & Martines, D. 2004. Increased risk of hepatocellular carcinoma and liver cirrhosis in vinyl chloride workers: synergistic effect of occupational exposure with alcohol intake. *Environ Health Perspect,* 112(11)**,** pp 1188-92.

McClain, C. J., Barve, S. S., Barve, A. & Marsano, L. 2011. Alcoholic liver disease and malnutrition. *Alcoholism, clinical and experimental research,* 35(5)**,** pp 815-820.

McGuire, M. R., Mukhopadhyay, D., Myers, S. L., Mosher, E. P., Brookheart, R. T., Kammers, K., Sehgal, A., Selen, E. S., Wolfgang, M. J., Bumpus, N. N. & Espenshade, P. J. 2021. Progesterone receptor membrane component 1 (PGRMC1) binds and stabilizes cytochromes P450 through a heme-independent mechanism. *J Biol Chem,* 297(5)**,** pp 101316.

McKleroy, W., Lee, T. H. & Atabai, K. 2013. Always cleave up your mess: targeting collagen degradation to treat tissue fibrosis. *Am J Physiol Lung Cell Mol Physiol,* 304(11)**,** pp L709-21.

Medici, V. & Halsted, C. H. 2013. Folate, alcohol, and liver disease. *Mol Nutr Food Res,* 57(4)**,** pp 596-606.

Mesnage, R., Biserni, M., Balu, S., Frainay, C., Poupin, N., Jourdan, F., Wozniak, E., Xenakis, T., Mein, C. A. & Antoniou, M. N. 2018. Integrated transcriptomics and metabolomics reveal signatures of lipid metabolism dysregulation in HepaRG liver cells exposed to PCB 126. *Arch Toxicol,* 92(8)**,** pp 2533-2547.

Montone, R. C., Alonso, M. B., Santos, M. C. O., Méndez-Fernandez, P., Taniguchi, S., Barbosa, A. P. M., Gonçalves, R. M., Padilha, J. d. A., Bertozzi, C., da Silva, J., Marigo, J., Pereira, A. D. S. & Lourenço, R. A. 2023. Temporal trends of

persistent organic pollutant contamination in Franciscana dolphins from the Southwestern Atlantic. *Environmental Research,* 216(114473.

Mueller, K. M., Themanns, M., Friedbichler, K., Kornfeld, J. W., Esterbauer, H., Tuckermann, J. P. & Moriggl, R. 2012. Hepatic growth hormone and glucocorticoid receptor signaling in body growth, steatosis and metabolic liver cancer development. *Mol Cell Endocrinol,* 361(1-2)**,** pp 1-11.

Murray, I. A. & Perdew, G. H. 2020. How Ah Receptor Ligand Specificity Became Important in Understanding Its Physiological Function. *Int J Mol Sci,* 21(24)**,** pp.

Nakajima, T., Kamijo, Y., Tanaka, N., Sugiyama, E., Tanaka, E., Kiyosawa, K., Fukushima, Y., Peters, J. M., Gonzalez, F. J. & Aoyama, T. 2004. Peroxisome proliferator-activated receptor α protects against alcohol-induced liver damage. *Hepatology,* 40(4)**,** pp 972-980.

Nassir, F., Rector, R. S., Hammoud, G. M. & Ibdah, J. A. 2015. Pathogenesis and Prevention of Hepatic Steatosis. *Gastroenterology & hepatology,* 11(3)**,** pp 167-175.

Nault, R., Fader, K. A., Harkema, J. R. & Zacharewski, T. 2017. Loss of liver-specific and sexually dimorphic gene expression by aryl hydrocarbon receptor activation in C57BL/6 mice. *PLoS One,* 12(9)**,** pp e0184842.

Nault, R., Forgacs, A. L., Dere, E. & Zacharewski, T. R. 2013. Comparisons of differential gene expression elicited by TCDD, PCB126, βNF, or ICZ in mouse hepatoma Hepa1c1c7 cells and C57BL/6 mouse liver. *Toxicol Lett,* 223(1)**,** pp 52-9.

Neumann, N., Friz, S. & Forchhammer, K. 2022. Glucose-1,6-Bisphosphate, a Key Metabolic Regulator, Is Synthesized by a Distinct Family of α-Phosphohexomutases Widely Distributed in Prokaryotes. *mBio,* 13(4)**,** pp e0146922.

Nguyen, N. T., Hanieh, H., Nakahama, T. & Kishimoto, T. 2013. The roles of aryl hydrocarbon receptor in immune responses. *International Immunology,* 25(6)*,* pp 335-343.

Nicoll, R., Gerasimidis, K. & Forrest, E. 2022. The Role of Micronutrients in the Pathogenesis of Alcohol-Related Liver Disease. *Alcohol Alcohol,* 57(3)*,* pp 275-282.

Nivukoski, U., Niemelä, M., Bloigu, A., Bloigu, R., Aalto, M., Laatikainen, T. & Niemelä, O. 2020. Combined effects of lifestyle risk factors on fatty liver index. *BMC gastroenterology,* 20(1)*,* pp 109-109.

Nukaya, M., Takahashi, Y., Gonzalez, F. J. & Kamataki, T. 2004. Aryl hydrocarbon receptor-mediated suppression of GH receptor and Janus kinase 2 expression in mice. *FEBS Lett,* 558(1-3)*,* pp 96-100.

Obenauer, J. C., Cantley, L. C. & Yaffe, M. B. 2003. Scansite 2.0: Proteome-wide prediction of cell signaling interactions using short sequence motifs. *Nucleic Acids Res,* 31(13)*,* pp 3635-41.

Pandey, G., Kuykendall, A. T. & Reuther, G. W. 2022. JAK2 inhibitor persistence in MPN: uncovering a central role of ERK activation. *Blood Cancer Journal,* 12(1)*,* pp 13.

Pedroza, D. A., Rajamanickam, V., Subramani, R., Bencomo, A., Galvez, A. & Lakshmanaswamy, R. 2020. Progesterone receptor membrane component 1 promotes the growth of breast cancers by altering the phosphoproteome and augmenting EGFR/PI3K/AKT signalling. *Br J Cancer,* 123(8)*,* pp 1326-1335.

Petri, B. J., Piell, K. M., Wahlang, B., Head, K. Z., Andreeva, K., Rouchka, E. C., Cave, M. C. & Klinge, C. M. 2023. Polychlorinated biphenyls alter hepatic m6A mRNA methylation in a mouse model of environmental liver disease. *Environ Res,* 216(Pt 3)*,* pp 114686.

Petri, B. J., Piell, K. M., Wahlang, B., Head, K. Z., Andreeva, K., Rouchka, E. C., Pan, J., Rai, S. N., Cave, M. C. & Klinge, C. M. 2022. Multiomics analysis of the impact of polychlorinated biphenyls on environmental liver disease in a mouse model. *Environ Toxicol Pharmacol,* 94(103928.

Petriello, M. C., Brandon, J. A., Hoffman, J., Wang, C., Tripathi, H., Abdel-Latif, A., Ye, X., Li, X., Yang, L., Lee, E., Soman, S., Barney, J., Wahlang, B., Hennig, B. & Morris, A. J. 2018. Dioxin-like PCB 126 Increases Systemic Inflammation and Accelerates Atherosclerosis in Lean LDL Receptor-Deficient Mice. *Toxicol Sci,* 162(2)**,** pp 548-558.

Petriello, M. C., Hoffman, J. B., Sunkara, M., Wahlang, B., Perkins, J. T., Morris, A. J. & Hennig, B. 2016. Dioxin-like pollutants increase hepatic flavin containing monooxygenase (FMO3) expression to promote synthesis of the pro-atherogenic nutrient biomarker trimethylamine N-oxide from dietary precursors. *J Nutr Biochem,* 33(145-53.

Plaza-Díaz, J., Solís-Urra, P., Rodríguez-Rodríguez, F., Olivares-Arancibia, J., Navarro-Oliveros, M., Abadía-Molina, F. & Álvarez-Mercado, A. I. 2020. The Gut Barrier, Intestinal Microbiota, and Liver Disease: Molecular Mechanisms and Strategies to Manage. *Int J Mol Sci,* 21(21)**,** pp.

Qian, M., Liu, J., Zhao, D., Cai, P., Pan, C., Jia, W., Gao, Y., Zhang, Y., Zhang, N., Zhang, Y., Zhang, Q., Wu, D., Shan, C., Zhang, M., Schnabl, B., Yang, S., Shen, X. & Wang, L. 2022. Aryl Hydrocarbon Receptor Deficiency in Intestinal Epithelial Cells Aggravates Alcohol-Related Liver Disease. *Cell Mol Gastroenterol Hepatol,* 13(1)**,** pp 233-256.

Raffetti, E., Speziani, F., Donato, F., Leonardi, L., Orizio, G., Scarcella, C., Apostoli, P. & Magoni, M. 2017. Temporal trends of polychlorinated biphenyls serum levels in subjects living in a highly polluted area from 2003 to 2015: a follow-up study. *Int J Hyg Environ Health,* 220(2 Pt B)**,** pp 461-467.

Rakhra, G. & Rakhra, G. 2021. Zinc finger proteins: insights into the transcriptional and post transcriptional regulation of immune response. *Mol Biol Rep,* 48(7)**,** pp 5735-5743.

Rey-Cadilhac, L., Cariou, R., Ferlay, A., Jondreville, C., Delavaud, C., Faulconnier, Y., Alcouffe, S., Faure, P., Marchand, P., Le Bizec, B., Jurjanz, S. & Lerch, S. 2020. Undernutrition combined with dietary mineral oil hastens depuration of stored dioxin and polychlorinated biphenyls in ewes. 1. Kinetics in blood, adipose tissue and faeces. *PLoS One,* 15(3)**,** pp e0230629.

Rosato, V., Masarone, M., Dallio, M., Federico, A., Aglitti, A. & Persico, M. 2019. NAFLD and Extra-Hepatic Comorbidities: Current Evidence on a Multi-Organ Metabolic Syndrome. *International journal of environmental research and public health,* 16(18)**,** pp 3415.

Rosenfeld, R. G., Belgorosky, A., Camacho-Hubner, C., Savage, M. O., Wit, J. M. & Hwa, V. 2007. Defects in growth hormone receptor signaling. *Trends Endocrinol Metab,* 18(4)**,** pp 134-41.

Sabbir, M. G. 2019. Progesterone induced Warburg effect in HEK293 cells is associated with post-translational modifications and proteasomal degradation of progesterone receptor membrane component 1. *The Journal of Steroid Biochemistry and Molecular Biology,* 191(105376.

Safe, S., Bandiera, S., Sawyer, T., Robertson, L., Safe, L., Parkinson, A., Thomas, P. E., Ryan, D. E., Reik, L. M., Levin, W. & et al. 1985. PCBs: structure-function relationships and mechanism of action. *Environ Health Perspect,* 60(47-56.

Safe, S., Jin, U. H., Park, H., Chapkin, R. S. & Jayaraman, A. 2020. Aryl Hydrocarbon Receptor (AHR) Ligands as Selective AHR Modulators (SAhRMs). *Int J Mol Sci,* 21(18)**,** pp.

Schlageter, M., Terracciano, L. M., D'Angelo, S. & Sorrentino, P. 2014. Histopathology of hepatocellular carcinoma. *World J Gastroenterol,* 20(43)**,** pp 15955-64.

Seitz, H. K., Bataller, R., Cortez-Pinto, H., Gao, B., Gual, A., Lackner, C., Mathurin, P., Mueller, S., Szabo, G. & Tsukamoto, H. 2018. Alcoholic liver disease. *Nat Rev Dis Primers,* 4(1)**,** pp 16.

Shan, Q., Li, H., Chen, N., Qu, F. & Guo, J. 2020. Understanding the Multiple Effects of PCBs on Lipid Metabolism. *Diabetes, metabolic syndrome and obesity : targets and therapy,* 13(3691-3702.

Shi, H., Hardesty, J. E., Jin, J., Head, K. Z., Falkner, K. C., Cave, M. C. & Prough, R. A. 2019a. Concentration dependence of human and mouse aryl hydrocarbon receptor responsiveness to polychlorinated biphenyl exposures: Implications for aroclor mixtures. *Xenobiotica,* 49(12)**,** pp 1414-1422.

Shi, H., Jan, J., Hardesty, J. E., Falkner, K. C., Prough, R. A., Balamurugan, A. N., Mokshagundam, S. P., Chari, S. T. & Cave, M. C. 2019b. Polychlorinated biphenyl exposures differentially regulate hepatic metabolism and pancreatic function: Implications for nonalcoholic steatohepatitis and diabetes. *Toxicol Appl Pharmacol,* 363(22-33.

Shirpoor, A., Heshmati, E., Kheradmand, F., Gharalari, F. H., Chodari, L., Naderi, R., Majd, F. N. & Samadi, M. 2018. Increased hepatic FAT/CD36, PTP1B and decreased HNF4A expression contributes to dyslipidemia associated with ethanol-induced liver dysfunction: Rescue effect of ginger extract. *Biomed Pharmacother,* 105(144-150.

Singh, V., Huang, E., Pathak, V., Willard, B. B., Allende, D. S. & Nagy, L. E. 2022. Phosphoproteomics identifies pathways underlying the role of receptor-interaction protein kinase 3 in alcohol-associated liver disease and uncovers apoptosis signal-regulating kinase 1 as a target. *Hepatol Commun,* 6(8)**,** pp 2022-2041.

Soto, M., Chaumontet, C., Even, P. C., Azzout-Marniche, D., Tomé, D. & Fromentin, G. 2017. Metabolic effects of intermittent access to caloric or non-caloric sweetened solutions in mice fed a high-caloric diet. *Physiol Behav,* 175(47-55.

Steiner, J. L., Crowell, K. T. & Lang, C. H. 2015. Impact of Alcohol on Glycemic Control and Insulin Action. *Biomolecules,* 5(4)**,** pp 2223-2246.

Steiner, J. L. & Lang, C. H. 2014. Alcohol impairs skeletal muscle protein synthesis and mTOR signaling in a time-dependent manner following electrically stimulated muscle contraction. *Journal of Applied Physiology,* 117(10)**,** pp 1170-1179.

Stiers, K. M., Kain, B. N., Graham, A. C. & Beamer, L. J. 2016. Induced Structural Disorder as a Molecular Mechanism for Enzyme Dysfunction in Phosphoglucomutase 1 Deficiency. *J Mol Biol,* 428(8)**,** pp 1493-505.

Suk, K. T. & Kim, D. J. 2015. Staging of liver fibrosis or cirrhosis: The role of hepatic venous pressure gradient measurement. *World J Hepatol,* 7(3)**,** pp 607-15.

Sun, L., Yin, H., Liu, M., Xu, G., Zhou, X., Ge, P., Yang, H. & Mao, Y. 2019. Impaired albumin function: a novel potential indicator for liver function damage? *Annals of medicine,* 51(7-8)**,** pp 333-344.

Szklarczyk, D., Gable, A. L., Lyon, D., Junge, A., Wyder, S., Huerta-Cepas, J., Simonovic, M., Doncheva, N. T., Morris, J. H., Bork, P., Jensen, L. J. & Mering, C. V. 2019. STRING v11: protein-protein association networks with increased coverage, supporting functional discovery in genome-wide experimental datasets. *Nucleic Acids Res,* 47(D1)**,** pp D607-d613.

Tanos, R., Murray, I. A., Smith, P. B., Patterson, A. & Perdew, G. H. 2012. Role of the Ah receptor in homeostatic control of fatty acid synthesis in the liver. *Toxicological sciences : an official journal of the Society of Toxicology,* 129(2)**,** pp 372-379.

Thejer, B. M., Adhikary, P. P., Kaur, A., Teakel, S. L., Van Oosterum, A., Seth, I., Pajic, M., Hannan, K. M., Pavy, M., Poh, P., Jazayeri, J. A., Zaw, T., Pascovici, D., Ludescher, M., Pawlak, M., Cassano, J. C., Turnbull, L., Jazayeri, M., James, A. C., Coorey, C. P., Roberts, T. L., Kinder, S. J., Hannan, R. D., Patrick, E., Molloy, M. P., New, E. J., Fehm, T. N., Neubauer, H., Goldys, E. M., Weston, L. A. & Cahill, M. A. 2020. PGRMC1 phosphorylation affects cell shape, motility,

glycolysis, mitochondrial form and function, and tumor growth. *BMC Molecular and Cell Biology,* 21(1), pp 24.

Trapnell, C., Roberts, A., Goff, L., Pertea, G., Kim, D., Kelley, D. R., Pimentel, H., Salzberg, S. L., Rinn, J. L. & Pachter, L. 2012. Differential gene and transcript expression analysis of RNA-seq experiments with TopHat and Cufflinks. *Nature Protocols,* 7(3), pp 562-578.

Van den Berg, M., Birnbaum, L. S., Denison, M., De Vito, M., Farland, W., Feeley, M., Fiedler, H., Hakansson, H., Hanberg, A., Haws, L., Rose, M., Safe, S., Schrenk, D., Tohyama, C., Tritscher, A., Tuomisto, J., Tysklind, M., Walker, N. & Peterson, R. E. 2006. The 2005 World Health Organization reevaluation of human and Mammalian toxic equivalency factors for dioxins and dioxin-like compounds. *Toxicol Sci,* 93(2), pp 223-41.

Van Horn, C. G. & Cunningham, C. C. 1999. Contributions of dietary carbohydrate and ethanol to alterations in liver glycogen levels and glycolytic activity. *Alcohol,* 19(2), pp 139-44.

Wahlang, B., Alexander, N. C., 2nd, Li, X., Rouchka, E. C., Kirpich, I. A. & Cave, M. C. 2021. Polychlorinated biphenyls altered gut microbiome in CAR and PXR knockout mice exhibiting toxicant-associated steatohepatitis. *Toxicol Rep,* 8(536-547.

Wahlang, B., Beier, J. I., Clair, H. B., Bellis-Jones, H. J., Falkner, K. C., McClain, C. J. & Cave, M. C. 2013a. Toxicant-associated steatohepatitis. *Toxicologic pathology,* 41(2), pp 343-360.

Wahlang, B., Falkner, K. C., Clair, H. B., Al-Eryani, L., Prough, R. A., States, J. C., Coslo, D. M., Omiecinski, C. J. & Cave, M. C. 2014a. Human receptor activation by aroclor 1260, a polychlorinated biphenyl mixture. *Toxicological sciences : an official journal of the Society of Toxicology,* 140(2), pp 283-297.

Wahlang, B., Falkner, K. C., Gregory, B., Ansert, D., Young, D., Conklin, D. J., Bhatnagar, A., McClain, C. J. & Cave, M. 2013b. Polychlorinated biphenyl 153 is

a diet-dependent obesogen that worsens nonalcoholic fatty liver disease in male C57BL6/J mice. *The Journal of nutritional biochemistry,* 24(9), pp 1587-1595.

Wahlang, B., Hardesty, J. E., Jin, J., Falkner, K. C. & Cave, M. C. 2019a. Polychlorinated biphenyls and nonalcoholic fatty liver disease. *Current Opinion in Toxicology,* 14(21-28.

Wahlang, B., Jin, J., Beier, J. I., Hardesty, J. E., Daly, E. F., Schnegelberger, R. D., Falkner, K. C., Prough, R. A., Kirpich, I. A. & Cave, M. C. 2019b. Mechanisms of Environmental Contributions to Fatty Liver Disease. *Curr Environ Health Rep,* 6(3), pp 80-94.

Wahlang, B., Jin, J., Hardesty, J. E., Head, K. Z., Shi, H., Falkner, K. C., Prough, R. A., Klinge, C. M. & Cave, M. C. 2019c. Identifying sex differences arising from polychlorinated biphenyl exposures in toxicant-associated liver disease. *Food Chem Toxicol,* 129(64-76.

Wahlang, B., Perkins, J. T., Petriello, M. C., Hoffman, J. B., Stromberg, A. J. & Hennig, B. 2017. A compromised liver alters polychlorinated biphenyl-mediated toxicity. *Toxicology,* 380(11-22.

Wahlang, B., Song, M., Beier, J. I., Cameron Falkner, K., Al-Eryani, L., Clair, H. B., Prough, R. A., Osborne, T. S., Malarkey, D. E., States, J. C. & Cave, M. C. 2014b. Evaluation of Aroclor 1260 exposure in a mouse model of diet-induced obesity and non-alcoholic fatty liver disease. *Toxicol Appl Pharmacol,* 279(3), pp 380-390.

Wang, C., Petriello, M. C., Zhu, B. & Hennig, B. 2019. PCB 126 induces monocyte/macrophage polarization and inflammation through AhR and NF-κB pathways. *Toxicology and Applied Pharmacology,* 367(71-81.

Werder, E. J., Beier, J. I., Sandler, D. P., Falkner, K. C., Gripshover, T., Wahlang, B., Engel, L. S. & Cave, M. C. 2020. Blood BTEXS and heavy metal levels are associated with liver injury and systemic inflammation in Gulf states residents. *Food Chem Toxicol,* 139(111242.

WHO 2018. *Global status report on alcohol and health 2018*, Geneva: World Health Organization.

Willibald, M., Bayer, G., Stahlhut, V., Poschmann, G., Stühler, K., Gierke, B., Pawlak, M., Seeger, H., Mueck, A. O., Niederacher, D., Fehm, T. & Neubauer, H. 2017. Progesterone receptor membrane component 1 is phosphorylated upon progestin treatment in breast cancer cells. *Oncotarget; Vol 8, No 42*.

Witkiewitz, K., Litten, R. Z. & Leggio, L. 2019. Advances in the science and treatment of alcohol use disorder. *Sci Adv,* 5(9)**,** pp eaax4043.

Wong, F., Hung, H., Dryfhout-Clark, H., Aas, W., Bohlin-Nizzetto, P., Breivik, K., Mastromonaco, M. N., Lundén, E. B., Ólafsdóttir, K., Sigurðsson, Á., Vorkamp, K., Bossi, R., Skov, H., Hakola, H., Barresi, E., Sverko, E., Fellin, P., Li, H., Vlasenko, A., Zapevalov, M., Samsonov, D. & Wilson, S. 2021. Time trends of persistent organic pollutants (POPs) and Chemicals of Emerging Arctic Concern (CEAC) in Arctic air from 25 years of monitoring. *Science of The Total Environment,* 775(145109.

Xu, J., Xu, Y., Li, Y., Jadhav, K., You, M., Yin, L. & Zhang, Y. 2016. Carboxylesterase 1 Is Regulated by Hepatocyte Nuclear Factor 4α and Protects Against Alcohol- and MCD diet-induced Liver Injury. *Sci Rep,* 6(24277.

Yakar, S., Liu, J. L., Fernandez, A. M., Wu, Y., Schally, A. V., Frystyk, J., Chernausek, S. D., Mejia, W. & Le Roith, D. 2001. Liver-specific igf-1 gene deletion leads to muscle insulin insensitivity. *Diabetes,* 50(5)**,** pp 1110-8.

Yang, T., Poenisch, M., Khanal, R., Hu, Q., Dai, Z., Li, R., Song, G., Yuan, Q., Yao, Q., Shen, X., Taubert, R., Engel, B., Jaeckel, E., Vogel, A., Falk, C. S., Schambach, A., Gerovska, D., Araúzo-Bravo, M. J., Vondran, F. W. R., Cantz, T., Horscroft, N., Balakrishnan, A., Chevessier, F., Ott, M. & Sharma, A. D. 2022a. Corrigendum to 'Therapeutic HNF4A mRNA attenuates liver fibrosis in a preclinical model' [J Hepatol (2021) 1420-1433]. *J Hepatol,* 77(1)**,** pp 270.

Yang, Z., Han, S., Zhang, T., Kusumanchi, P., Huda, N., Tyler, K., Chandler, K., Skill, N. J., Tu, W., Shan, M., Jiang, Y., Maiers, J. L., Perez, K., Ma, J. & Liangpunsakul, S. 2022b. Transcriptomic Analysis Reveals the Messenger RNAs Responsible for the Progression of Alcoholic Cirrhosis. *Hepatology Communications,* 6(6)**,** pp 1361-1372.

You, M. & Arteel, G. E. 2019. Effect of ethanol on lipid metabolism. *J Hepatol,* 70(2)**,** pp 237-248.

Young, T. A., Bailey, S. M., Van Horn, C. G. & Cunningham, C. C. 2006. CHRONIC ETHANOL CONSUMPTION DECREASES MITOCHONDRIAL AND GLYCOLYTIC PRODUCTION OF ATP IN LIVER. *Alcohol and Alcoholism,* 41(3)**,** pp 254-260.

Younossi, Z., Anstee, Q. M., Marietti, M., Hardy, T., Henry, L., Eslam, M., George, J. & Bugianesi, E. 2018. Global burden of NAFLD and NASH: trends, predictions, risk factors and prevention. *Nat Rev Gastroenterol Hepatol,* 15(1)**,** pp 11-20.

Yu, G., Wang, L. G., Han, Y. & He, Q. Y. 2012. clusterProfiler: an R package for comparing biological themes among gene clusters. *Omics,* 16(5)**,** pp 284-7.

Zhang, H. F., Lin, X. H., Yang, H., Zhou, L. C., Guo, Y. L., Barnett, J. V. & Guo, Z. M. 2012a. Regulation of the activity and expression of aryl hydrocarbon receptor by ethanol in mouse hepatic stellate cells. *Alcoholism, clinical and experimental research,* 36(11)**,** pp 1873-1881.

Zhang, L., Ruan, X., Gu, M. & Mueck, A. O. 2022. E2 + norethisterone promotes the PI3K-AKT pathway via PGRMC1 to induce breast cancer cell proliferation. *Climacteric,* 25(5)**,** pp 467-475.

Zhang, M., Robitaille, M., Showalter, A. D., Huang, X., Liu, Y., Bhattacharjee, A., Willard, F. S., Han, J., Froese, S., Wei, L., Gaisano, H. Y., Angers, S., Sloop, K. W., Dai, F. F. & Wheeler, M. B. 2014. Progesterone receptor membrane component 1 is a functional part of the glucagon-like peptide-1 (GLP-1) receptor complex in pancreatic β cells. *Mol Cell Proteomics,* 13(11)**,** pp 3049-62.

Zhang, W., Sargis, R. M., Volden, P. A., Carmean, C. M., Sun, X. J. & Brady, M. J. 2012b. PCB 126 and other dioxin-like PCBs specifically suppress hepatic PEPCK expression via the aryl hydrocarbon receptor. *PLoS One,* 7(5)**,** pp e37103.

Zhong, W., Zhao, Y., Sun, X., Song, Z., McClain, C. J. & Zhou, Z. 2013. Dietary zinc deficiency exaggerates ethanol-induced liver injury in mice: involvement of intrahepatic and extrahepatic factors. *PLoS One,* 8(10)**,** pp e76522.

Zhou, Z., Wang, L., Song, Z., Saari, J. T., McClain, C. J. & Kang, Y. J. 2005. Zinc supplementation prevents alcoholic liver injury in mice through attenuation of oxidative stress. *Am J Pathol,* 166(6)**,** pp 1681-90.

APPENDICIES

Appendix I: Supporting Information for Chapter II

Supporting Table S1: List of housekeeping gene and genes of interest used in RT-PCR analysis.

Gene of Interest name	Abbreviated name	Assay ID
Glyceraldehyde-3-Phosphate Dehydrogenase (Applied Biosystems)	*Gapdh*	Ref: 4351309
Peroxisomal Proliferator Receptor α	*Pparα*	Mm00440939
Cytochrome P450 family 4, subfamily a, polypeptide 10	*Cyp4a10*	Mm02601690
Constitutively activated Androstane Receptor	*Car (Nr1i3)*	Mm01283978
Cytochrome P450 family 2, subfamily b, polypeptide 10	*Cyp2b10*	Mm01972453
Aryl Hydrocarbon Receptor	*Ahr*	Mm00478932
Cytochrome P450 family 1, subfamily a, member 2	*Cyp1a2*	Mm00487224
Fatty Acid Synthase	*Fasn*	Mm00662319
Stearoyl-CoA Desaturase 1	*Scd-1*	Mm00772290
Sterol Regulatory Element Binding Transcription Factor 1	*Srebf1*	Mm00550338
Albumin	*Alb*	Mm00802090
Cluster Differentiation 36 (Fatty Acid Translocase)	*Cd36*	Mm00432403
Fatty Acid Binding Protein	*Fabp1*	Mm00443440
Carnitine Palmitoyltransferase 1α	*Cpt1a*	Mm01231183
Carnitine Palmitoyltransferase 2	*Cpt2*	Mm00487205
Apolipoprotein B	*Apob*	Mm01545150
Microsomal Triglyceride Transfer Protein	*Mttp*	Mm00435015
Pyruvate Kinase L/R	*Pklr*	Mm00443090
Phosphoenolpyruvate Carboxykinase 1	*Pck1*	Mm01247058
Glucose-6-Phosphatase Catalytic Subunit 1	*G6pc*	Mm00839363
Glycogen Synthase	*Gys2*	Mm01267381
Glycogen Phosphorylase	*Pygl*	Mm01289790
Tumor Necrosis Factor α	*TNFα*	Mm00443258
C-X-C Motif Chemokine Ligand 2	*Cxcl2*	Mm00441242
C-C Motif Chemokine Ligand 2	*Ccl2*	Mm00441242
Tight junction protein 1	*Tjp1*	Mm00493699
Occludin	*Ocln*	Mm00500912
Claudin 3	*Cldn3*	Mm00515499
Mucin 2	*Muc2*	Mm01276696
DNA Damage Inducible Transcript 3	*Chop*	Mm00492097

Activating Transcription Factor 3	*Atf3*	Mm00476033
Activating Transcription Factor 4	*Atf4*	Mm00515324

Supporting Table S2: Repeated Measures ANOVA analyses performed for within-subjects using general linear models on SAS (ver. 9.4). The table represents a list of p-values reflecting the Wilks' Lambda, Pillai's Trace, Hotelling-Lawley Trace, and Roy's Greatest Root tests for significance where an alpha level is set to 0.05. Null hypotheses tested for change in body weight over days (H_{01}), change in body weight over days dependent on feeding (H_{02}), change in body weight over days dependent on exposure (H_{03}), and change in body weight over days dependent on combined feeding and exposure (H_{04}).

Supporting Table S2. Repeated Measure ANOVA: p-values for Within-Subjects Test				
Null Hypothesis	H_{01}	H_{02}	H_{03}	H_{04}
Test: No Effect for	Day	Day*Feeding	Day*Exposure	Day*Feeding *Exposure
Wilks' Lambda	**<.0001**	**<.0001**	**0.0055**	**0.0011**
Pillai's Trace	**<.0001**	**<.0001**	**0.0055**	**0.0011**
Hotelling-Lawley Trace	**<.0001**	**<.0001**	**0.0055**	**0.0011**
Roy's Greatest Root	**<.0001**	**<.0001**	**0.0055**	**0.0011**

Supporting Table S3: Repeated Measures ANOVA analyses performed for between-subjects using general linear models on SAS (ver. 9.4). The table represents p-values describing between-subjects (ignoring within-subjects) for feeding effect on body weight, exposure effects on body weight, and combined feeding and exposure effects on body weight.

| Supporting Table S3. Repeated Measure ANOVA: p-values for Between-Subjects Test					
Source	DF	Type III SS	Mean Square	F Value	Pr > F
Feeding	1	8.151220	8.151220	0.27	0.6085
Exposure	1	52.575120	52.575120	1.71	0.1961
Feeding*Exposure	1	0.009004	0.009004	0.00	0.9864
Error	56	1720.065877	30.715462		

Pair-feeding
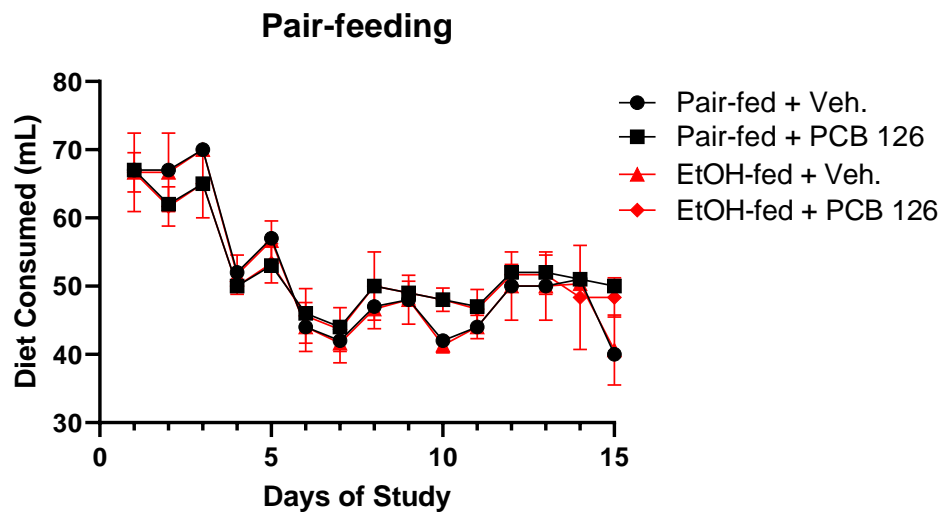
Supporting Figure S1: Consumption of the ethanol- and pair-fed diet was recorded daily. Ethanol- and pair-fed diet (mL) consumed was plotted over the entire duration of study. All values are represented as mean ± SD. EtOH, ethanol; Veh., vehicle.
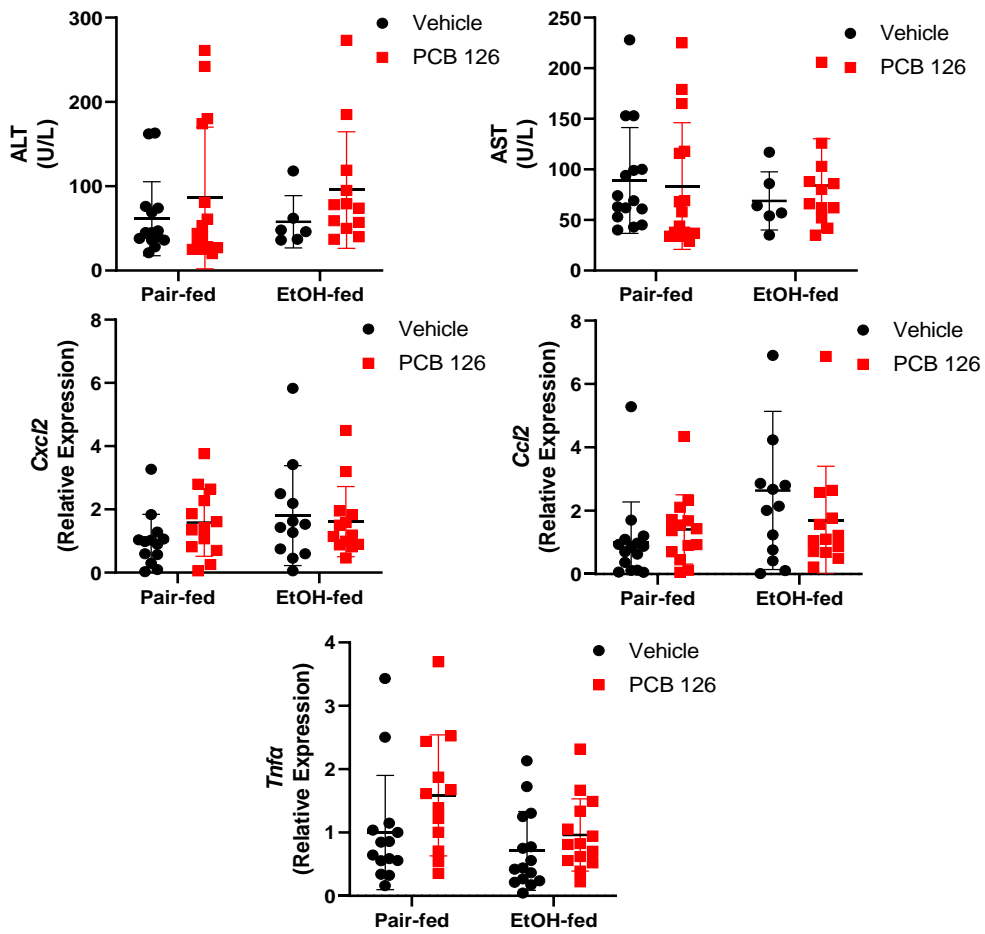
Outcome	EtOH	PCB 126	Interaction	Pair-fed (Veh. vs. PCB126)	EtOH-fed (Veh. vs. PCB126)	Veh. (Pair-fed vs. EtOH-fed)	PCB126 (Pair-fed vs. EtOH-fed)
ALT	n.s.	n.s.	n.s.	n.s.	n.s.	n.s.	n.s.
AST	n.s.	n.s.	n.s.	n.s.	n.s.	n.s.	n.s.
Cxcl2	n.s.	n.s.	n.s.	n.s.	n.s.	n.s.	n.s.
Ccl2	**0.0441**	n.s.	n.s.	n.s.	n.s.	n.s.	n.s.
Tnfα	**0.0328**	**0.0493**	n.s.	n.s.	n.s.	n.s.	n.s.

Supporting Figure S2: Plasma was isolated from whole blood and ALT and AST were measured *via* Piccolo Xpress Chemistry Analyzer. RT-PCR analysis was performed to measure hepatic mRNA levels of *Cxcl2*, *Ccl2*, and *Tnfα*. All values are represented as mean ± SD with an alpha level set to 0.05. A complete list of P-values, as determined by two-way ANOVA and Tukey's post-hoc test, is provided in the accompanying table. EtOH, ethanol; Veh., vehicle; ALT, alanine aminotransferase; AST, aspartate aminotransferase; Cxcl2, C-X-C Motif Chemokine Ligand 2; Ccl2, C-C Motif Chemokine Ligand 2; Tnfα, tumor necrosis factor α.
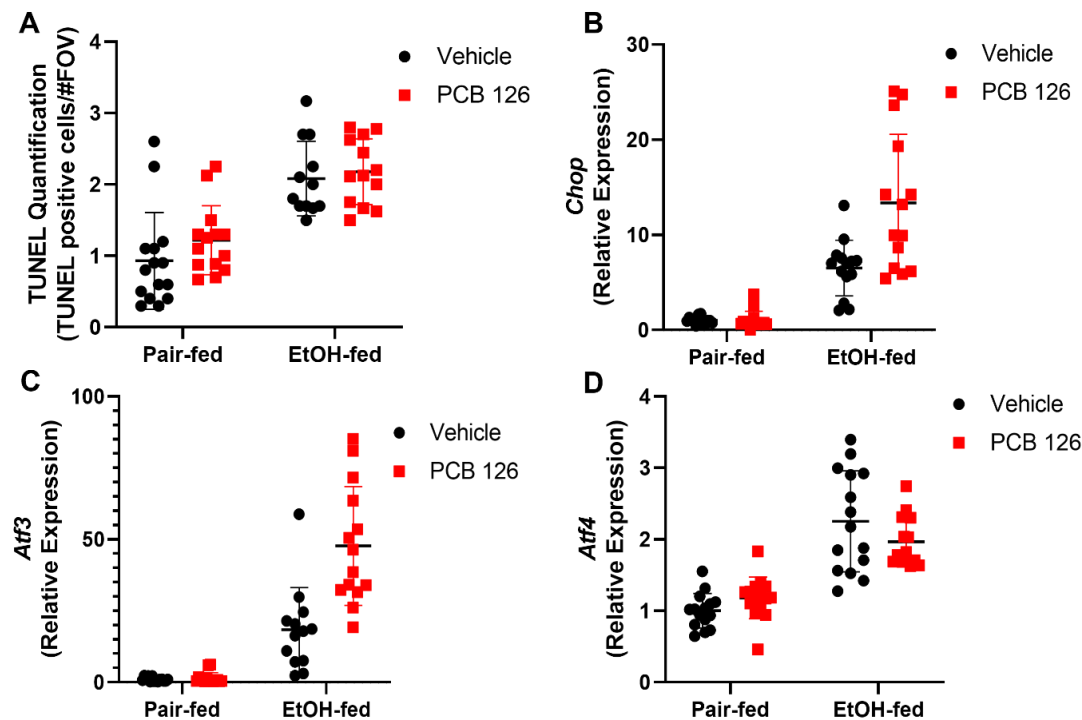
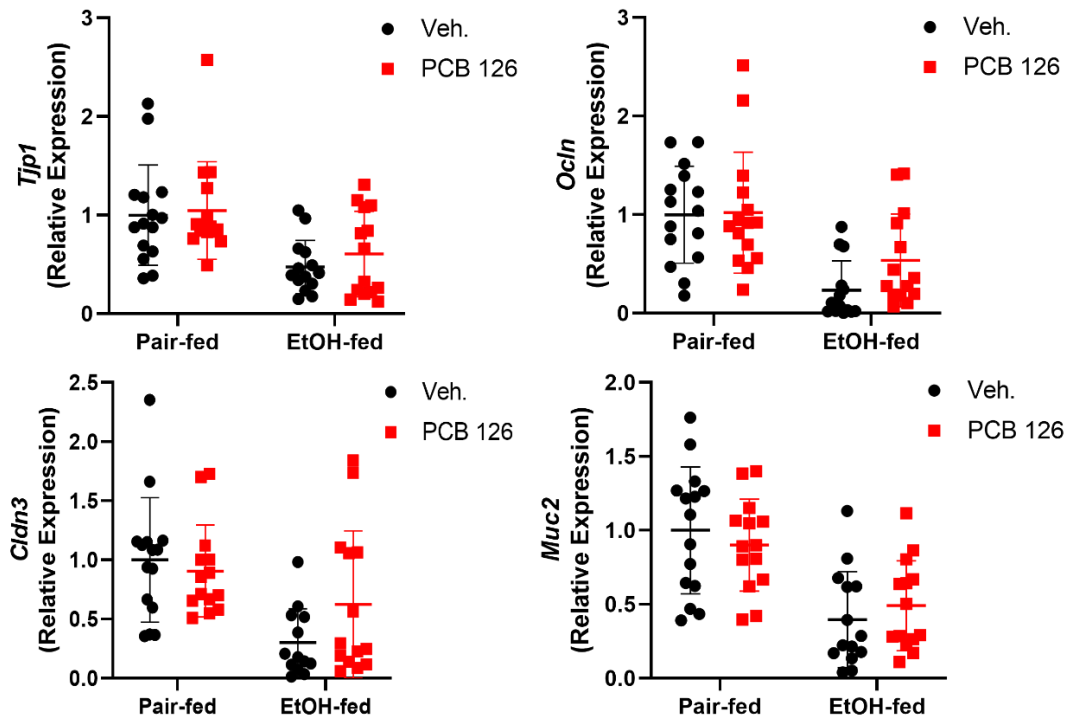| Outcome	EtOH	PCB 126	Interaction	Pair-fed (Veh. vs. PCB126)	EtOH-fed (Veh. vs. PCB126)	Veh. (Pair-fed vs. EtOH-fed)	PCB126 (Pair-fed vs. EtOH-fed)
TUNEL Quant.	<0.0001	n.s.	n.s.	n.s.	n.s.	<0.0001	0.0002
Chop	<0.0001	0.0015	0.0017	n.s.	0.0001	0.0023	<0.0001
Atf3	<0.0001	<0.0001	<0.0001	n.s.	<0.0001	0.0042	<0.0001
Atf4	<0.0001	n.s.	0.0463	n.s.	n.s.	<0.0001	<0.0001

Supporting Figure S3: (A) 5μm thin TUNEL stained liver sections were analyzed and quantified to detect hepatocytes undergoing apoptosis or necrosis (TUNEL positive staining) at 20x magnification. TUNEL scoring was performed by

counting positively stained nuclei for up to ten fields of view for each study animal. Counts were normalized by dividing by

the number of fields of view for each study animal. RT-PCR was performed to measure hepatic mRNA levels of **(B)** *Chop*,

(C) *Atf3*, and **(D)** *Atf4*. Values are represented as mean ± SD with an alpha level set to 0.05. A complete list of P-values, as

determined by two-way ANOVA and Tukey's post-hoc test, is provided in the accompanying table. EtOH, ethanol; Veh.,

vehicle; TUNEL, Terminal deoxynucleotidyl transferase dUTP nick end labeling; Chop, DNA Damage Inducible Transcript

3; Atf3, Activating Transcription Factor 3; Activating Transcription Factor 4.
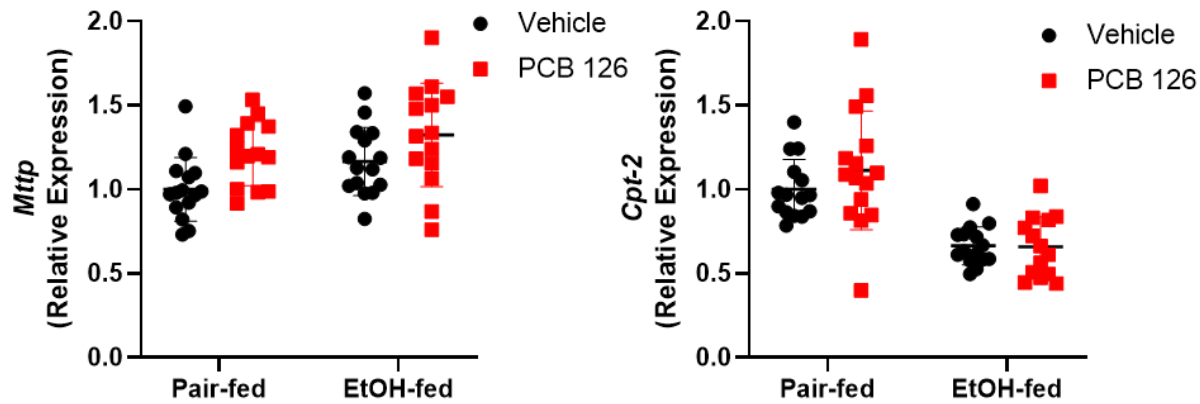
Outcome	EtOH	PCB 126	Interaction	Pair-fed (Veh. vs. PCB126)	EtOH-fed (Veh. vs. PCB126)	Veh. (Pair-fed vs. EtOH-fed)	PCB126 (Pair-fed vs. EtOH-fed)
Mttp	0.0236	0.0031	n.s.	n.s.	n.s.	n.s.	n.s.
Cpt-2	<0.0001	n.s.	n.s.	n.s.	n.s.	0.0008	<0.0001

Supporting Figure S4: RT-PCR analysis was performed to measure hepatic mRNA levels of *Mttp* and *Cpt-2*. Values are

represented as mean ± SD with an alpha level set to 0.05. A complete list of P-values, as determined by two-way ANOVA

and Tukey's post-hoc test, is provided in the accompanying table. EtOH, ethanol; Veh., vehicle; Mttp, microsomal triglyceride

transfer protein; Cpt-2, carnitine palmitoyltransferase 2.

Outcome	EtOH	PCB 126	Interaction	Pair-fed (Veh. vs. PCB126)	EtOH-fed (Veh. vs. PCB126)	Veh. (Pair-fed vs. EtOH-fed)	PCB126 (Pair-fed vs. EtOH-fed)
Tjp1	**0.0001**	n.s.	n.s.	n.s.	n.s.	**0.0115**	**0.0445**
Ocln	**<0.0001**	n.s.	n.s.	n.s.	n.s.	**0.0005**	**0.0459**
Cldn3	**0.0003**	n.s.	n.s.	n.s.	n.s.	**0.0017**	n.s.
Muc2	**<0.0001**	n.s.	n.s.	n.s.	n.s.	**0.0001**	**0.0150**

Supporting Figure S5: RT-PCR analysis was performed to measure ileal mRNA levels of *Tjp1*, *Ocln*, *Cldn3*, and *Muc2*. Values are represented as mean ± SD with an alpha level set to 0.05. A complete list of P-values, as determined by two-way ANOVA and Tukey's post-hoc test, is provided in the accompanying table. EtOH, ethanol; Veh., vehicle; Tjp1, tight junction protein 1; Ocln, occludin; Cldn3, claudin 3; Muc2, mucin 2.

Appendix II: Supporting Information for Chapter III

Supporting Table S4: Number of Differentially Expressed Genes (DEGs) detected *via* DESeq2 analyses for all pairwise comparisons performed.

Group Comparison	DEGs (p≤0.05; q≤0.05; |log2FC|≥0; FPKM≥1 in ≥3 samples; AVG FPKM≥1)		
	TOTAL	UP	DOWN
EF v PF	5919	2834	3085
Veh. v PCB126	449	278	171
Veh.(PF v EF)	4474	2231	2243
PCB126(PF v EF)	4832	2214	2618
PF(Veh. v PCB126)	503	339	164
EF(Veh. v PCB126)	907	536	371

Supporting Table S5: Top 20 up- and downregulated DEGs sorted by lowest *p*-value. DEGs were determined by DESeq2 analyses.

Top 20 UP DEGs			Top 20 DOWN DEGs		
Gene	Log$_2$FC	p-value	Gene	Log$_2$FC	p-value
Cyp1a1	8.64	1.86e-218	*Ugt1a6b*	-1.01	9.64e-22
Cyp1a2	3.63	2.29e-110	*Plin4*	-1.76	2.09e-14
Slc46a3	2.55	1.67e-67	*Cyp3a11*	-1.26	7.36e-12
Cyfip2	3.51	4.57e-46	*Cyp2d40*	-0.88	1.56e-11
Ugt1a9	2.15	3.07e-43	*Alas2*	-0.86	1.86e-11
Pkm	1.99	8.08e-39	*Rnf169*	-0.48	7.47e-11
Htatip2	1.59	4.56e-38	*Fam210b*	-0.53	3.39e-10
Gpx2	3.95	2.94e-36	*Paqr9*	-0.85	5.13e-10
Maoa	1.55	2.93e-33	*1810055G02Rik*	-0.81	6.09e-10
Aldh3b1	2.06	7.72e-29	*Apoa1*	-1.02	8.61e-10
Pcp4l1	2.19	1.88e-26	*St3gal3*	-0.58	1.56e-09
Rtn4rl2	2.91	2.71e-26	*Nrbp2*	-0.70	1.98e-09
Tuba8	1.55	9.95e-25	*Elovl2*	-0.63	2.58e-09
Selenbp1	1.31	2.63e-24	*Smarcc2*	-0.35	4.44e-09
Coro6	2.20	1.60e-19	*Ulk1*	-0.64	5.59e-09
Cyp1b1	2.99	1.55e-18	*Serpina11*	-0.75	7.53e-09
Insl6	2.26	5.27e-17	*Zfp865*	-0.46	9.02e-09
Nqo1	1.49	4.24e-16	*Ldha*	-0.68	2.17e-08
Tmem86b	1.07	5.32e-15	*Scp2*	-0.49	7.65e-08
Tgfb2	2.50	2.04e-14	*Gm50136*	-1.14	9.11e-08
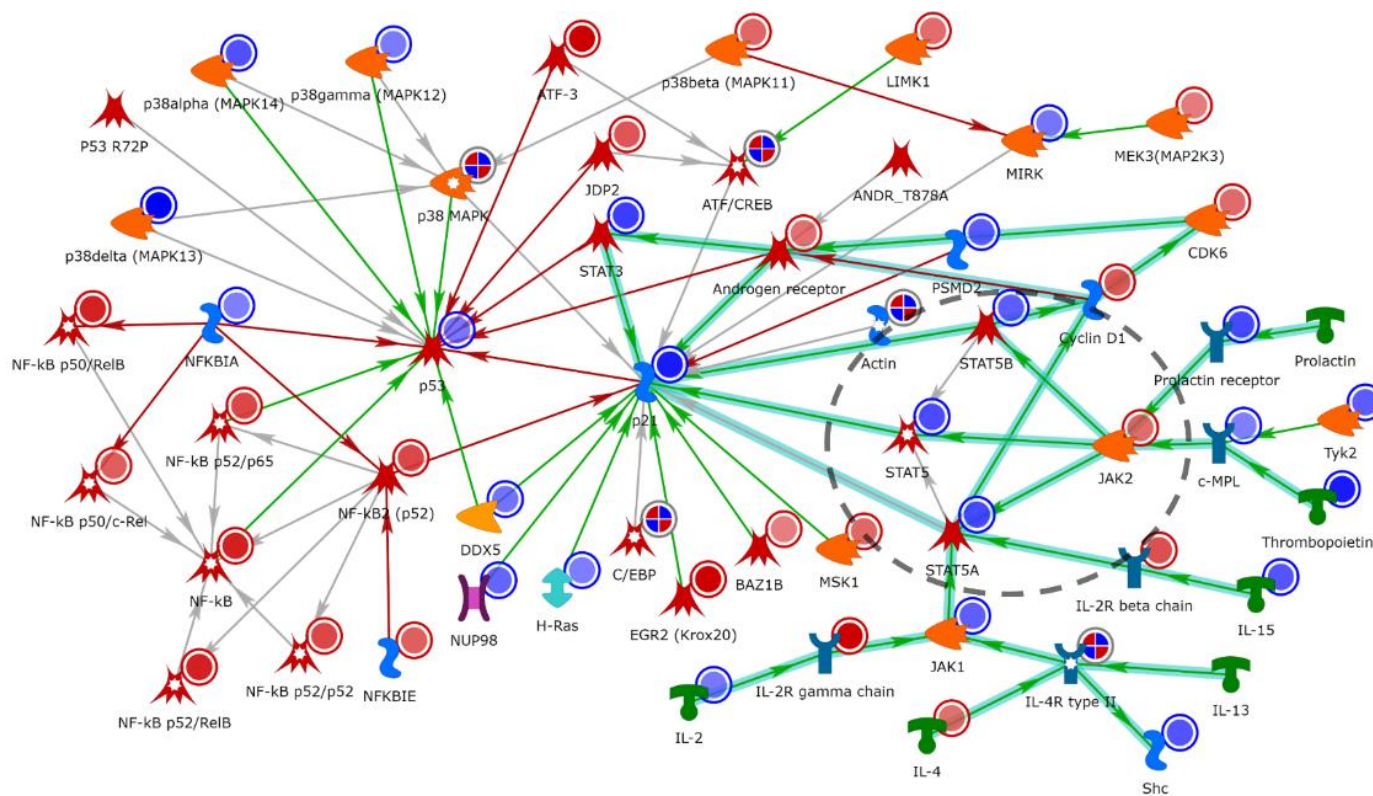
Supporting Figure S6: MetaCore network analysis of the term "peptidyl-tyrosine modifications", where JAK2 and STAT5 are encircled by a gray dash line. Green lines indicate activation, red lines indicate inhibition, and gray lines indicate an unknown interaction. Red circles indicate upregulation and blue circles indicate downregulation, where darker color indicates a higher magnitude of fold change and lighter color indicates smaller magnitude of fold change.

Supporting Table S6: Top 25 enriched GO molecular function processes generated on MetaCore. Processes were filtered

by down signals for a false discovery rate threshold of 0.05.

#	Enriched GO Molecular Functions | EF(Veh. v PCB 126) | DOWN	p-value	FDR	In Data
1	protein binding	1.3013E-133	5.07E-130	5750
2	binding	4.6623E-103	9.0823E-100	6443
3	catalytic activity	1.05167E-55	1.36577E-52	2585
4	**ion binding**	3.96767E-52	3.86451E-49	2574
5	organic cyclic compound binding	1.11826E-46	8.7135E-44	2616
6	heterocyclic compound binding	6.79609E-45	4.41293E-42	2579
7	**metal ion binding**	1.28796E-32	7.16844E-30	1798
8	cation binding	2.03499E-32	9.9104E-30	1838
9	transcription factor binding	4.72748E-29	2.04647E-26	394
10	nucleoside phosphate binding	7.03134E-27	2.73941E-24	1023
11	nucleotide binding	9.58535E-27	3.37514E-24	1022
12	small molecule binding	1.03957E-26	3.37514E-24	1205
13	DNA-binding transcription factor binding	6.02271E-26	1.80496E-23	298
14	chromatin binding	4.29744E-23	1.19592E-20	354
15	nucleic acid binding	6.35743E-23	1.65124E-20	1706
16	transcription coregulator activity	8.82227E-23	2.14822E-20	295
17	enzyme binding	2.16828E-22	4.96918E-20	1031
18	**transition metal ion binding**	5.8704E-22	1.27061E-19	724
19	anion binding	7.19611E-21	1.47558E-18	1066
20	purine nucleotide binding	2.68221E-20	5.22494E-18	885
21	**zinc ion binding**	4.32103E-20	8.01654E-18	589
22	transferase activity	6.09936E-20	1.08014E-17	1047
23	adenyl nucleotide binding	1.84881E-19	3.13172E-17	742
24	RNA binding	2.72757E-19	4.42775E-17	751
25	RNA polymerase II-specific DNA-binding transcription factor binding	2.9894E-19	4.65868E-17	219
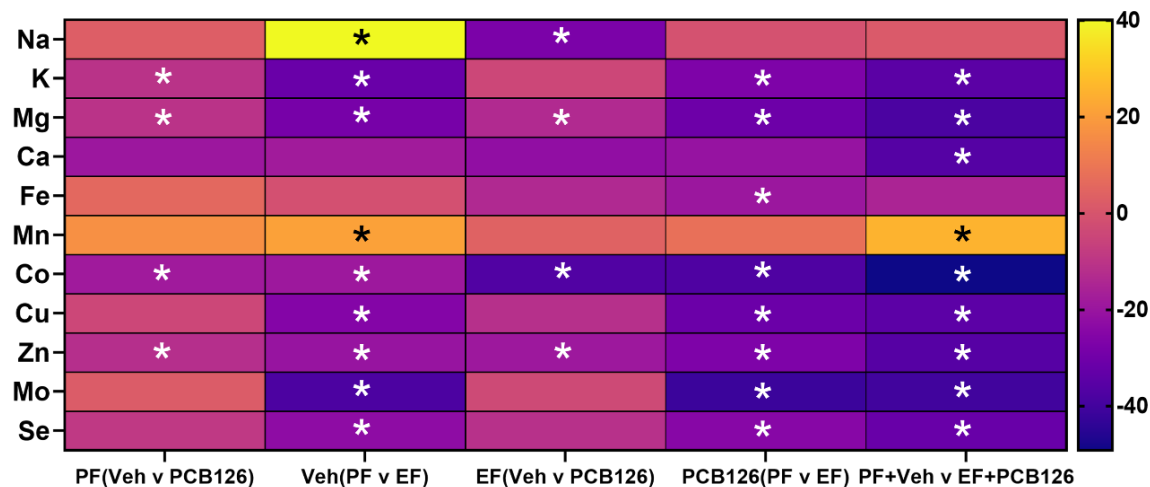
| Percent change of mean for essential metals					
Metal	PF(Veh. v PCB126)	Veh.(PF v EF)	EF(Veh. v PCB126)	PCB126(PF v EF)	PF+Veh. v EF+PCB126
Sodium (Na)	2.54% ↑	40.1% ↑*	27.8% ↓*	1.3% ↓	1.2% ↑
Potassium (K)	10.9% ↓*	31.7% ↓*	4.6% ↓	27.0% ↓*	34.9% ↓*
Magnesium (Mg)	10.8% ↓*	28.7% ↓*	13.6% ↓*	30.9% ↓*	38.4% ↓*
Calcium (Ca)	19.6% ↓	18.2% ↓	22.3% ↓	20.9% ↓	36.4% ↓*
Iron (Fe)	5.3% ↑	1.8% ↓	13.9% ↓	19.7% ↓*	15.4% ↓
Manganese (Mn)	16.3% ↑	20.8% ↑*	3.6% ↑	7.6% ↑	25.1% ↑*
Cobalt (Co)	18.5% ↓*	19.3% ↓*	37.1% ↓*	37.6% ↓*	49.2% ↓*
Copper (Cu)	4.7% ↓	25.6% ↓*	12.0% ↓	31.2% ↓*	34.5% ↓*
Zinc (Zn)	12.2% ↓*	20.7% ↓*	19.2% ↓*	27.1% ↓*	36.0% ↓*
Molybdenum (Mo)	1.9% ↑	38.3% ↓*	3.8% ↓	41.7% ↓*	40.6% ↓*
Selenium (Se)	9.2% ↓	23.2% ↓*	11.4% ↓	25.0% ↓*	31.9% ↓*

Supporting Figure S7: Heatmap reflecting the percent change of mean metal levels between group comparisons. This heatmap was generated on GraphPad Prism where group comparisons are on the x-axis, and individual metals are on the y-axis. The accompanied table lists the actual percent change between the respective groups. Metals were measured by

ICP-MS and normalized to the initial hepatic tissue weight. Asterisks (*) represents a significant two-way ANOVA Tukey's post-hot test between groups. Na, sodium; K, potassium; Mg, magnesium; Ca, calcium; Fe, Iron; Mn, manganese; Co, cobalt; Cu, copper; Zn, zinc; Mo, molybdenum; Se, selenium.
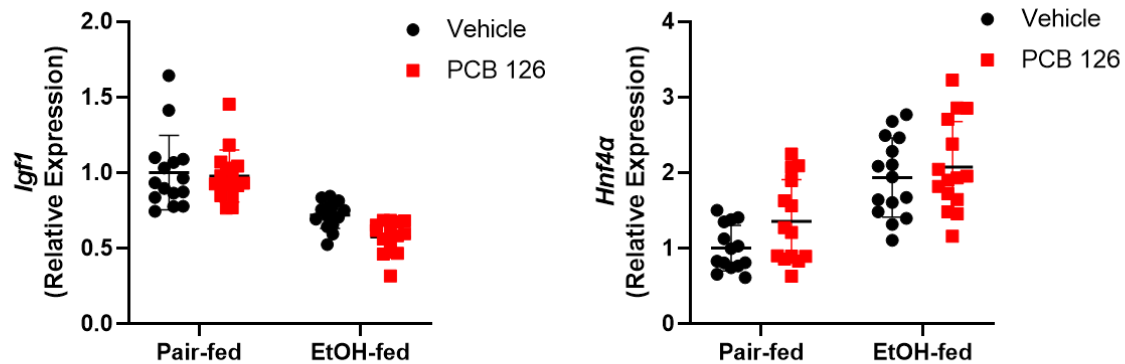
Outcome	EtOH	PCB 126	Interaction	Pair-fed (Veh. vs. PCB 126)	EtOH-fed (Veh. vs. PCB 126)	Veh. (Pair-fed vs. EtOH-fed)	PCB 126 (Pair-fed vs. EtOH-fed)
Igf1	<0.0001	n.s.	n.s.	n.s.	n.s.	0.0001	<0.0001
Hnf4α	<0.0001	n.s.	n.s.	n.s.	n.s.	<0.0001	0.0020

Supporting Figure S8: Hepatic RT-PCR analysis of *Igf1* and *Hnf4α*. Measured mRNA transcripts of *Igf1* and *Hnf4α* are displayed where values are represented as mean±SD with an alpha level set to 0.05. A complete list of p-values, as determined by two-way ANOVA and Tukey's post-hoc test, is provided in the accompanying table. *Igf1*, insulin-like growth factor 1; *Hnf4α*, hepatocyte nuclear factor 4 alpha.
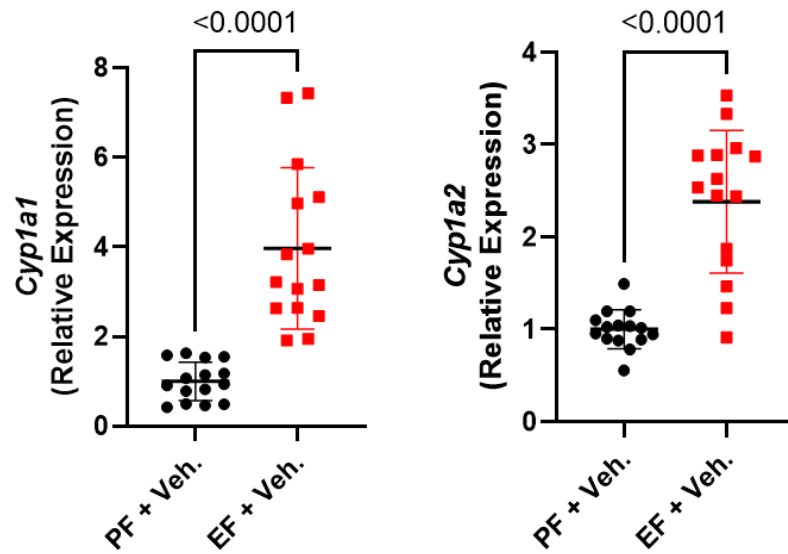
Supporting Figure S9: Hepatic RT-PCR analysis of *Cyp1a1* and *Cyp1a2*. Measured mRNA transcripts of *Cyp1a1* and *Cyp1a2* are displayed where values are represented as mean±SD with an alpha level set to 0.05. Students t-test was performed on GraphPad Prism and p-values for each gene are shown above each figure for the Veh.(PF v EF) comparison. *Cyp1a1*, cytochrome P450, family 1, subfamily a, polypeptide 1;*Cyp1a2*, cytochrome P450, family 1, subfamily a, polypeptide 2.
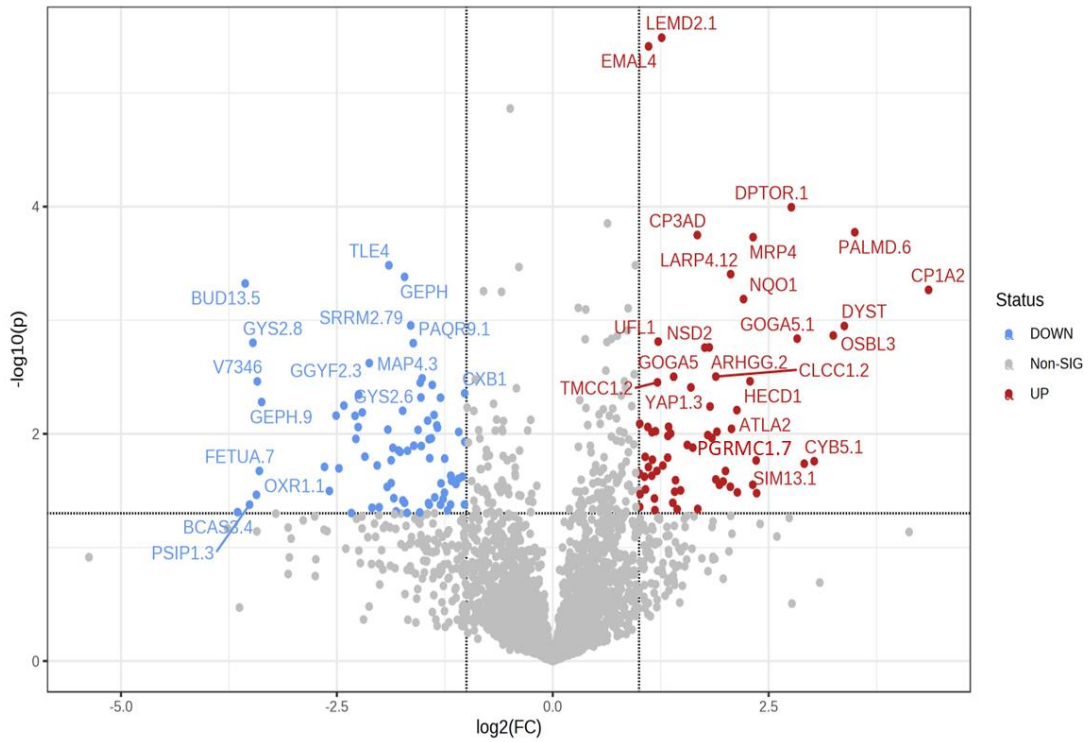
Supporting Figure S10: Volcano plot of all phospho-peptides differentially impacted in the EF(Veh. v PCB126) comparison. A volcano plot was generated on MetaboAnalyst for both EtOH-fed groups, where outlier EF_PCB3 was removed. Phospho-peptide p-value cutoff was set to 0.05.

Supporting Table S7: Scansite 4.0 predicted kinases that phosphorylate PGRMC1 at the phosphoacceptor sites, Y180 and S181.

Score	Percentile	Motif Group	Phospho-site	Gene Alias
0.487	1.592%	SH2	Y180	Fgr
0.463	2.437%	SH2	Y180	Lck
0.550	3.886%	SH2	Y180	Nck
0.496	4.984%	Tyrosine kinase	Y180	Pdgfrb
0.343	0.204%	SH2	Y180	Inpp5d
0.696	4.447%	SH2	Y180	Pik3r1
0.386	0.210%	Acidophilic serine/threonine kinase	S181	Csnk2b
0.512	0.884%	DNA damage kinase	S181	Prkdc

Predicted kinases were revealed by Scansite 4.0 (scansite4.mit.edu/#home) for a low stringency property. SH2, Src homology 2 group; Fgr, Feline Gardner-Rasheed proto-oncogene; Lck, T-Cell-Specific Protein Tyrosine Kinase; Nck, Non-Catalytic Region of Tyrosine Kinase; Pdgfrb, Platelet-Derived Growth Factor Receptor beta; Inpp5d, Inositol Polyphosphate-5-Phosphatase D; Pik3r1, Phosphoinositide-3-Kinase Regulatory Subunit 1; Csnk2b, Casein Kinase 2 beta; Prkdc, Protein Kinase, DNA-Activated, Catalytic Subunit.
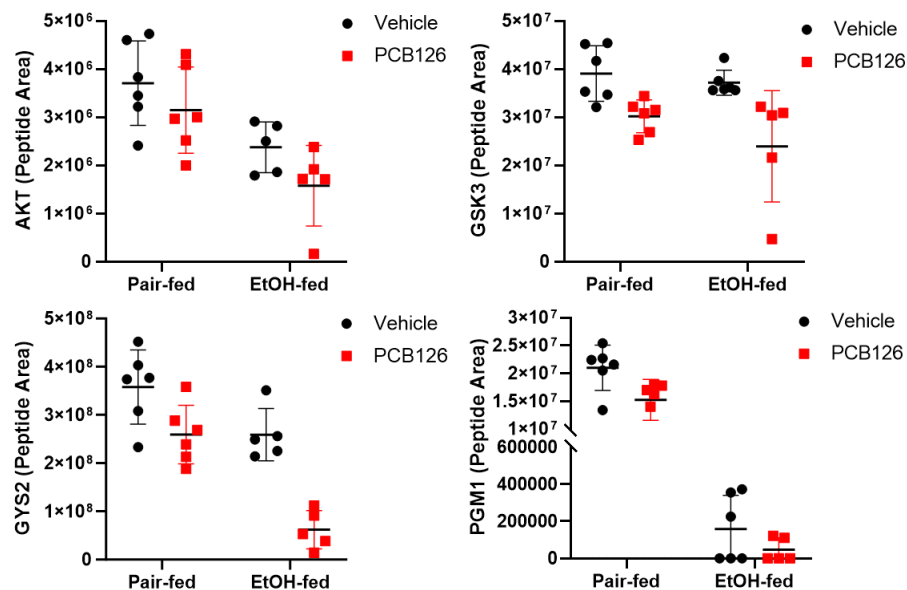
Outcome	EtOH	PCB 126	Interaction	Pair-fed (Veh. vs. PCB 126)	EtOH-fed (Veh. vs. PCB 126)	Veh. (Pair-fed vs. EtOH-fed)	PCB 126 (Pair-fed vs. EtOH-fed)
AKT	0.0005	n.s.	n.s.	n.s.	n.s.	n.s.	0.0230
GSK3	n.s.	0.0006	n.s.	n.s.	0.0154	n.s.	n.s.
GYS2	<0.0001	<0.0001	n.s.	n.s.	0.0004	n.s.	0.0002
PGM1	<0.0001	0.0219	0.0268	0.0106	n.s.	<0.0001	<0.0001

Supporting Figure S11: Peptide area evaluation of most prominent phospho-peptides residing in AKT, GSK3, and PGM1.

Phospho-peptides normalized by TIC were exported from our phosphoproteomic dataset and imported into GraphPad Prism

for statistical analysis. A two-way ANOVA and Tukey's post-hoc test was used where values are represented as mean±SD

with an alpha level set to 0.05. A complete list of p-values, as determined by two-way ANOVA and Tukey's post-hoc test, is

provided in the accompanying table. Akt, protein kinase B; GSK3, glycogen synthase kinase 3; GYS2, Glycogen Synthase

2; PGM1, phosphoglucomutase 1.

CURRICULUM VITAE

Tyler C. Gripshover, M.S.

Ph.D. Candidate

University of Louisville, School of Medicine

Department of Pharmacology & Toxicology

Kosair Charities Clinical & Translational Research Building

505 S Hancock St., Room 527D

Louisville, KY 40202

Academic Email: tcgrip01@louisville.edu

Personal Email: tygripshover72@gmail.com

LinkedIn: linkedin.com/in/tyler-gripshover

ORCID: 0000-0003-2191-910

Education

2021-present (Expected 2023)	Ph.D. Pharmacology & Toxicology University of Louisville School of Medicine Louisville, Kentucky
2019-2021	M.S. Pharmacology & Toxicology University of Louisville School of Medicine Louisville, Kentucky
2014-2018	B.S. Chemistry (Biochemistry concentration) Eastern Kentucky University College of Science Richmond, Kentucky

Employment Experience

2019 (Feb-July)	Laboratory Technician Mentors: Dr. Bernhard Hennig & Dr. Hollie Swanson University of Kentucky Lexington, Kentucky
2019 (May-July)	Near-peer Mentor – SURES program Director: Dr. Hollie Swanson University of Kentucky Lexington, Kentucky

2017	Undergraduate Research Trainee – SURES program
(May-July)	Mentor: Dr. Yvonne Fondufe-Mittendorf
	University of Kentucky
	Lexington, Kentucky

Funding Appointments

| 2021-2023 | NIEHS T32 Institutional Training Grant \| UofL Environmental Health Science Training Program (5T32ES011564-17) |

Honors & Awards

2020-2022	GSC & CIEHS travel awards (x6), University of Louisville
2015-2018	Dean's List (x7), Eastern Kentucky University
2014, 2018	President's List (x2), Eastern Kentucky University
2014-2018	Presidential Scholarship, Eastern Kentucky University

Professional Memberships

2021-present	American Association for the Study of Liver Diseases (AASLD)
2020-present	Ohio Valley Society of Toxicology (OVSOT)
2019-present	Superfund Research Program (SRP)
2019-present	Society of Toxicology (SOT)

Continuing Education & Elective Coursework

Spring 2023	Advanced Discovery Toxicology: Integrating Toxicology with Other Functions on the Team (AM03) – SOT Annual Meeting
Spring 2022	How Advances in Exposure Science and Toxicology Are Changing Assessments of the Effects of Chemical Mixtures on Human Health (AM04) – SOT Annual Meeting
Fall 2021	Toxicology Excellence for Risk Assessment (TERA) Dose-Response Boot Camp – Introduction to Human Risk Assessment
Spring 2021	Immunology (MBIO 602); Molecular Toxicology (PHTX 661)

Mentorship

Summer 2023	Mentored and trained University of Louisville second-year medical students, Zayna Qaissi and Joshua Abramson; post-doctoral fellow, Frederick Ekuban; and senior undergraduate student, Ashton Reed
Summer 2022	Mentored and trained University of Louisville second-year medical student Muhammad Mustafa
Spring '22-present	Assisted in the training of two graduate students, Oluwanifemi Bolatimi and Ngozi Adiele; and two undergraduate students, Bana Luulay and Shikshita Singh
Fall 2021	Assisted in the training of a rotating first-year graduate students, Oluwanifemi Bolatimi and Ngozi Adiele
Summer 2019	Near-peer mentor to undergraduate SURES student, Nicholas Meredith

Publications

1. **Gripshover TC**, Wahlang B, Head KZ, Luo J, Bolatimi OE, Smith ML, Rouchka EC, Chariker JH, Xu J, Cai L, Cave MC. PCB126 Modifies the Murine Hepatic Transcriptome and Metallome to Promote Alcohol-associated Liver Disease Pathogenesis. *Under review with Environmental Health Perspectives (2023)*.

2. Luo J, Watson WH, **Gripshover TC**, Qaissi Z, Wahlang B. Sex-specific effects of acute chlordane exposure in the context of steatotic liver disease, energy metabolism and endocrine disruption. Food Chem Toxicol. 2023 Sep 4;180:114024. doi: 10.1016/j.fct.2023.114024. Epub ahead of print. PMID: 37666290.

3. Groswald AM, **Gripshover TC**, Watson WH, Wahlang B, Luo J, Jophlin LL, Cave MC. Investigating the Acute Metabolic Effects of the N-Methyl Carbamate Insecticide, Methomyl, on Mouse Liver. Metabolites. 2023 Aug 1;13(8):901. doi: 10.3390/metabo13080901. PMID: 37623845; PMCID: PMC10456691.

4. Head KZ, Bolatimi OE, **Gripshover TC**, Tan M, Li Y, Audam TN, Jones SP, Klinge CM, Cave MC, Wahlang B. Investigating the effects of long-term Aroclor 1260 exposure on fatty liver disease in a diet-induced obesity mouse model. Front Gastroenterol (Lausanne). 2023;2:1180712. doi: 10.3389/fgstr.2023.1180712. Epub 2023 May 12. PMID: 37426695; PMCID: PMC10327714.

5. Bolatimi OE, Head KZ, Luo J, **Gripshover TC**, Lin Q, Adiele NV, Watson WH, Wilkerson C, Cai L, Cave MC, Young JL. Can Zinc Supplementation Attenuate High Fat Diet-Induced Non-Alcoholic Fatty Liver Disease? Int J Mol Sci. 2023 Jan 16;24(2):1763. doi: 10.3390/ijms24021763. PMID: 36675277; PMCID: PMC9864360.

6. **Gripshover TC**, Wahlang B, Head KZ, Young JL, Luo J, Mustafa MT, Kirpich IA, Cave MC. The environmental pollutant, polychlorinated biphenyl 126, alters liver function in a rodent model of alcohol-associated liver disease. Alcohol Clin Exp Res. 2023 Jan;47(1):60-75. doi: 10.1111/acer.14976. Epub 2022 Dec 1. PMID: 36377258; PMCID: PMC9974797.

7. Wahlang B*, **Gripshover TC***, Gao H*, Krivokhizhina T, Keith RJ, Sithu ID, Rai SN, Bhatnagar A, McClain CJ, Srivastava S, Cave MC. Associations Between Residential Exposure to Volatile Organic Compounds and Liver Injury Markers. Toxicol Sci. 2021 Dec 28;185(1):50-63. doi: 10.1093/toxsci/kfab119. PMID: 34668566; PMCID: PMC8714366. *First Co-Authors*

8. Werder, E. J., Beier JI, Sandler DP, Falkner KC, **Gripshover T**, Wahlang B, Engel LS, Cave MC. Blood BTEXS and heavy metal levels are associated with liver injury and systemic inflammation in Gulf states residents. Food Chem Toxicol. 2020 May;139:111242. doi: 10.1016/j.fct.2020.111242. Epub 2020 Mar 20. PMID: 32205228; PMCID: PMC7368391.

9. Rea, M., **Gripshover T**, Fondufe-Mittendorf Y. Selective inhibition of CTCF binding by iAs directs TET-mediated reprogramming of 5-hydroxymethylation patterns in iAs-transformed cells. Toxicol Appl Pharmacol. 2018 Jan 1;338:124-133. doi: 10.1016/j.taap.2017.11.015. Epub 2017 Nov 22. PMID: 29175454; PMCID: PMC5738917.

Presentations

1. **Gripshover TC**. "The Impact of Environmental Pollutants on Alcohol-associated Liver Disease Pathogenesis" Pharmacology and Toxicology Department Seminar. November 8th, 2023. *Oral Dissertation Defense*.

2. **Gripshover TC**, Wahlang B, Head KZ, Rouchka EC, Young JL, Luo J, Kirpich IA, Cave MC. "Polychlorinated Biphenyl 126 alters the Hepatic Transcriptome to enhance Alcohol-associated Liver Disease" Ohio Valley Chapter of the Society of Toxicology Annual Meeting 2023. *Poster Presentation*.

3. **Gripshover TC**. "Altered Phospho- Signaling Promotes Fatty Liver Disease in an Alcohol+PCB126 Model" Annual Pharmacology and Toxicology Department Seminar. June 15th, 2023. *Oral Presentation*.

4. **Gripshover TC**, Wahlang B, Head KZ, Rouchka EC, Young JL, Luo J, Kirpich IA, Cave MC. "Polychlorinated Biphenyl 126 alters the Hepatic

Transcriptome to enhance Alcohol-associated Liver Disease" Society of Toxicology Annual Meeting 2023. *Poster Presentation*.

5. **Gripshover TC**, Wahlang B, Head KZ, Mustafa MT, Young JL, Luo J, Cave MC. "Environmental pollutant, Polychlorinated biphenyl 126, alters energy metabolism in a rodent ALD model" Superfund Research Program Annual Meeting 2022. *Poster Presentation*.

6. **Gripshover TC**, Wahlang B, Head KZ, Mustafa MT, Young JL, Luo J, Cave MC. "Environmental pollutant, Polychlorinated biphenyl 126, alters energy metabolism in a rodent ALD model" American Association for the Study of Liver Diseases Annual Meeting 2022. *Poster Presentation*.

7. **Gripshover TC**, Wahlang B, Head KZ, Mustafa MT, Young JL, Luo J, Cave MC. "Environmental pollutant, Polychlorinated biphenyl 126, alters energy metabolism in a rodent ALD model" Ohio Valley Chapter of the Society of Toxicology Annual Meeting 2022. *Poster Presentation*.

8. **Gripshover TC**, Wahlang B, Head KZ, Mustafa MT, Young JL, Luo J, Cave MC. "Environmental pollutant, Polychlorinated biphenyl 126, alters energy metabolism in a rodent ALD model" Research! Louisville Annual Meeting 2022. *Poster Presentation*.

9. **Gripshover TC**, Mustafa MT, Wahlang B, Head KZ, Luo J, Young JL, Cave MC. "Investigating the Effects of PCB126 on Gut-Liver Interactions in Mice consuming an Ethanol Diet" Ohio Valley Chapter of the Society of Toxicology Summer Student Meeting 2022. *Oral Presentation*.

10. **Gripshover TC**, Wahlang B, Head KZ, Young JL, Luo J, Cave MC. "Investigating the Effects of PCB126 in an Acute Rodent Alcohol Model" Research Society on Alcoholism Annual Meeting 2022. *Poster Presentation*.

11. **Gripshover TC**. **"**Environmental pollutant, PCB126, alters Liver Function in a Rodent ALD Model" Annual Pharmacology and Toxicology Department Seminar. May 26th, 2022. *Oral Presentation*.

12. **Gripshover TC**, Wahlang B, Head KZ, Young JL, Luo J, Cave MC. "Investigating the Effects of PCB126 in an Acute Rodent Alcohol Model" Society of Toxicology Annual Meeting 2022. *Poster Presentation*.

13. **Gripshover TC**, Wahlang B, Head KZ, Young JL, Luo J, Cave MC. "Investigating the Interaction of PCB-126 and Ethanol in a Rodent Alcohol Model." Ohio Valley Chapter of the Society of Toxicology Annual Meeting 2021. *Poster Presentation*.

14. **Gripshover TC**, Wahlang B, Warner JB, Prough RA, Kirpich IA, Cave MC. "Investigating the Effects of Perfluorooctanoic Sulfonate (PFOS) and Ethanol on Fatty Liver Disease using a modified NIAAA Model." American Association for the Study of Liver Diseases Annual Meeting 2021. *Poster Presentation*.

15. **Gripshover TC**, Wahlang B, Warner JB, Prough RA, Kirpich IA, Cave MC. "Investigating the Effects of Perfluorooctanoic Sulfonate (PFOS) and Ethanol on Fatty Liver Disease using a modified NIAAA Model." Research! Louisville Annual Meeting 2021. *Poster Presentation*.

16. **Gripshover TC**. "Investigating the Effects of Perfluorooctanoic Sulfonate (PFOS) and Ethanol on Fatty Liver Disease using a Modified NIAAA Model" Master's Defense and PhD Proposal. Pharmacology and Toxicology Department Seminar Series. May 20th, 2021. *Oral Presentation*.

17. **Gripshover TC**, Wahlang B, Head KZ, Warner JB, Smith SE, Cave MC. "Investigating the Effects of Perfluorooctanoic Sulfonate (PFOS) and Ethanol on Fatty Liver Disease using a modified NIAAA Model." Society of Toxicology Annual Meeting 2021. *Poster Presentation*.

18. **Gripshover TC**, Wahlang B, Riggs D, Smith SE, Krivokhizhina T, Keith R, McClain CJ, Srivastava S, Cave MC. "Volatile Organic Compound Exposures Are Positively Associated with Liver Apoptosis in a Residential Cohort." Superfund Research Program Annual Meeting 2020. *Oral and Poster presentation*.

19. **Gripshover TC**, Wahlang B, Riggs D, Smith SE, Krivokhizhina T, Keith R, McClain CJ, Srivastava S, Cave MC. "Volatile Organic Compound Exposures Are Positively Associated with Liver Apoptosis in a Residential

Cohort." American Association for the Study of Liver Diseases Annual Meeting 2020. *Poster presentation.*

20. **Gripshover TC**. "Investigating the effects of PFAS and Ethanol co-exposures on Fatty Liver Disease and Fibrosis" Annual Pharmacology and Toxicology Department Seminar. April 2nd, 2020. *Oral Presentation.*

21. **Gripshover TC**, Wahlang B, Riggs D, Smith SE, Krivokhizhina T, Keith R, McClain CJ, Srivastava S, Cave MC. "Volatile Organic Compound Exposures Are Positively Associated with Liver Apoptosis in a Residential Cohort." Society of Toxicology Annual Meeting 2020. *Poster presentation.*

22. **Gripshover, T.**, Rea, M., Fondufe-Mittendorf, Y. "Profiling of Functional Reprogramming of 5-hydroxymethylCytosine during iAs-mediated EMT." SURES student presentations 2017. *Poster presentation.*